SYNTHESIS OF SUPPORTED METAL NANOPARTICLES AND THEIR ELECTROCHEMICAL AND CATALYTIC APPLICATIONS

A Thesis Submitted to Gauhati University for the Award of Degree of Doctor of Philosophy in Chemistry
(Faculty of Science)

By
Subrat Jyoti Borah
Department of Chemistry
Gauhati University, Guwahati-781014
Assam, India, August-2017

UNIVERSITY OF GAUHATI
Department of Chemistry
Guwahati-781014, Assam, India

Dr. Diganta Kumar Das, Ph.D
Professor

Mobile: (+91) 9864273744
E.Mail-digantakdas@gmail.com
diganta_chem@gauhati.ac.in
Tel: +91-0361-2570535
Fax: +91-0361-2570311

CERTIFICATE

This is to certify that the work described in the thesis entitled **"Synthesis of supported metal nanoparticles and their electrochemical and catalytic applications"** was carried out by **Subrat Jyoti Borah** in the Department of Chemistry, Gauhati University, Guwahati, under my guidance and supervision. He has fulfilled all the requirements under Ph.D. rules and regulations for submitting the thesis for the award of Ph.D. degree. The results embodied in the thesis are his own-investigations and no part of the thesis is submitted to any other university or institution for the award of any other degree.

Date: **(Dr. Diganta Kumar Das)**

DECLARATION

      The thesis entitled **"Synthesis of supported metal nanoparticles and their electrochemical and catalytic applications"** for the award of degree of Doctor of Philosophy in Chemistry, is a presentation of my original research work which has been carried out under the guidance of **Dr. Diganta Kumar Das**, Professor, Department of Chemistry, Gauhati University, Guwahati, Assam, India. I would like to declare that the research work included in the thesis has not been submitted to any other university or institution for the award of any other degree.

Date: **(Subrat Jyoti Borah)**

GAUHATI UNIVERSITY

Gopinath Bordoloi Nagar
Guwahati – 781014

Certificate

This is to certify that ...Subrat Jyoti Borah... bearing Enrollment number **Chem-10/14** year ...2014... is a bona fide Ph. D. student enrolled in the Department of ...Chemistry... under Faculty of ...Science..., Gauhati University, for the session (...2014...).

He/She has successfully completed Ph. D. Course work as partial fulfillment of Doctor of Philosophy (Ph. D.).

His/Her performance in the Course work is as follows :

Course Number	Course Name	Grade
	Ph.D. course work, 2014	B

Binchi Kr. Das
Dean FRC/HOD
Date : 9/7/2015

মৰবী অধ্যাপক
রসায়নিজ্ঞান বিভাগ, গুৱাহাটী বিশ্ববিদ্যালয়
Prof. & Head
Chemistry Department, Gauhati University

(Academic Registrar)
Academic Registrar
Gauhati University
Gauhati-781014 (Assam)
Gauhati University

Acknowledgement

---

am also thankful to Pallab Da, Kokil Da, Dipanka Da, Bibek Da, Prabhash Da, Jyotish Da, Binod Da, Rajesh Da, Dibya Da, Pranjal Da, Rupjyoti Da, Barhai Da, Bulbul Da, Manash Da, Arup Da, Krishna Da, Naba Da, Monjit Da, Ali Da, Trinayan Da, Dipankar, Papuli, Tina, Rit, Moumon, Momi ba, Sumi Baido, Suna Bou, Sujit Bhindo and Dada for their support and encouragement.

I gratefully acknowledge to all my teachers of 4-No Ward L.P. School Jorhat, Jorhat Govt Boys' H.S. School, J. B. College Jorhat and Gauhati University, Guwahati for whom what I am today.

I am grateful to NRL management for allowing me to carry out the Ph.D. work. I convey my sincere thanks to all the members of Quality Management Centre, NRL for their constant encouragement throughout the journey of my research work.

I extend my gratitude and love to my Parents, my wife Pompy who were always there to support and inspire me and suffered personal sacrifices to make me competent enough to carry out my Ph.D. work. Finally, I express my gratitude to all my family members for their immense moral support and affection which inspired me to have this goal.

Date: **(Subrat Jyoti Borah)**

Place: Guwahati

Contents   Pages

Abbreviations

AA	Ascorbic acid
BET	Brunauer-Emmett-Teller
BJH	Barrett-Joyner-Halenda
C-C	Carbon-Carbon
$CDCl_3$	Deuterated chloroform
CV	Cyclic voltammetry
δ	Chemical Shift in NMR
d	Doublet
DA	Dopamine
DCM	Dichloromethane
DMSO	Dimethylsulfoxide
fcc	Face centered cubic
FT-IR	Fourier Transform Infra-Red
g	Gram
GC	Gas chromatography
h	Hour
J	Coupling constant
mg	Miligram
min	Minute
mL	Mililitre
mmol	Milimole
Modified mmt	Modified Montmorillonite
MRC	Magnetically Recoverable Catalyst
nm	Nanometer
^{o}C	Degree centigrade
ppm	parts per million
PVP	Polyvinylpyrrolidone
RE	Reference Electrode

R. T.	Room Temperature
s	Singlet
SAED	Selected area electron diffraction
SPR	Surface Plasmon Resonance
SWV	Square Wave Voltammetry
t	Triplet
UV	Ultra violet
WE	Working Electrode
XRD	X-ray diffraction

In this thesis, syntheses of supported metal and metal oxide nanoparticles have been reported. The synthesized nanoparticles are utilized as electrode modifying agents to develop voltammetric sensors for some biologically active compounds and as heterogeneous catalysts for various organic transformations. The main outcomes of the research work are listed below.

(1) Modified montmorillonite shows catalytic activity for the synthesis of different benzimidazole derivatives under mild reaction condition.

(2) The silver nanoparticles supported on modified montmorillonite serve as efficient heterogeneous catalysts for the synthesis of different propargylamines and Baeyer-Villiger oxidation of cyclic and aromatic ketones.

(3) The clay supported Fe_3O_4 nanoparticles are used to develop voltammetric sensor for dopamine and ascorbic acid. The Fe_3O_4 nanoparticles also show efficient magnetically recoverable catalysts for the synthesis different dihydropyrimidinones via the Biginelli reaction.

(4) The clay supported Cu^0-nanoparticles are evaluated as heterogeneous catalytic precursor for the synthesis of different thiourea based dihydropyrimidinones and as electrode modifying agents for voltammetric determination of dopamine and ascorbic acid.

Abstract

Chapter 1: Introduction and Experimental

This chapter gives an overview of nanoscience and nanotechnology. It explains the basic concept, history, properties and types of nanomaterials, importance of nanoscience and nanotechnology. The various synthetic routes and applications of metal nanoparticles are also described here. It also describes the different experimental procedure, materials / reagents used and various experimental techniques with principles adopted in the research work. The aims and objectives of the work are also highlighted in this chapter.

Chapter 2: Modified Montmorillonite and Application

This chapter discusses modification of montmorillonite K10 by acid treatment to develop a high surface area and porous matrix and its characterizations by different analytical techniques. It also discusses the application of the modified clay as catalyst for the synthesis of different benzimidazoles.

Chapter 3: Silver Nanoparticles and Applications

This chapter contains description of synthesis, characterization and catalytic activities of silver nanoparticles supported on modified montmorillonite. The silver nanoparticles of sizes below 10 nm were prepared by reduction of $AgNO_3$ impregnated on modified montmorillonite. The reduction was carried out by adding $NaBH_4$ to the aqueous dispersion $AgNO_3$-montmorillonite clay composite. The characterization of modifed montmorillonite clay supported silver nanoparticles (Ag-NPs@mmt) by standard analytical techniques like UV-Visible spectroscopy, powder XRD, N2 adsorption-desorption, SEM-EDX and TEM analysis. The application of the synthesized silver nanoparticles as heterogeneous catalyst has been demonstrated for the one-pot three components coupling of aldehyde, amine and alkyne to synthesize propargylamine. The silver nanoparticles also found to be as active catalyst for the Baeyer-Villiger oxidation of cyclic and aromatic ketones.

Chapter 4: Fe$_3$O$_4$ Nanoparticles and Applications

This chapter discusses synthesis of Fe$_3$O$_4$ nanoparticles using both modified and unmodified montmorillonite as support material and their characterization by different analytical techniques such as powder XRD, N$_2$ adsorption-desorption, TEM and XPS analysis. It describes the application of the synthesized Fe$_3$O$_4$ nanoparticles supported on unmodified clay in the development of voltammetric sensor for dopamine and ascorbic acid. The modified clay supported Fe$_3$O$_4$ nanoparticles also found to be an efficient magnetically recoverable heterogeneous catalyst for synthesis of different dihydropyrimidinones via the Biginelli reaction. The recyclability of the recovered catalyst for several run has been demonstrated.

Chapter 5: Cu^0-Nanoparticles and Applications

In this chapter, we report generation of Cu^0-nanoparticles into the pores of both modified and unmodified montmorillonite as stabilizer. The Cu^0-nanoparticles were generated by impregnation of CuCl$_2$ on montmorillonite followed by reduction with NaBH$_4$. Powder XRD, N$_2$ adsorption-desorption and TEM etc. analysis were carried out to characterize the synthesized nanoparticles. It also describes the use of unmodified clay supported Cu^0-nanoparticles as electrode modifying agents for selective voltammetric determination of dopamine and ascorbic acid. The use of Cu^0-nanoparticles supported on modified montmorillonite as heterogeneous catalyst has also been described for the synthesis of different thiourea based dihydropyrimidinones under mild reaction condition.

List of Publications

(A) Articles Published / Submitted in Journals:

(1) Modified montmorillonite clay stabilized silver nanoparticles: An active heterogeneous catalytic system for the synthesis of propargylamines, Subrat Jyoti Borah, Diganta Kumar Das, *Catal. Lett. 146*, 657-666 **(2016)**.

(2) Fe_3O_4 nanoparticles stabilized on mmt: An efficient magnetically recoverable catalyst for the synthesis of dihydropyrimidinones, Subrat Jyoti Borah, Diganta Kumar Das, *J. Chem. Pharm. Res. 8(7)*, 347-356 **(2016)**.

(3) Montmorillonite clay supported copper nanoparticles: An efficient electrode modifying agent for voltammetric determination of dopamine and ascorbic acid, Subrat Jyoti Borah, Diganta Kumar Das (Communicated).

(4) Efficient Baeyer-Villiger oxidation catalysed by Silver Nanoparticles stabilized on modified montmorillonite, Subrat Jyoti Borah, Diganta Kumar Das (Communicated).

(B) Abstract of the paper published in Conference / Seminar / symposium:

(1) Fe_3O_4 nanoparticles stabilized on K-10 clay: An active and magnetically recoverable catalyst for the three component coupling reaction, Subrat Jyoti Borah, Diganta Kumar Das, "International Conference on Harnessing Natural Resources for Sustainable Development: Global Trends" held at Cotton College, Guwahati from 29th -31st January, 2014 (PP32).

(2) Cu^0-nanocomposite film on Gold electrode: An efficient voltammetric sensor for dopamine and ascorbic acid, Subrat Jyoti Borah, Diganta Kumar Das, "National Seminar on Recent Trends in Fundamental and Applied Chemical Sciences" held at Dibrugarh University from 19th to 21st November, 2014 (PP78).

(3) Fe_3O_4 nanocomposite@Platinum electrode: An efficient voltametric sensor for Dopamine and Ascorbic acid, Subrat Jyoti Borah, Diganta Kumar Das, "An International

Symposium on Recent Advances in Chemistry" held at NEHU, Shillong from 3rd to 5th March, 2015 (PP89).

(4) Modified montmorillonite clay stabilized silver nanoparticles: An active heterogeneous catalytic system for the synthesis of propargylamines, Subrat Jyoti Borah, Diganta Kumar Das, "UGC-SAP National Seminar on Emerging Trends in Chemical Sciences-2015" held at Department of Chemistry, Gauhati University from 5th to 6th November, 2015 (PP34)**.**

Chapter-1

Introduction and Experimental

1. Introduction

1.1. Overview

Nanoscience and nanotechnology arouse considerable interest in the recent time and has become one of the most important and exciting forefront area of research because of their wide range of applications in the field of catalysis, sensors, electronics, medicine, bio-sciences, drug delivery, opto-electronics, abatement of pollution etc. [1-3]. 'Nanoscience' is now at the cutting edge of science. It is highly multidisciplinary and deals with all branches of science. Nanoscience and nanotechnology is based on the concept that the particles of any materials with 0-100 nanometer (nm) in size impart new and novel properties and behaviour. Such nanoparticles exhibit improved physico-chemical properties, phenomena and processes which are correspond neither to those of free atoms or molecules making up the particles nor to those of bulk solids with same chemical composition. Nanotechnology involves the use of nanomaterials in various areas such as chemical and textiles industries, sensors, catalysis, biotechnology, electronics, medicine to provide better and improved technologies to the society [1-4]. Nanoparticles are characterized by a large value of the surface to volume ratio, which signifies that a large fraction of the atoms are exposed on the surface and can be involved in surface activities like catalysis [4-5]. As the size of the particle increases, the number of atoms on the surface will decrease. Thus, the overall performance of nanomaterials is dependent on shape, size and the textural parameters of the particles along with the stabilizer/support used for the synthesis of nanoparticles [6-7]. Different type of support materials such as polymers, organic ligands, mesoporous materials, activated carbon, metal oxides etc. have been used to stabilize metal nanoparticles. Therefore, there is great scope to develop supported metal and metal oxide nanoparticles and their applications in various fields.

1.2. Meaning of Nanoscience and Nanotechnology

The term nanoscience itself is a combination of two words i.e. nano from the Greek 'nanos' meaning 'Dwarf' (extremely small) and the word science. The word

'nano' refers to the numerical value 10^{-9} and its placement on the metric scale (1 nm = 10^{-9} m) clearly demonstrated the size of the nanoparticles. As a comparison, a single human hair is about 100000 nm thick. In general, Nanoscience is the study of properties of structures of various objects whose size is less than 100 nm. Any objects whose lateral dimensions fall within 100 nm are referred as 'Nanoparticles'. The above classification is somewhat arbitrary but it is widely established in scientific literature. The term Nanotechnology refers the techniques for research and technological development such as developing, manufacturing and designing these nanomaterials along with their applications in different fields of science.

1.3. History of Nanoscience

Although the concept of Nanoscience and Nanotechnology is very recent, it was practiced for different purposes in ancient time. In the Middle Ages, metal nanoparticles in the form of colloids, were used by man to dye fabrics, ornamental decoration, color glass etc. In 17th century, Andreus Cassius discovered *purple of cassius*. It was a coated gold colloid used a pigment in glass and chinaware. The windows of Medieval Cathedrals (Fig. 1.1) are one of the outstanding examples where the beautiful colors on the windows are due the presence of metal nanoparticles in the glass [1, 8]. In 18th century, nanoparticles of silver were used in photography [1].

Fig.1.1. Windows of Medieval Cathedrals.

The best example to explain nanoscience is nature where numerous examples of nanotechnology-based system already exist. Some of the examples are, in photosynthesis, the chloroplasts that convert light and carbon dioxide into biochemical energy; contain nanoscale molecular machinery arranged inside the stacked structures. Geckos, a lizard, can climb walls and hang from ceilings with a single toe by using millions of its nano toe pads [1,9]. Animal cells are another example of busy multifunctional nano-systems. Animal cells are very tiny i.e. a few nanometers in size. They can store information, move around, capable of replicating themselves and also manufacture various substances requires by the organism.

Michael Faraday was the first person who gave the systematic properties of colloidal metal. Faraday recognized the connection between the color and the size of the particles and explained the mechanism of formation colloidal gold particles from chloroaurate $[AuCl_4]^-$ solutions using phosphorus as reducing agent [8c]. The systematic study and description of nanoparticles was first established scientifically with colloidal chemistry at the beginning of 19th century. Besides Faraday, the other pioneers were Thomas Graham, Marian Smoluchowsky, Richard Zsigmondy, Wilhelm, and Wolfgang Ostwald [6b]. The widespread interest of modern nanoscience and its applications was begun after the visionary lecture by the famous Physicist Richard P. Feynman in 1959 at the annual meeting of American Physical Society held at The California Institute of Technology, USA. Feynman in his lecture described the future possibility of nanosized devises and related technologies by the vision, '*There's Plenty of Room at the Bottom*'. He also predicted that 'It would be possible to put the 24 volumes of Encyclopedia Britannica on the head of a pin'.

The particles with nano dimension cannot be seen with naked eye or even with a powerful optical microscope. Thus in early nineteenth century, the development of nanoscience was in an infant stage due to the lack of sophisticated imaging instrument. But its development has been enabled after the invention of electron microscopy and its imaging technique in the nano scale. These are scanning electron microscope (SEM), transmission electron microscope (TEM), atomic force microscope (AFM) and scanning

tunneling microscope (STM). The invention of these instruments practically opened the doors of modern nanoworld.

1.4. Properties of nanoparticles

Nanoparticles show different properties and behaviour from that of bulk materials. Some of the physical properties such as color, conductivity, melting point of bulk material changes in when it is transformed to nanoparticles. The properties which are responsible for these changes are described below.

1.4.1. Surface dependent properties

The most important factor which is responsible changing the properties of nanoparticles is the surface to volume ratio. In case of bulk solids, change of size does not change the property to large extent. These properties only become dominant in case of nanoparticles due to their high surface to volume ratio. For example, a particle with 1 nm size, which consists of about 13 numbers of atoms, has approximately 92% of atoms exposed on the surface [Fig. 1.2]. Thus, a large fraction of the atoms are exposed on the surface due to which nanoparticles exhibited special properties such as higher surface conductivity, chemical reactivity etc [1a]. The number of particles on the surface will decrease with increase in particle size.

| Number of atoms | 13 | 55 | 147 | 309 |
| Atoms on the surface | 92 % | 76 % | 62 % | 52 % |
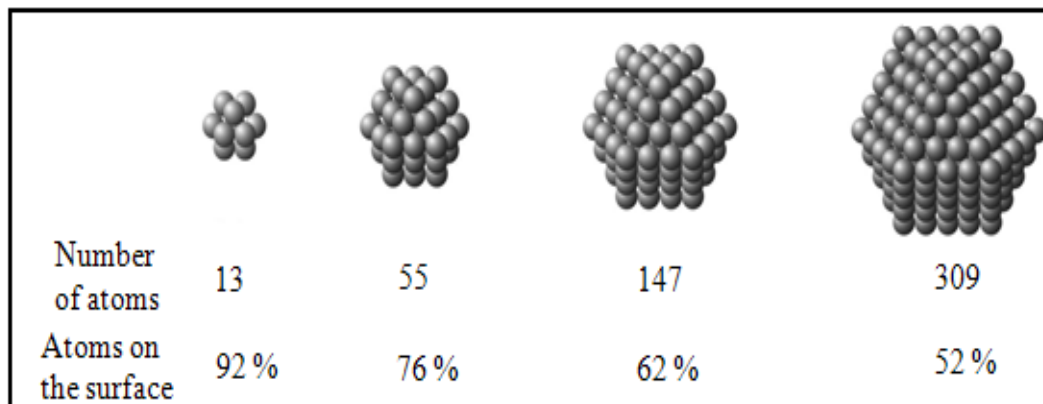
Fig. 1.2. Magic number cluster and surface atoms (%).

1.4.2. Size dependent properties

Most of the properties of nanoparticles are directly related to their size. For example, bulk gold melts at $1064^{o}C$, whereas gold nanoparticles with less than 2 nm size melt at about $500-600^{o}C$. The melting point of nanoparticles decreases dramatically with decrease in size. Again, gold is inert in bulk form while nanoparticles of gold show catalytic properties [9-10]. The color of the colloidal solution of metal nanoparticles also changes with change in particle size.

1.4.3. Quantum effect

Nanoparticles with particle size below 2 nm are known as quantum dots due to the quantum confinement of the electrons [11]. When the electronic structure of nanoparticles is influenced directly by the size, it is called size dependent quantum effect. This effect is due to the transition of an atom or molecule with defined energy levels to the dispersed bands of collective assembly of atoms. The size dependent color and shift in the plasmon resonance of gold nanoparticles are the examples of quantum effects [11].

1.4.4. Surface Plasmon Resonance (SPR)

Surface Plasmon Resonance (SPR) is an optical phenomenon where an interaction occurs between an electromagnetic wave and the free electrons within the conduction band in some metal. The electron cloud of the nanoparticles undergoes oscillation by the interaction of electric field component of incident light. Then the electron density in the particle is polarized to one surface and oscillates in resonance with the frequency of incident light causing a standing oscillation. This condition is found to depend on size, shape and the dielectric constant of both the metal and surrounding medium and is determined by absorption and scattering spectroscopy [10]. For example, silver nanoparticles show an SPR peak at about 400 nm.

1.5. Types of nanomaterials

There are various types of nanomaterials. Depending on the nature, dimension, shape and crystalline properties, nanomaterials are classified into following groups.

1.5.1. Carbon based nanomaterials

The carbon based nanomaterials are generally composed of carbon in the form of hollow spheres, ellipsoids or tubes. The spherical and ellipsoidal forms of carbon based nanomaterials are called fullerenes while the cylindrical types are known as carbon nanotube. These nanotubes belong to the fullerene family and they are stronger than steel wires, can conduct higher electricity and can bear weight million times more than their own weight [1c]. The two dimensional nanomaterials graphene consists of layers of carbon arranged in six-member ring and it becomes a hot topic of research in recent years. It has some special properties and used make different sensors, electrochemical devices etc. [12].

1.5.2. Metal based nanomaterials

The metal based nanomaterials are quantum dots (e.g. CdSe, CdS etc.), metal nanoparticles (e.g. Cu, Ag, Au, Ni etc.) and metal oxide nanoparticles (e.g. TiO_2, ZrO, Fe_3O_4 etc.). The quantum dots are closely packed semiconductor nanoparticles with particles size below 2 nm and are significant for optical application due to their high extinction co-efficient [5b]. Metal and metal oxide nanoparticles find their application various field such as catalysis, sensor, biosciences, electronics etc. [1-6].

1.5.3. Dendrimers

Dendrimers are spherical polymeric molecules with numerous chain ends on their surface. These chain ends can be tailored to carry out specific chemical functions such as catalysis. In addition to that, dendrimers can also act as nanoscale carrier molecules which can be useful in drug delivery.

1.5.4. Nano-composite materials

The nano-composites are combined materials with one or more dimension in the nano range [6b]. Some of the examples are clay, zeolite, polymeric materials, graphite etc. Out of various nano-composite materials, clay is relatively cheap and widely available materials for commercial use. Due to high thermal and mechanical properties, clays are being used in various products ranging from car parts to packaging materials.

1.6. Synthesis of nanoparticles

There are various synthetic techniques for obtaining nanoparticles or nanomaterials by physical and chemical methods. Generally, two approaches namely 'top-down' and 'bottom-up' are used for the synthesis of nanoparticles. In 'top-down' approach, nanoparticles are made from large objects by means of mechanical force like grinding, milling etc. Photolithography, electron beam lithography etc. are some techniques used in 'top-down' approach. But the disadvantage of this approach is the imperfection of the morphology of the nanostructure. In 'bottom-up' approach nanoparticles are constructed from atom or molecular level using the principles of molecular recognition and self assembly. This includes chemical procedure, sol-gel technique, thermal decomposition techniques etc. This approach gives nanomaterials with less defects and more homogeneous chemical composition.

Among the various nanomaterials, metal and metal oxide nanoparticles get special attention because of their unique properties and applications in different fields like sensor, catalysis, electronics, biology etc. Although, various techniques are developed for the construction of nanomaterials, still there is a scope for improvement in the methodologies employed for this purpose [13]. Some of the general chemical routs for the preparation of metal nanoparticles are described below.

1.6.1. Wet chemical reduction of metal salts

The first reproducible synthesis of metal nanoparticles by wet chemical reduction was done by Turkevich and his coworkers. They synthesized a stable deep red dispersion Au^0-nanoparticles using sodium citrate as both reductant and stabilizer and also proposed a mechanism for the formation of nanopartilces [8c]. This method is now become the most common method for synthesis of metal nanoparticles. Schematically, it can be represented by the following equation.

$$xM^{n+} + nxe^- + \text{stabilizer} \longrightarrow nM^o \text{ (cluster)}$$
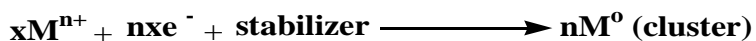
Here, the reducing agent (e.g. hydrogen, hydrazine etc.) is added to the metal salt precursor in presence of stabilizing agent such as ligands, porous materials etc. The stabilizers/supports prevent undesired agglomeration and help in the formation of well-dispersed nanoparticles. The size, shape and morphology of the metal nanoparticles depend on many factors such as type of reducing agent used, metal salt precursor, concentration, temperature, solvent and reaction time.

1.6.2. Sol-gel technique

The sol-gel technique is a wet-chemical process which uses either a chemical solution or colloidal particles to produce an integrated network (gel). Typical precursors are metal alkoxides and metal chlorides which undergo hydrolysis and polycondensation reaction to form colloidal nanoparticles. On evaporation, a continuous inorganic framework with a liquid phase (gel) is obtained. The metal centers get connected with oxo (M-O-M) or hydroxo (M-OH-M) bridges and generate metal-oxo or metal-hydroxo polymers in solution. The liquid phase is removed from the gel by drying. After that, a thermal treatment such as calcination may be performed to enhance the mechanical properties [14].

1.6.3. Impregnation

This technique involves wetting of the solid support with a solution of the metal precursor. In this process, the metal precursor which is used for the synthesis of nanoparticles is dissolved in the minimum quantity of solvent. The solution obtain is then added to the support material and the metal precursor fills the pores of the support so that a thick paste is formed. The solvent is removed in rotary evaporator to get the solid mass. It is then dried in an oven and finally calcined or reduced by appropriate reducing agents to the metal nanoparticles [15]. This methodology gives dispersed nanoparticles depending on the metal, nature of support and amount of loading.

1.6.4. Co-precipitation technique

This method involves the instantaneous precipitation of both the metal and the support. This results in the incorporation of metal nanoparticles into the porous structure

of support material [16]. Bao and coworkers reported a co-precipitation approach for the synthesis supported silver nanoparticles on silica [16b]. The synthetic route consisted of capping of Ag^+ ions in solution with dodecylamine, followed by reduction to Ag (0) using formaldehyde and then tetraethyl orthosilicate (TEOS) was added as silica source to get the eventual self assembly of the material.

1.6.5. Precipitation-deposition technique

The precipitation-deposition technique involves dissolution of the metal salt precursor followed by pH adjustment to alkaline medium to get complete precipitation of metal hydroxide (e.g. $Au(OH)_3$), which is deposited on the surface of the support [17]. The hydroxide obtained is finally calcined and reduced to the elemental metal. The nanoparticles obtained by this method generally give broad particle size distribution due to poor control of the nanoparticles size.

1.6.6. Microemulsion

Microemulsion is thermodynamically stable, homogeneous like combination of water, oil and surfactant [18]. In this process, the principle of formation of reverse micelles was used as an alternative for the preparation of metal nanoparticles. The support material used for stabilization of metal nanoparticles is first impregnated with a Microemulsion containing the dissolved metal salt precursor. Then microemulsion-support interactions occur and finally it is reduced by suitable reducing agent. During the process, the microemulsion-support interactions can be boosted by increasing the hydrophobicity of the support material (e.g. silylation of hydroxy-rich surfaces) and make it chemically well-suited with the emulsion during the deposition step [18].

1.6.7. Thermal decomposition

In this process, nanoparticles of various metals are prepared by thermal decomposition of metal surfactant complexes and organometallic compounds in hot surfactant solutions [19a]. Traditional thermal decomposition of metal salts without any stabilizer results nanoparticles broad size distributions. But the same process gave highly improved results when the thermolysis was carried out in presence of some stabilizing

polymers such as PVP (polyvinylpyrrolidone). Lacante's group has reported synthesis of Ru, Rh and Co nanoparticles from their organometallic precursors by this technique [19b].

1.7. Support / Stabilizer for the synthesis of metal nanoparticles

Naked nanoparticles are thermodynamically and kinetically unstable, highly reactive and tend to aggregate once they formed. It is due to the fact that most of the atoms in nanoparticles are remained in the surface which makes them highly reactive. Thus, to control the shape and size of metal nanoparticles, some stabilizers or supporting materials are required. The main role of stabilizers or supports is to prevent particle aggregation and control of particle size. There are three conventional mechanisms for stabilization of metal nanoparticles. The mechanisms are electrostatic, steric and combination of both. In electrostatic stabilization, cations and anions from the starting material remain in solution and associate with the nanoparticles by an electrical double layer. This develops a Coulombic repulsion which prevents the aggregation of nanoparticles. In the second one i.e. steric stabilization, particle aggregation is prevented by the adsorption of large molecules such as polymers, surfactants etc. The third option i.e. combination of both electrostatic and steric stabilization is called electrosteric stabilization. Depositing nanoparticles on porous support material is one of the best techniques for stabilization as it prevents the particle growth upto the size of the pores. Some of the important supports / stabilizers used for nanoparticles stabilization are discussed below.

1.7.1. Organic ligands

The use of organic ligand as stabilizer for the synthesis of nanoparticles is of particular interest as it can form metal nanoparticles with small size, narrow size distributions and high thermal stability [20a]. Depending on the basis of donor site affinity and structural suitability, ligands are selected for stabilization of metal nanoparticles. Different types of ligands like amines, phosphines, thiols etc. have been widely used for stabilization of metal nanoparticles [20]. The biphasic (liquid-liquid)

procedure has also been used for stabilization of metal nanoparticles in organic solvent using various ligands. One of the advantages of the biphasic method is that the nanoparticles can be separated as solid mass and can be directly used for further applications.

1.7.2. Polymers

Polymers are one of the most extensively employed stabilizers for nanoparticles synthesis due to their easy availability, high stability, low cost and excellent resistance to particle aggregation. The size and shape of the metal nanoparticles can be controlled by adjusting the concentration, chain length and functionality on the polymer chain. For example, polyvinylpyrrolidone (PVP) is used for synthesis of small size Ru^0 nanoparticles [21a], poly(methylphenylphosphazene) (PMPP) is used to stabilize Au^0 nanoparticles [21b]. Recently, biopolymers such as cellulose, starch have also been utilized for preparation and stabilization of metal nanoparticles [21c].

1.7.3. Porous materials

The porous materials are generally solid substances having pores (voids) in their interconnected network. Natural substances such as rocks, clays and synthetic materials like metal oxide, ceramics, carbonaceous materials etc. are the examples of porous materials. These materials are characterized by their porosity (macro, meso and micro porosity) and their textural properties, which in turn depend on their constituents. The porous materials can be advantageously used as supports for the synthesis of metal nanoparticles. Furthermore, it is possible to tune the textural properties of the porous supports by different techniques which help to control the shape and size of metal nanoparticles [22a]. A few examples of porous materials are described below.

1.7.3.1. Carbon based materials

Carbon based materials acquires great attention in recent time due to their well-defined porosities and high surface area and ease of modification of their surfaces. For example, charcoal is a commercially available carbon based material used as a support for the synthesis of metal nanoparticles [23a]. Activated carbon is another example of

carbon based material that can be used as a support for nanoparticles synthesis. The surfaces of these materials can also be modified to improve their surface area and porosity. Recently, Budrain and coworkers have reported synthesis of various metal nanoparticles using carbonized starch as support material [23b].

1.7.3.2. Metal oxides

Metal oxides are generally thermally and chemically stable, have well-developed porous structure with high surface areas, which make them attractive to use as a support for the synthesis of nanoparticles. Metal oxides can be further functionalized for their value addition to use as catalyst or support. Various metal oxides such as Mg, Al, Ti, Si, Ce and Zr oxides are widely used as support materials for preparation of various metal nanoparticles [22, 24]. Kantam and coworkers have recently reported nanocrystalline magnesium oxide as support for gold nanoparticles and its application as heterogeneous catalyst in three component coupling reaction [25a]. The use of metal oxides with magnetic property such as Fe_3O_4 have recently attained great attention as catalyst and support for nanoparticles due to the improve separation capabilities [25b]. The most important property such support is that the materials can be easily recovered magnetically and reused several times for further applications.

1.7.3.3. Clay minerals

Environmentally benign, efficient, economical and green synthesis of nanoparticles and the use of environmental friendly materials have now become more important to address industrial and environmental concern [26]. Thus, there has been increasing demand to use cheap and environmental friendly supports for the stabilization of metal nanoparticles. Clay minerals are one of the best examples, as it is environmentally benign, cheap and abundant in nature. They possess high surface area with absorptive and ion-exchange properties which have been advantageously used for various applications such as catalysis [27]. Clay minerals are crystalline materials of layered silicates with particle size ranging from 150 to less than 1 micron. There are two basic building blocks in clay minerals which are common to all clay minerals. The

building blocks are tetrahedral silicates and octahedral aluminate layers. The classifications of different clay minerals are represented in Table 1.1.

Among the various clay minerals, Montmorillonite clay is the most widely studied clay of the smectite group [27-28]. It is a hydrated 2:1 layered aluminosilicate of the smectite group and composed of two tetrahedral silicate sheets, which are bonded to either side of an octahedral aluminate sheet. Isomorphous substitution of Si^{4+} and Al^{3+} by lower valence cations such as Mg^{2+} results in charge imbalance in the clay structure. It is balanced by hydrated exchangeable cations which occupy the position between clay layers. The montmorillonite clay structure is pictorially is shown in Fig. 1.3.

Table 1.1. Classification of clay minerals.

Type*	Name of the group	Common species
1 : 1	Kaolinite and Serpentine	Kaolinite, Halloysite, Chrysotile
2 : 1	Micas	Illite
	Vermiculite	Vermiculite
	Smectite	Montmorillonite, Beidellite, Nontronite, Saponite
	Pyrophyllite and Talc	Pyrophyllite, Talc
2 : 1 : 1	Chlorite	Donbassite
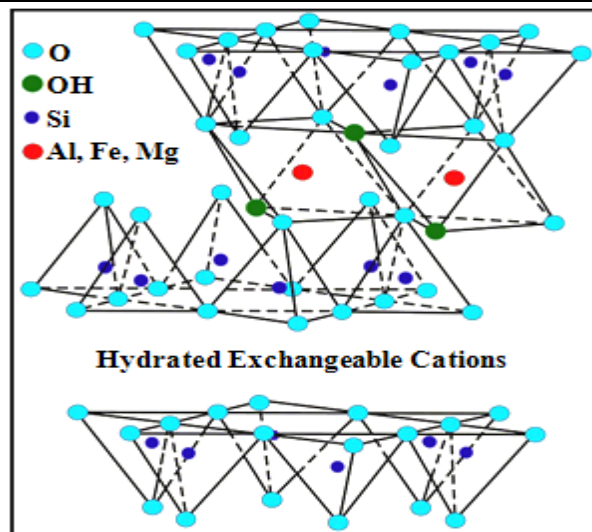
Fig. 1.3. Montmorillonite clay structure.

The modified montmorillonite clay has attracted much attention of the chemists because of their large applications in various catalytic reactions [29]. Montmorillonite clay can be modified by treatment with mineral acid under controlled conditions to give partially delaminated clay with higher surface area and contain micro and mesopores with diameters 0-10 nm. This highly porous material can be advantageously used as a support for generation of metal nanoparticles. The specific surface area, pore volume and pore diameter of the clay can also be varied by controlling the acid treatment in the clay modification process.

1.8. Applications of supported metal nanoparticles

The supported metal nanoparticles have found wide range of applications in various fields such as catalysis, biology, electrochemical sensor and electronics etc. Herein, we highlighted some catalytic and electrochemical applications of supported Ag^0, Cu^0 and Fe_3O_4 nanoparticles.

1.8.1. Catalytic applications of Ag^0, Cu^0 and Fe_3O_4 nanoparticles

Silver nanoparticles have become increasingly popular in catalysis. In homogeneous system, silver metal complexes have been used for various important reactions such as carbon-carbon coupling reaction, oxidation reaction, dehydrogenation reaction etc. Due to growing environmental concern, researchers have attracted for heterogeneous system of metals in catalysis. Supported silver nanoparticles have been used as active catalysts for various organic transformations like three component coupling reaction, rearrangement reaction, cycloaddition reaction, oxidation reaction etc [30-31]. The advantage of using these heterogeneous nanocatalysts is that they require only mild reaction conditions to produce high yields of products in short reaction times and their easy recyclability for further use [26].

Supported Cu^0-nanoparticles have been prepared in various supports and used for different catalytic reactions. The reactions catalyzed by supported Cu^0-nanoparticles provide the advantage of high atom efficiency, simplified isolation of product, easy

recovery and recyclability of the catalyst. Copper nanoparticles supported on Al_2O_3 have been used for the reduction of NO [32a]. Copper nanoparticles stabilized on different supports have been used as active catalysts for the synthesis of 1,2,3-triazole by coupling of various alkyl azide and terminal alkynes [32b]. Like Cu^0-nanoparticles, CuO nanoparticles also show catalytic activity for various organic transformations. Supported copper and copper oxide (CuO) nanoparticles have been used as catalysts in a number of reaction such as three component coupling reaction, C-N cross coupling, alcohol oxidation [33] etc.

Among the various nanostructured materials, magnetic nanoparticles like Fe_3O_4 get particular interest in catalysis due to the facile isolation of product and catalyst by magnetic separation technique and easy catalyst reusability. Supported Fe_3O_4 magnetic nanoparticles have been used as magnetically recoverable catalyst (MRC) for various organic syntheses like synthesis of propargylamines, Baeyer-Villiger oxidation, condensation reactions, Sonagashira-Hagihara reaction etc. [34-35]. Besides, Fe_3O_4 nanoparticles are also used as a support material for preparation of nanocatalysts of other metal like copper, nickel, palladium, platinum etc. to get the advantage of magnetic separation.

1.8.2. Electrochemical applications of Cu^0 and Fe_3O_4 nanoparticles

Metal nanoparticles with different properties have found various applications in analytical chemistry [36a]. The utilization of metal nanoparticles to construct novel and improved sensing devices such as electrochemical sensor is a great challenge for the researchers. An electrochemical sensor is basically a molecular system which can detect events or make changes in its environments electrochemically into a compatible signal which can be easily read by an observer. Different nanoparticles like metal and metal oxide nanoparticles have been widely used in electrochemical sensors. The basic functions of metal nanoparticles in electrochemical sensing systems are: immobilization of target molecules, catalysis of electrochemical reactions, enhancement of electron transfer, labeling of target molecules and acting as reactant.

Copper nanoparticles prepared on various supports have been used for electrochemical sensing different molecules. For example, copper nanoparticles supported on graphene have been used for electrochemical sensing of glucose and hydrogen peroxide [36b]. Chen's group has reported graphene-copper nanocomposite as electrochemical sensor for carbohydrates [36c]. Li and co-workers have reported copper nanoparticles deposited on ITO electrode as electrochemical sensor for carbohydrates [37a]. Copper nanoparticles deposited on MWCNT-modified glassy carbon electrode have been used as electrochemical sensors for nicotine and dopamine [37b-c].

The applications of nanoparticles of non-precious metals such as iron has received great attention in recent years due to easy availability and less cost price of the metal salts and growing environmental regulations. As an example, Fe_3O_4 functionalized graphene oxide-gold nanocomposite has been used for simultaneous electrochemical determination of catechol and hydroquinone [38a]. Cao and co-workers have reported Fe_3O_4 nanoparticles as electrode materials for hydrogen peroxide electrochemical sensor [38b]. Zhang's group has reported carbon-encapsulated Fe_3O_4 nanoparticles coated glassy carbon electrode as electrochemical sensor for Pb(II) [38c]. Chitosen / Fe_3O_4 nanoparticles based screen printed electrodes have been used for electrochemical detection of short HIV sequences [38d]. Besides, Fe_3O_4 nanoparticles are also used as electrode modifying agents for electrochemical determination of other species arsenic(III), tramadol etc. [39].

1.9. Objectives of the Thesis

❖ Modification of montmorillonite K10 clay by executing controlled acid treatment to generate a high surface area and porous matrix and its catalytic application.

❖ Synthesis of metal (Ag, Cu) and metal oxide nanoparticles (Fe_3O_4) using modified montmorillonite and raw montmorillonite as support materials by following greener procedure.

❖ Evaluation of reactivities of the synthesized nanocomposites as heterogeneous catalyst precursors for various organic transformations.

❖ Utilizations of the synthesized nanocomposites as electrode modifying agents for selective voltammetric determination of dopamine and ascorbic acid.

1.10. Experimental

The chemicals/materials, their purification or modification and characterization techniques used in the course of this research work are described in this chapter. The instrument used for the characterizations are also stated in this chapter.

1.10.1. Materials

$FeCl_3$, $FeCl_2.4H_20$, $NaBH_4$, Dopamine hydrochloride were purchased from M/S Sigma Aldrich, USA. L-ascorbic acid, $NaNO_3$ were purchased from Loba Chemie, India. $CuCl_2.2H_2O$, $AgNO_3$, ethanol, ethylene glycol and NH3 solution were purchased from Merck Chemicals. Analytically pure common chemicals such as n-hexane, ethyl acetate, dichloromethane, methanol, acetonitrile, toluene etc. were purchased from Rankem Chemicals. Different aldehydes, amines, alkynes, urea, thiourea, active methylene compounds, cyclic and aromatic ketones were purchased from M/S Sigma Aldrich, USA and are used as received. The gold and platinum working electrodes were obtained from CH instruments, USA.

Montmorillonite K10 was purchased from M/S Sigma Aldrich, USA. It was purified by sedimentation technique to separate the < 2 μm Montmorillonite rich fraction.

1.10.2. Separation of < 2 μm fraction of Montmorillonite K10

The lower fraction (< 2 μm) of montmorillonite K10 clay was obtained by sedimentation technique. The aqueous suspension of the clay was allowed to settle and

different particle size fractions of the clay were separated by applying Stoke's law [40]. The mathematical representation of Stoke's law can be expressed as:

$$r = \left[\frac{9\eta h}{2(d_1 - d_2)gt} \right]^{1/2}$$

Where, r = radius of the particles to be separated

η = coefficient of viscosity of water at 25 ^{o}C

d_1 = density of the clay suspension

d_2 = density of the water

h = height

t = time

The rate of fall of particles having different size by a certain distance was calculated from Stoke's equation and the desired size fraction of the clay was separated by using this equation. The < 2 µm fraction of montmorillonite K10 was separated from a 2% aqueous suspension of the raw clay. In this process, about 20 g of clay was dispersed in 1000 mL of distilled water in a glass beaker and the suspension obtained was allowed to stand for 12 h. It was then siphoned out from the 20 cm depth of the beaker into flat trays and was allowed to dry in a hot air oven at 50°C for 15 h. The clay after drying was hand ground to get the powdered clay and kept in dry bottles.

1.10.3. Acid modification of Montmorillonite K10

The modification montmorillonite K10 was carried out with mineral acid to get a porous matrix with high surface area having micro and mesopores on the surface. Acid treatment of clay leached out octahedral alumina from the clay matrix and increased the porosity of the clay matrix [41-42]. Here, an amount of 10 g of Montmorillonite K10 (10 g) was dispersed in 200 ml 2M HCl and the mixture was refluxed for different time intervals (30 min, 1 h, 2 h and 3 h). After cooling, the supernatant liquid was discarded and the activated clay was continuously washed with deionised water till the removal of all the Cl$^-$ ions. The removal of Cl$^-$ ions was confirmed by AgNO$_3$ test. The modified

clays were dried in air oven at 50°C over for 12 h and they were named as modified mmt-I, II, III and IV with respect to refluxing time 30 min, 1, 2 and 3 h.

1.10.4. Characterization techniques and principles

1.10.4.1. CHNS Elemental analysis

CHNS elemental analysis provides the simultaneous determination of amount of C, H, N and S in organic matrices and other types of materials. Samples such as solid, liquid, viscous sample etc. can be used for CHNS analysis. This process requires high temperature combustion in an oxygen-rich environment which is generally carried out by introduction of a set volume of O_2 for a set period of time. On combustion (furnace temperature about 1000°C) carbon is converted to carbon dioxide; hydrogen to water; nitrogen to N_2 gas / oxides of nitrogen and sulphur to sulphur dioxide. The combustion products are then swept out from the combustion chamber by inert carrier gas like Helium and passed over heated copper (about 600 ^{o}C) which is situated at the base of the chamber. The main function of copper is to remove any oxygen not used in the combustion process and to convert oxides of nitrogen to N_2 gas. The results are obtained as mass percent. In this study, CHNS analysis was done by using LECO CHNS analyzer, USA. Standard reference material is used for calibration of the instrument.

1.10.4.2. FTIR spectroscopic analysis

Infrared (IR) spectroscopy deals with the study of infrared region of electromagnetic spectrum and is used to identify the structural information of a molecule or compound. This technique measures absorption of different IR frequencies by a sample positioned in the path of an IR radiation. The absorption is measured in terms of wave numbers in the range 400-4000 cm^{-1}. FTIR (Fourier Transform Infrared Spectroscopy) is an improved version of IR spectroscopic technique with superior speed and sensitivity. Instead of measuring each component frequency successively as in dispersive IR spectrophotometer, all frequencies are measured simultaneously in FTIR

spectrophotometer. The result is obtained in the form a spectrum with wave number as the x-axis and absorption intensity or percent transmittance as the y-axis. In this study, FTIR spectra were recorded in the range 400-4000 cm^{-1} using Perkin Elmer, RX-1 spectrophotometer. The medium used in this study is KBr discs.

1.10.4.3. NMR spectroscopic analysis

Nuclear magnetic resonance (NMR) is a very important spectroscopic technique to study the properties of the molecules having nuclei spin. NMR study gives detail information about the structure and chemical environment of the molecules under investigation. It occurs when nuclei of certain atoms such as ^{1}H, ^{13}C, ^{31}P etc. which have spin value are exposed to an external magnetic field. In presence of external magnetic field, the magnetically active nuclei absorb electromagnetic radiation at a frequency characteristic of the isotope i.e. energy transfer takes place at a wavelength that corresponds to radio frequencies and get excited to higher energy level. When it returns to the ground state, energy is emitted at same frequency and this signal is measured and processed to give an NMR spectrum for the concern nucleus. The energy of absorption, resonant frequency and intensity of the signal is directly related to the strength of the magnetic field. The NMR analysis results a spectrum that contains series of peaks corresponds to different applied field strength and each peak represents a set of nuclei at same magnetic environment. In this work, ^{1}H NMR and ^{13}C NMR spectra were recorded in a Bruker Ultrashield 300 spectrometer by using aprotic solvents CDCl$_3$, DMSO-d$_6$ etc. The chemical shifts are reported in δ values in parts per million (ppm) relative to tetramethylsilane (TMS) as internal standard.

1.10.4.4. Electrochemical analysis

The voltammetric electrochemical analysis were carried out in a CHI 600B electrochemical analyser (CH Instruments, USA) with a three electrode cell assembly which consisted of a working electrode, a counter electrode and a reference electrode. The working electrodes used were gold and platinum electrode, the counter electrode was platinum wire and the reference electrode was Ag/AgCl. 0.1 M NaNO$_3$ was used as

electrolyte. A schematic representation of a three electrode assembly system is shown in Fig. 1.4. In this work, square wave voltammetry technique was used for electrochemical studies.
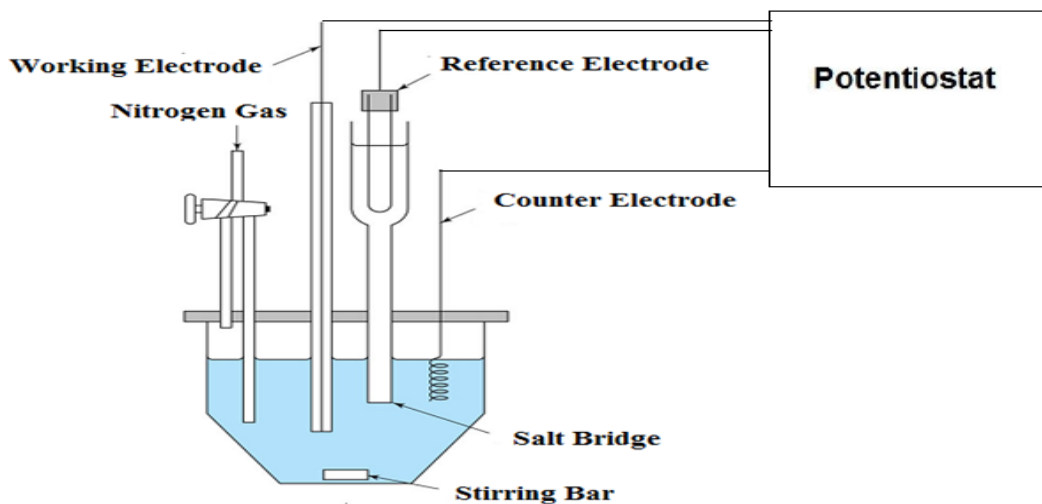

Fig. 1.4. Schematic representation of a three electrode system.

1.10.4.4.1. Square wave voltammetry (SWV)

Square wave voltammetry (SWV) is a pulse voltammetric technique which offers distinctive advantages in terms of sensitivity, speed and detection limit [43]. This technique works much faster than other electrochemical techniques, which typically run at scan rates of 1-10 mV/sec. The square wave voltammetry technique can be operated at scan rate of 1 V/sec or faster, thereby allowing much faster determinations. The oxidation or reduction of the analyte occurs at a potential at which the analyte begins to be oxidized or reduced and it is obtained as a peak or trough in the current signal. In SWV, the excitation signal consists of a symmetrical square wave pulse of amplitude Esw superimposed on staircase waveform of step height ΔE, where the forward pulse of the square wave coincides with the staircase step (pulse direction same as the scan direction) [44]. The forward pulse measures the cathodic current (i_{for}) while the reverse pulse measures the anodic current (i_{rev}) and their difference (i_{for} - i_{rev}) gives the net current which appears in the square wave voltammogram. A graphical representation for a typical potential excitation function for square wave voltammetry is given in Fig. 1.5.

22
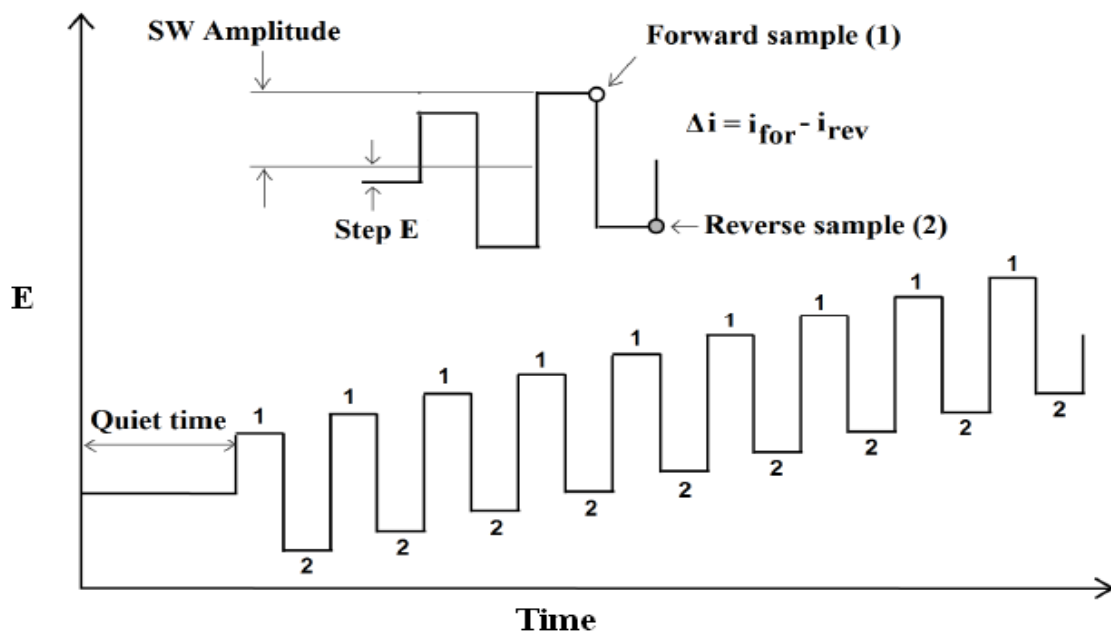
Fig. 1.5. Graphical representation for square wave potential excitation.

The peak height obtained in the voltammogram is directly proportional to the concentration of the analyte in the solution and direct detection limit as low as 10^{-8} M is possible. A typical square wave voltammetric response for a reversible redox couple is represented in Fig. 1.6.
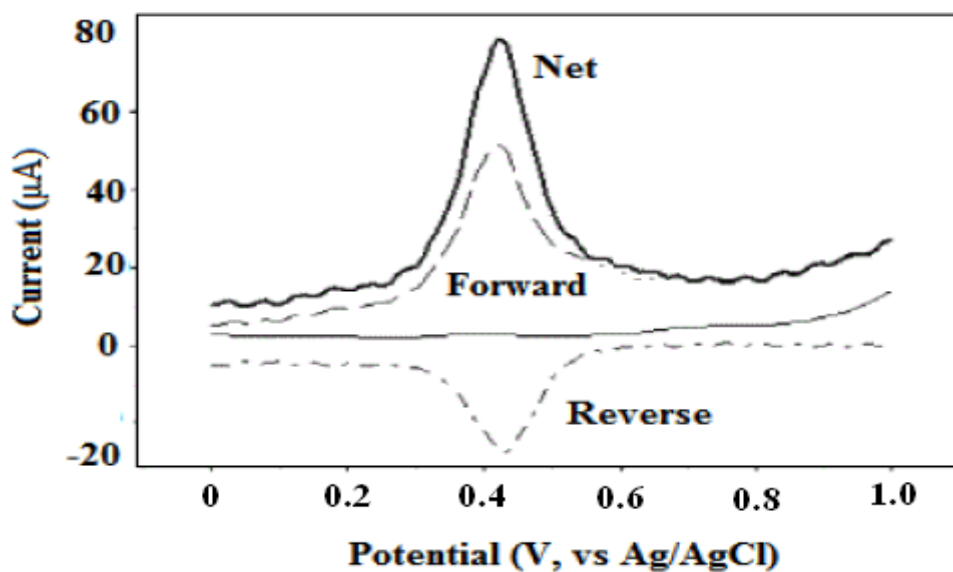

Fig. 1.6. Typical square wave voltammetric response for a reversible redox couple.

1.10.4.5. UV-Visible spectroscopy

UV-Visible spectroscopy is a very useful technique for the determination of nanoparticles formation of transition metal ions, transition metal ions and conjugated organic compounds etc. [45]. This spectroscopic technique gives the wavelength a transition and the corresponding molar extinction coefficient (ε) of the analyte under investigation. The wavelength of light that a molecule or analyte will absorb is characteristic of its chemical structure. Absorption of UV-Visible radiation results excitation of electrons in both atoms and molecules to higher energy states. The absorption is further influenced by the environmental condition of the molecule or analyte which can alter the relative energy of the ground and excited states. The result is obtained as a spectrum with wavelength (nm) of transition as x-axis and absorbance as y-axis. The absorbance is directly related to concentration of the analyte which can be obtained by Beer-Lambert law. The mathematical expression for Beer-Lambert law is-

$$A = \varepsilon c l$$

Where, A = absorbance

ε = molar absorptivity ($M^{-1}cm^{-1}$)

 l = cell path length in cm

c = molar concentration of the analyte.

In this work, UV-Visible spectra were recorded on a Shimadzu UV-1800 spectrophotometer at room temperature using aqueous dispersion.

1.10.4.6. Powder X-ray diffraction

Powder XRD is very important technique and is used to determine the crystal structure of the solids, identification of unknown materials, formation of metal nanoparticles, preferred orientation of polycrystals etc. In powder X-ray diffraction, the sample to be investigated should be homogeneous with a plane surface. So prior to investigation, non-homogeneous sample must be ground to make it uniform one and then it can be placed in sample holder to get a smooth flat surface. A collimated beam of X-rays (λ ranging from 0.7 to 2 Å) is allowed to fall on the sample and it is diffracted by the

crystalline phases present in the sample according to Bragg's Law. The Bragg's Law can be expressed as : $\lambda = 2d \sin\theta$

Where, d = spacing between atomic planes in crystalline phases

λ = X-ray wavelength

θ = scattering angle

The result is obtained as a spectrum where the intensity of diffracted X-ray is measured as a function of diffraction angle 2θ. From the diffraction pattern obtained, one can determine the crystalline phases and structural properties of the sample under investigation. In this work, powder XRD analysis were carried out on Rigaku, Ultima-IV X-ray diffractometer in the range 2-90^0 2θ at a scan rate 3^0 per min using Cu-Kα as X-ray source (λ = 1.5406 Å). The samples for powder XRD analysis were prepared as front coated packed powders in glass sample holders.

1.10.4.7. Surface area, pore diameter and pore volume analysis

The tendency of a solid surface to attract surrounding gas molecules such as N_2 gives the process known as gas sorption. It provides useful information about the characteristics of a solid substance such as surface area and pore size distribution. Prior to surface area analysis, the powdered solid substance must be freed from contaminants such as water and oils etc. So the test samples are degassed (surface cleaning) in the range of 50-250^{0}C for about 3 h under inert gas environment (e.g., helium) prior to N_2 adsorption analysis. Then small amount of N_2 gas (adsorbate) are admitted in steps into the evacuated sample chamber where they get adsorbed on the surface of every pore in the solid substance. The surface area of the sample can be calculated from the monolayer amount using Brunauer-Emmett-Teller (BET) method. In this work, surface area, average pore diameter and pore volume analysis of various samples were carried out on Autosorb-1 (Quantachrome, USA). The surface areas of the powdered samples were measured by adsorption of N_2 gas at 77 K and applying Brunauer-Emmett-Teller (BET)

calculation. Pore size distributions of the samples were determined from desorption isotherms by using the Barrett-Joyner-Halenda (BJH) method.

1.10.4.8. Scanning electron microscope (SEM) and Energy dispersive X-ray (EDX)

SEM is a high magnification microscope which uses a focused scanned electron beam to produce images of the sample. It is one of the most widely used surface characterization technique for various materials such as clay, porous materials, nanomaterials etc. It provides not only topographical information but also gives the chemical composition information of the test sample near the surface. Here, a source electron is focused into a beam with energy ranging from a few hundred to 50 KeV and it is rastered over the surface of the sample by deflection coils. A number of interactions occur when the electrons strike and penetrate the surface and this result in the emission of electrons and photons from the sample. The SEM images are obtained by collecting the emitted electrons on a cathode ray tube. The principle images obtained from SEM investigation are: secondary electron images; back scattered electron images and elemental X-ray maps. Energy dispersive X-ray (EDX) is a spectroscopic technique and is used for chemical characterization of a sample in conjunction with scanning electron microscope (SEM). The intensity of the peak obtained in EDX spectrum is directly proportional to the concentration of the corresponding element in the sample. In this work, SEM images, X-ray element mapping images and EDX of the selected samples were obtained from a Supra 35VP Carl Zeiss (Germany) instrument.

1.10.4.9. Transmission electron microscope (TEM) and High resolution transmission electron microscope (HRTEM)

Transmission electron microscope (TEM) works on the same basic principles as the light microscope but it uses electrons instead of light. TEM gives an image of a specimen by passing an accelerated a beam of electrons through it. The electron source is an electron gun which consists of tungsten filament and it emits electron when it is heated. The electrons are accelerated to 100 KeV or higher and then projected to the specimen by condenser lens system. The sample holder contains mechanical arm which

holds the specimen. The imaging system consists of electromagnetic lens system and a screen with a phosphorescent plate. When the electrons after passing through the specimen strikes the plate, it glows and the image is recorded. One of the advantages of TEM investigation is that it offers the high magnification ranging from 50 to 10^6 and it provides both image and diffraction information from a single sample. In this work, TEM and HRTEM analysis of various samples were carried out on JEOL JEM-2011 electron microscope. The sample specimens were prepared by dispersing the samples in isopropanol and 2-3 drops of the dispersed samples were placed on carbon coated 300 mesh copper grids. The copper grids were allowed to dry and used for TEM and HRTEM analysis.

1.10.4.10. X-ray photoelectron spectroscopy (XPS)

X-ray photoelectron spectroscopy (XPS) is a spectroscopic technique which is surface sensitive and used to analyze the chemical and electronic state of elements within a material, surface chemistry of a material etc. XPS experiment is performed by irradiating the sample with a beam of x-ray and simultaneously measuring the number of electrons that escape from the top 0-10 nm of the sample and their kinetic energy. The process requires a high vacuum condition. The XPS spectrum is a plot of intensity which is related number of electrons detected (y-axis) against the binding energy of the detected electrons (x-axis). The element that exists in or on the surface of a material can be identified with its electronic state from the XPS spectrum as each element produces characteristic XPS peaks at characteristic binding energy values. In this work, XPS experiment of the test sample was carried out on Kratos ESCA Axis 165 spectrophotometer. All the measurements were performed using Mg-KP X-ray and the binding energy correction was done by the C_{1s} peak of carbon at 285 eV as reference.

1.10.4.11. Inductively coupled plasma-atomic emission spectroscopy (ICP-AES)

ICP-AES is an emission spectroscopic technique which can be used for both qualitative and quantitative multiple elements analysis in a sample at a given time. It works on the fact that each element emits energy at specific wavelength peculiar to its

atomic character as they return to the ground state after excitation by high temperature argon plasma. When the electrons from the excited state fall down to ground state, the energy transfer (or wavelength of light emitted) is unique to each element as it depends upon the electronic configuration of the orbital. The intensity of the energy emitted at a particular wavelength is proportional to the concentration of that element in the analyte. By determining the wavelengths and intensities, the amount of different elements in a sample can be evaluated. In this work, the amounts of metal present in different catalysts were determined with the help of ICP-AES analysis. The ICP-AES analysis was performed in Perkin Elmer Optima DV instrument. The instrument was calibrated using standard solutions. The instrument can be used for the analysis of both aqueous and organic solutions for metal with either an axial or radical plasma configuration.

Chapter-2

Acid modification of montmorillonite K10, its characterization and applications

2. Acid modification of montmorillonite K10, its characterization and applications.

2.1. Introduction

The development of environmentally benign, efficient and green synthetic methods has become the major current challenge to the chemists to address industrial and environmental concerns [46]. Due to growing environmental regulations, the chemical industry has to use manufacturing processes that do not cause any permanent damage to the environment or disturb the ecological balance [47]. The researchers also try to minimize the consumption of energy and raw materials required in synthesis so that optimal value of resources could be realized. Thus, development of clean technology for both material synthesis and organic synthesis is a great challenge for the researchers. In this context, the use of environmentally benign, easily available, robust and cheap materials as support for nanoparticles synthesis or directly as catalyst has gained interest in recent years [48]. Among the different materials, clays are widespread, easily available and cheap materials which show activities in both in their native state and numerous modified forms [49]. Now a day, clays are important materials with a large variety of applications in ceramics, oil drilling, and the metal and paper industry. Clays are furthermore used as adsorbents, decoloration agents, ion exchangers and molecular sieve catalysts [50-51].

Clays are lamellar aluminosilicates showing a large variety of physicochemical properties such as swelling, adsorption, surface acidity, ion exchange etc. Clays can be modified very easily by simple acid treatment and this provides the scope for altering their properties like surface area, pore size, acidity and other characteristics [48-49]. These properties make them attractive for utilization as catalysts or support materials for the development of metal nanocatalysts for organic synthesis. Due to their environmental acceptability, cheapness and wide range of possibilities for surface modification, much effort is expended to develop newer methods for organic transformations using clay based catalysts. Among the different clay minerals, the Smectite group of clays is most widely used for catalytic applications. Montmorillonite clay, which is included in the

Smectite group, has enjoyed a great deal of attention because of its useful cation exchanged, intercalation and adsorption properties [51- 56]. Montmorillonite clay is a hydrated 2:1 layered dioctahedral aluminosilicate of the smectite group. It is composed of two tetrahedral silicate sheets which are bonded to either side of an octahedral aluminate sheet. Isomorphous substitution of Si^{4+} and Al^{3+} by lower valence cation such as Mg^{2+} results in charge deficit. This layer charge is balanced by hydrated exchangeable cations which occupy the surfaces between clay layers. Montmorillonite clay has been used as active catalysts for various organic transformations and also as a support material for the synthesis of metal nanoparticles [54-56]. In this work, we have reported modification of montmorillonite K10 by treatment with HCl under refluxing conditions to get a high surface area and porous matrix. The modified clay has been utilized as an efficient heterogeneous catalyst for the heterocyclic condensation between different aromatic aldehydes and arene-1,2-diamines to give benzimidazoles under mild reaction conditions. The raw montmorillonite K10 is commercially available and is purchased from M/S Sigma Aldrich. Acid modification of montmorillonite K10 results the following changes of the clay matrix: exchange of hydrated interlayer charge compensating cations for H^+, leaching of Al from the octahedral sites of the clay matrix and formation of hydrous, poorly crystalline but highly porous clay phase with micro and mesopores.

Benzimidazoles are important synthetic intermediates in organic synthesis and are considered to be privileged sub-structure for drug design [57]. Benzimidazole derivatives have shown different pharmaceutical activities such as antiviral, antihypertension, anticancer and some other properties [58-59]. Thus, they are important building blocks in organic synthesis. The conventional method for the synthesis of benzimidazole involved condensation reaction between 1,2-diaminobenzene and carboxylic acid or acid derivative under acidic condition at high temperature [60]. In recent years, a lot of methods have been developed to synthesize benzimidazole derivatives. Some of the examples are intramolecular condensation, condensation of o-phenylenediamine with carboxylic acid or its halide derivative and condensation of o-phenylenediamine and aldehyde etc [61-63]. Among the various staring materials, aldehydes are desirable one

for the synthesis of benzimidazole because of their ready availability and non-toxic nature [64]. Although much progress has been made in this reaction, it is still highly desirable to develop efficient and green synthetic methods for the synthesis of benzimidazoles. Herein, we have reported a procedure for the synthesis of benzimidazole through the room temperature stirring of aromatic aldehyde and o-phenylenediamine using modified montmorillonite clay as catalyst and toluene as a solvent in presence of air.

2.2. Experimental

2.2.1. Acid modification of montmorillonite K10

Purified montmorillonite K10 was modified with mineral acid to get a porous matrix with high surface area having micro and mesopores on the surface. An amount of 10 g of Montmorillonite K10 (10 g) was dispersed in 200 ml 2M HCl and refluxed for different time intervals (30 min, 1 h, 2 h and 3 h). After cooling, the supernatant liquid was discarded and the activated montmorillonite was repeatedly washed with deionised water until no Cl$^-$ ions could be detected by the AgNO$_3$ test. The activated clays were dried in air oven at 50°C over for 12 h and the solid products were designated as modified mmt-I, II, III and IV with respect to refluxing time 30 min, 1, 2 and 3 h.

2.2.2. General procedure for the one-pot synthesis of benzimidazoles

Aldehyde (1 mmol), o-phenylenediamine (1.2 mmol), 20 mg catalyst (modified mmt-III) and 5 ml toluene were taken in a 25 ml round bottom flask and the reaction mixture was stirred in presence of air for stipulated time period (3 h). The progress of the reactions was monitored by TLC. After completion of the reaction, the solid catalyst was separated from the reaction mixture by filtration through a sintered funnel (G3) and the solvent was removed under low pressure in a rotary evaporator. The recovered catalyst was washed with acetone, dried in a desiccator and stored for another consecutive reaction run. The crude product obtained was then purified by silica gel column chromatography using ethyl acetate and hexane as eluents. The products were characterized by ^{1}H and ^{13}C NMR spectrometry.

2.3. Results and discussion

2.3.1. Characterization of modified montmorillonite

The characterization of different modified montmorillonite were thoroughly carried out with the help of different sophisticated analytical instruments like Powder-XRD, FTIR, N_2 adsorption-desorption and SEM-EDX analysis.

2.3.1.1. X-ray diffraction

The parent montmorillonite K10 exhibited an intense basal reflection at 7.10^o 2θ corresponding to a basal spacing of 12.7 Å (Fig. 2.1). The reflection intensity of the basal peak decreased with time during acid treatment and no basal reflection was seen after 2 h. It was due to the fact that acid treatment modified the layered structure of the clay by leaching out aluminium from octahedral sites and developed a porous amorphous silica phase. The formation of amorphous silica was also substantiated by the appearance of a low intense broad reflection at $20\text{-}30^o$ 2θ [65].
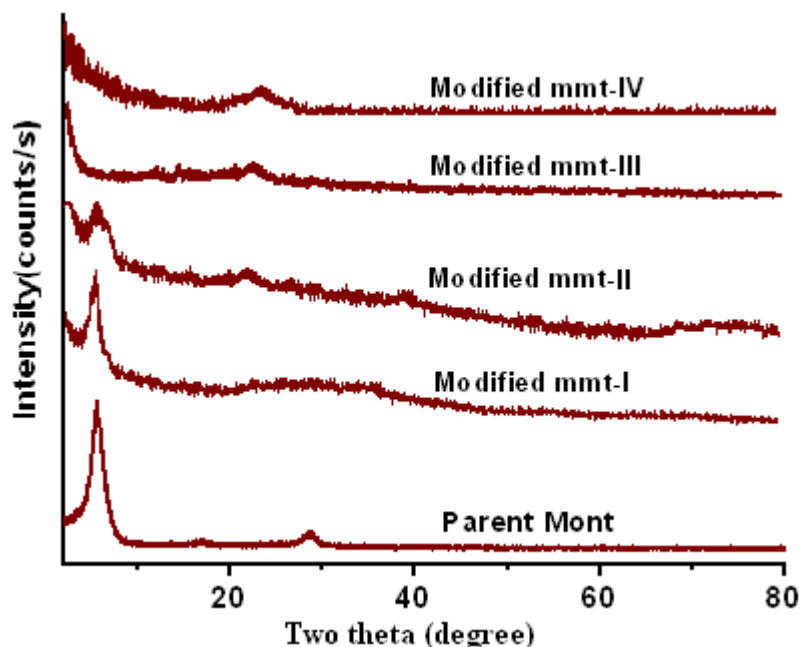
Fig. 2.1. Powder XRD pattern of different Montmorillonite clay.

2.3.1.2. Specific surface area and pore size distribution

The specific surface area and pore size distribution of modified montmorillonite determined by N_2-adsorption study revealed that the clay matrix contained both micro (< 2 nm) and mesopores (> 2 nm). The adsorption-desorption isotherms (Fig. 2.2) were of the type-IV with a H3 hysteresis loop at P/P_o ~ 0.4-0.9, indicating mesoporous solid.

The specific surface area of parent montmorillonite K10 was found to be 192 m^2/g with pore volume ~0.30 cm^3/g. After acid modification, the surface area of the clay increased with modification time and showed a maximum of 416 m^2/g with large specific pore volume 0.65 cm^3/g for modification time 2 h i.e. modified mmt-III (Table 2.1.). But after 2 h, further increased in acid modification time decreased surface area remarkably but the specific pore volume increased. The initial increase in surface area might be due to the formation of micro and mesopores during acid treatment which leached out aluminum from octahedral sites. Further increased in the acid treatment time decreased the surface area because of destruction of the pore walls which formed bigger pores.
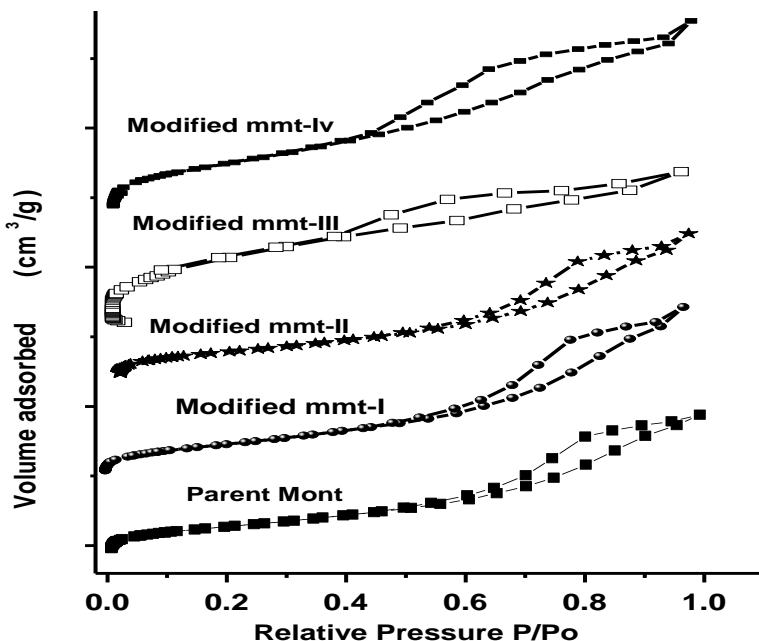
Fig. 2.2. N_2 adsorption / desorption isotherms of Parent Mont and different Modifed montmorillonite.
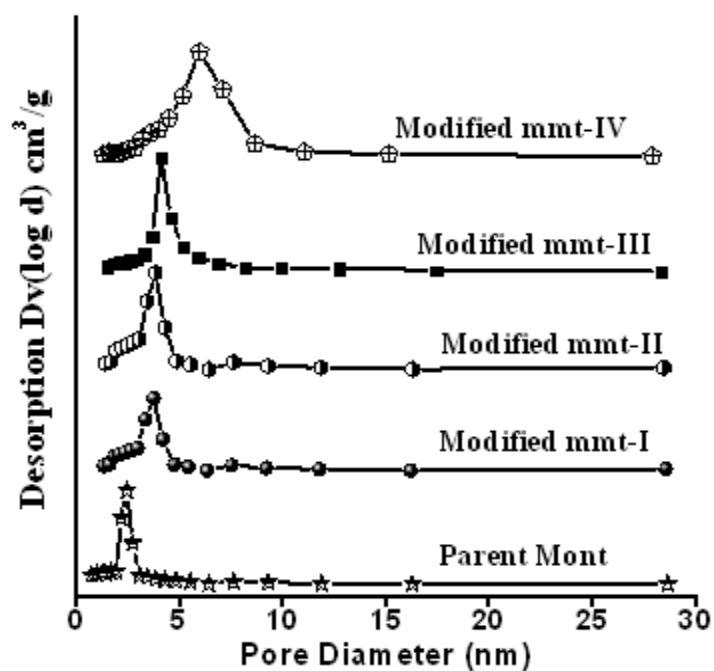
Fig. 2.3. BJH pore size distribution curves of Parent Mont and different Modified montmorillonite.

Table 2.1. Surface properties of parent mont and modified montmorillonite.

Samples	Specific Surface Area (m^2/g)	Pore Diameter (nm)	Specific Pore Volume (cm^3/g)
Parent Mont	192	3.82	0.30
Modified mmt-I	264	4.06	0.43
Modified mmt-II	373	4.45	0.55
Modified mmt-III	416	4.88	0.65
Modified mmt-IV	368	5.94	0.71

2.3.1.3. FTIR analysis

FTIR study revealed that the parent montmorillonite exhibited an intense absorption band at ~1051 cm^{-1} for Si-O stretching vibrations of tetrahedral sheet. It also showed

absorption bands at 3628 cm^{-1} due to stretching vibrations of OH groups of Al-OH. The bands near 525 and 462 cm^{-1} were due to Si-O-Al and Si-O-Si bending vibrations mode respectively [Fig. 2.4]. The band at 1618 cm^{-1} was due to bending vibration of O-H group of clay structure and the water molecule present there. During acid treatment, the Si-O stretching vibration band shifted from ~1051 cm^{-1} to ~1091 cm^{-1} indicating the change in bonding environment in tetrahedral layer and formation of amorphous silica phase. This was substantiated by the alteration of the band at 799 cm^{-1} which was due to the vibrations of amorphous SiO$_2$ [29 b].
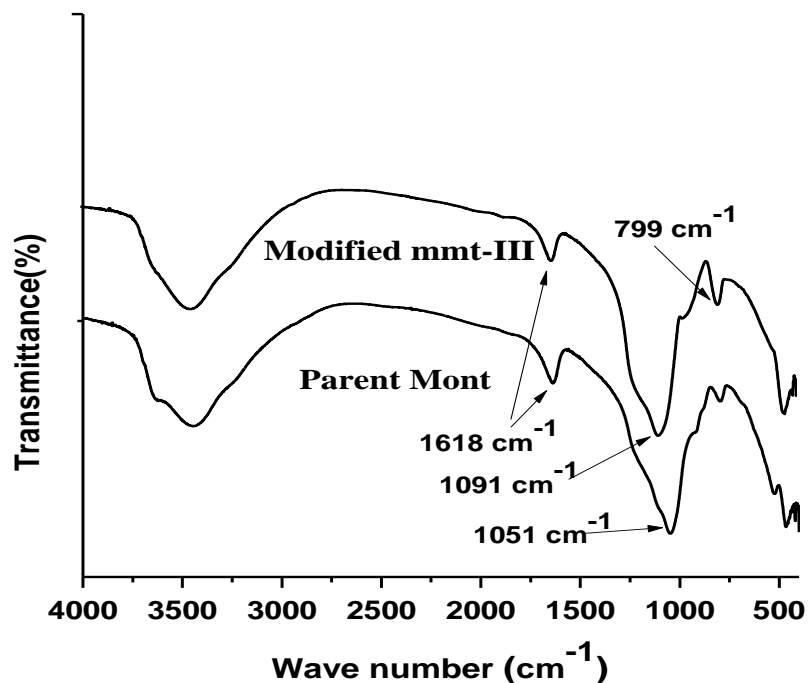
Fig. 2.4. FTIR spectra of Parent Mont and Modified mmt-III.

2.3.1.4. SEM-EDX analysis

The SEM analysis of parent and modified montmorillonite showed the formation of porous matrix on the surface of montmorillonite after acid treatment which was not observed on unmodified clay [Fig. 2.5 (a) and (c)]. The unmodified parent clay showed the uniform layered structure of the clay in the SEM image. EDX analysis showed a decrease in Al content after acid treatment which was due to the leaching of aluminium from the clay structure [Fig. 2.5 (b) and (d)]. Na, Mg present in the parent clay also

36

disappeared from the EDX spectra of modified montmorillonite as they were leached out during acid treatment.
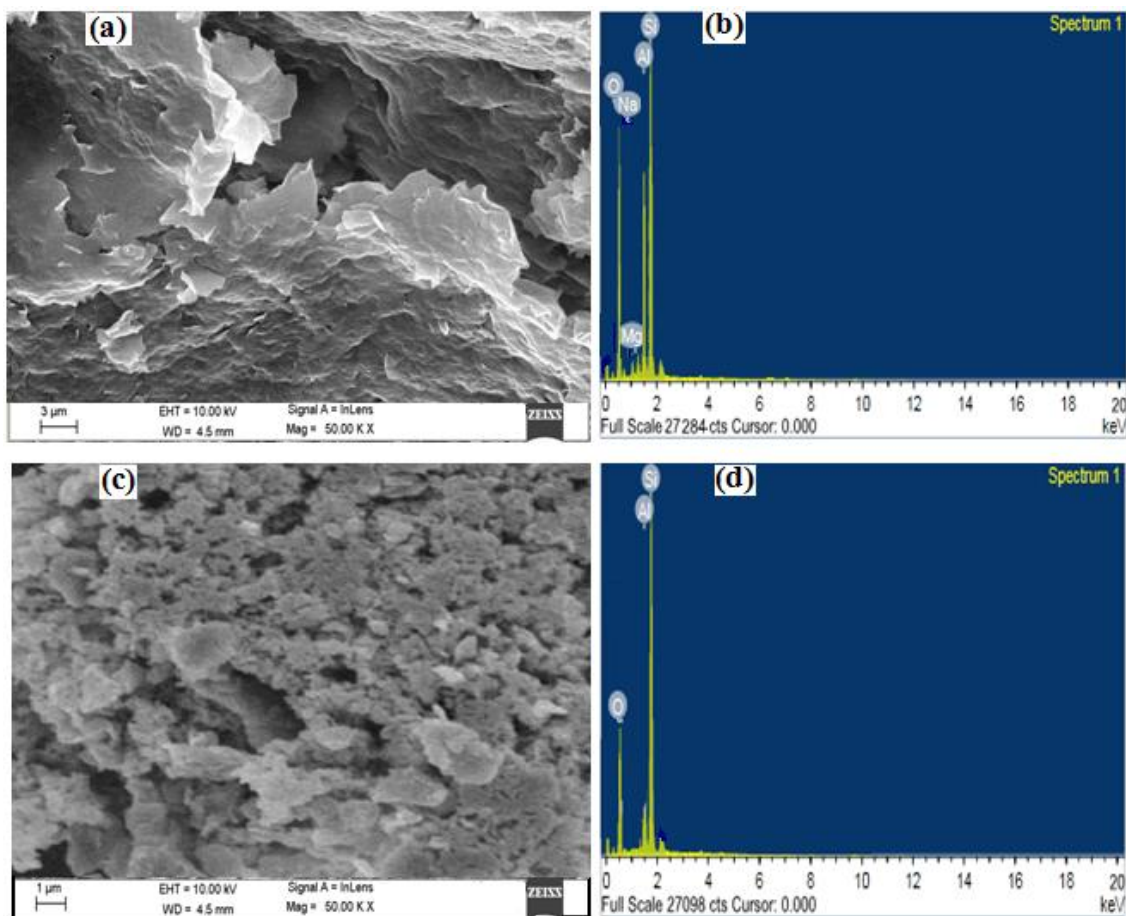

Fig. 2.5. (a) SEM image of Parent Mont, (b) EDX analysis of Parent Mont, (c) SEM image of modified montmorillonite, (d) EDX analysis of modified montmorillonite.

2.3.2. Catalytic activity

2.3.2.1. Synthesis of benzimidazoles using modified mmt as catalyst

The conditions for the synthesis of benzimidazoles were optimized by using the model substrates benzaldehyde and o-phenylenediamine. After screening a wide range of

reactions, we have found that our catalytic system i.e. modified mmt-III is most efficient at room temperature in toluene as solvent for the of benzimidazole synthesis. The reaction mixture was also stirred without catalyst to test its requirement for the reaction and we obtained only 12% yield of the desired product in 3 h. The use of unmodified montmorillonite as catalyst gave 48% yield in 3 h in the model reaction. To investigate the catalytic activity other modified montmorillonite in the synthesis of benzimidazole, the modified mmt-IV was also utilized as catalyst in the model reaction but we obtained the best result in modified mmt-III catalyst (Table 2.2.). Thus, the catalytic synthesis of benzimidazole was carried out with modified mmt-III catalyst. The higher catalytic activity of modified mmt-III might be due to its higher surface area compared to the other modified mmt catalysts. The model reaction gave maximum 86% yield using modified mmt-III as catalyst. A variation in the reaction was done by using different aldehydes with o-phenylenediamine and all these gave the expected benzimidazoles with excellent yield and selectivity. The various substrates and products were represented in table 2.3. In this study, it was observed that the aldehydes with electron withdrawing substituent gave slightly higher yield of product than the aldehydes with electron donating substituent. This might be due to the fact that the presence of electron withdrawing substituent on aldehyde made the carbonyl group more positive and this increased its reactivity.

Table 2.2. Screening of different montmorillonite catalyst for benzimidazole synthesis

Catalyst	Solvent	Time (h)	*Yield (%)
Parent Mont	Toluene	3	48
Modified mmt-III	Toluene	3	86
Modified mmt-IV	Toluene	3	75

*Yields are isolated products based on aldehyde after silica-gel column chromatography. **Reaction conditions:** Aldehyde (1 mmol), o-Phenylenediamine (1.2 mmol), Catalyst (20 mg), Room Temperature, Time: 3 h.
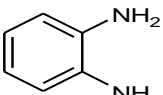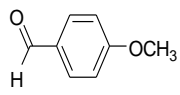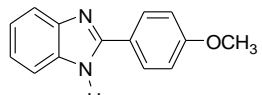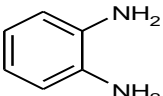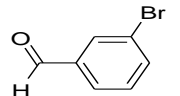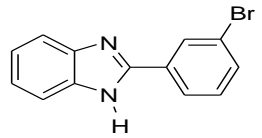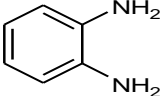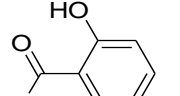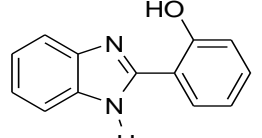
The recyclability of the catalyst was also investigated in this study. This is a very important factor in any catalytic application. Here, the recyclability of our modified

mmt-III catalyst was investigated with the substrates of entry S1 and entry S2. The catalyst was recovered by filtration after each experiment. It was then washed with acetone, dried and reused with fresh reaction mixture for another catalytic run. The modified mmt catalyst was successfully reused upto 3rd catalytic run without any significant loss in its catalytic activity (Table 2.3).

**Table 2.3.** Modified mmt-III catalysed synthesis of benzimidazoles.
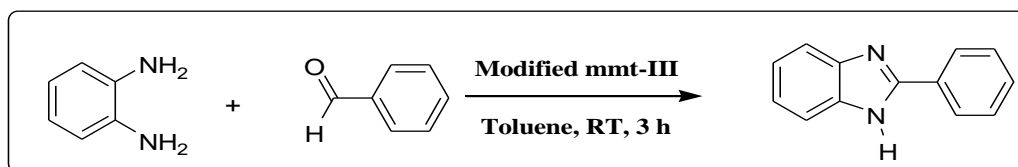
Entry	Arene-1,2-diamine	Aldehyde	Products	Yield[*](%)
S1				86
				84(2nd run)
				81(3rd run)
S2				88
				86(2nd run)
				84(3rd run)
S3				87
S4				82

39

S5	o-phenylenediamine (NH₂, NH₂)	4-methoxybenzaldehyde	2-(4-methoxyphenyl)benzimidazole	84
S6	o-phenylenediamine (NH₂, NH₂)	3-bromobenzaldehyde	2-(3-bromophenyl)benzimidazole	85
S7	o-phenylenediamine (NH₂, NH₂)	2-hydroxybenzaldehyde	2-(2-hydroxyphenyl)benzimidazole	81

[Note: structures shown in table cells]

*Yields are isolated products based on aldehyde after silica-gel column chromatography.
**Reaction conditions: Aldehyde (1 mmol), o-Phenylenediamine (1.2 mmol), Catalyst (20 mg), Solvent: Toluene, Room Temperature, Time: 3 h.

A plausible mechanism for the synthesis of benzimidazole catalysed modified mmt is proposed (Scheme 2.1.). First, the arene-1,2-diamine and aldehyde are adsorbed on the catalyst surface. Then arene-1,2-diamine and aldehyde undergo dehydration to give the intermediate imine. The imine undergoes cyclization to give the product and the catalyst is regenerated.
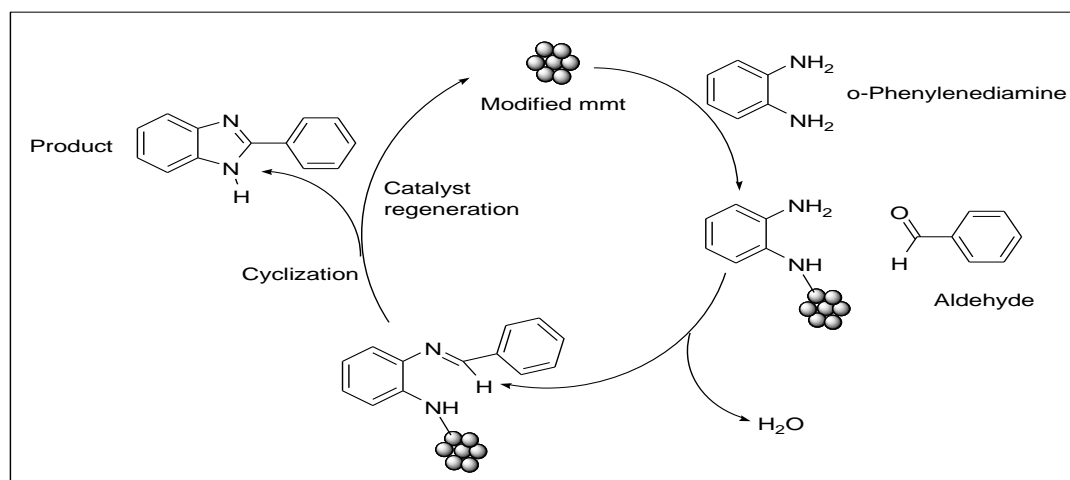
Scheme 2.1. Proposed mechanism for the synthesis of benzimidazole.

2.4. Conclusion

Modification of montmorillonite was carried out with 2M HCl for different time intervals. The different modified clays were characterized by Powder-XRD, FTIR, N_2 adsorption-desorption and SEM-EDX analysis. The modified clay with 2 h acid treatment (modified mmt-III) showed maximum specific surface area and it was evaluated as a heterogeneous catalyst for the synthesis of benzimidazoles under mild reaction condition. The used modified mmt-III catalyst was recovered and reused upto 3rd catalytic run without any significant loss in activity.

Chapter-3

Synthesis, characterization and applications of silver nanoparticles (Ag-NPs) stabilized on modified montmorillonite

3. Synthesis, characterization and applications of silver nanoparticles (Ag-NPs) stabilized on modified montmorillonite.

3.1. Introduction

The synthesis and characterization of metal and metal oxide nanoparticles have attracted great attention due to their potential applications in the field of electronics, opto-electronics, biosciences, medicine, sensor and catalysis [1]. The development of facile synthetic methods and choice of suitable support towards the synthesis of metal nanoparticles having uniform size and controllable preparation of nanoparticles with different shapes and exposed surfaces appear to be of key importance for the exploration of new research [66-67]. The utilization of metal and metal oxide nanomaterials as catalyst precursors for organic synthesis is a challenge for researchers [26]. Among the transition metal nanoparticles, silver and gold nanoparticles were extensively focused due to their relatively high stability [1, 26]. Recently, lot of research has been focused on silver nanoparticles due to their scientific and technological applications in antibacterial activities, optical sensors, color filters, optical switching and catalysis [68-69]. Silver nanoparticles were advantageously used as active catalysts in various organic reactions such as carbon-carbon coupling reaction, three-component coupling reaction, oxidation reaction, dehydrogenation reaction, Diels-Alder cycloaddition reaction. The advantage of using silver nanoparticles over traditional catalysts is that they require only mild reaction conditions to produce high yields of products in short reaction times and can also be recycled [30-31]. But due to their high surface reactivity, the metal nanoparticles immediately tend to aggregate once they are formed, which increases their particle size and make them inactive. To prevent the aggregation, various supports were used to stabilize metal nanoparticles [70-71]. A good support and stabilizer is the one which prevents aggregation of the nanoparticles during participation in any chemical activities like catalytic process but does not totally passivate the surfaces of the nanoparticles. In addition to that the use of stabilizer will also affect the shape, core diameter and size of the metal nanoparticles. Different types of supports / stabilizers like mesoporous

materials, activated carbons, polymers, dendrimers, metal oxides, organic ligands, zeolite, clay etc. have been employed to stabilize metal nanoparticles [70-72].

In recent years, metal nanoparticles were stabilized into the interlamellar spaces of clay minerals of the smectite group like montmorillonite, hectorite and saponite [15, 72-73]. Various methodologies for synthesizing and stabilizing metal nanoparticles into the interlayer space of modified montmorillonite clay were also developed and reported in the literature [74]. The micro and mesoporous materials supported metal nanoparticles are expected to behave very differently from bulk metals. They may exhibit unique catalytic activity, molecular selectivity and adsorption properties. Acid treated montmorillonite is partially delaminated clay with higher specific surface area and contains micro and mesopores. The surface properties of the montmorillonite clay such as specific surface area, the pore diameter and pore volume can be tuned by controlling the acid treatment conditions [74-75].

Propargylamines have been attracting considerable attention over the last few years due to their wide applications in drug discovery [76-78]. Propargylamines are versatile synthetic intermediates in organic synthesis, important structural elements in natural products and therapeutic drug molecules [79]. The propargylamine derivatives have gained much importance after the discovery of rasagiline, which contains propargylamine moiety (Azilect). Rasagiline is an FDA approved drug and used as monotherapy in early Parkinson's disease [80-81]. In 2003, Li's group first reported gold catalysed three component coupling reaction for the alkynylation of iminium ions [82 a]. Now, various metal based catalysts (e.g. Cu, Fe, Au, Ag, In etc.) have been extensively used for the synthesis of propargylamines via C-H alkyne activation [82-84]. Although, various catalytic systems have been developed for the synthesis of propargylamines, the main disadvantages of these systems are high reaction temperature, long reaction time and most of the catalytic systems are homogenous in nature which makes them economically and environmentally unattractive. Here, we have reported synthesis of different propargylamines using modified montmorillonite clay stabilized silver nanoparticles (Ag-NPs@mmt) as catalyst under mild reaction conditions. The

nanocatalysts can be reused several times without any significant loss in their catalytic activity.

Baeyer-Villiger (BV) oxidation is a very important class of organic reaction, where various value-added lactones and esters in many fields such as the production of antibiotics and steroids can be generated in one pot from their respective carbonyl compound in the presence of oxidants such as peroxides, per acids or persulfate salts [85-87]. When organic per acids are used, the reaction generates huge amount of hazardous byproducts which is a major problem often encountered in this reaction. Thus the use of H_2O_2 as oxidant gets the advantages over other peracids because of its ease of use, being environment friendly, produce water only as side product. Although both homogeneous and heterogeneous catalysts were used in this reaction, heterogeneous catalysts have more advantages than homogenous ones, because of facile separation and reusability of the catalyst and simple isolation of the product. Some of the recently developed heterogeneous catalytic systems for BV oxidation are: supported ionic liquids, supported sulfonic acids, Sn-doped microporous and mesoporous materials, mesoporous magnesium-aluminum mixed oxide, clay-supported Sn catalysts, stabilized Fe_3O_4 magnetic nanoparticles, Sn exchanged hydrotalcites [85-90] etc. In this study, we have reported efficient Baeyer-Villiger oxidation of cyclic and aromatic ketones catalysed silver nanoparticles stabilized on modified montmorillonite (Ag-NPs@mmt) under solvent free condition. The catalysts can be recycled and reused several times without significant loss of their catalytic activity.

This chapter, reports the synthesis of silver nanoparticles (Ag-NPs@mmt) using modified montmorillonite clay as stabilizer and their utilization as a heterogeneous catalyst precursor for the one pot three component coupling of aldehyde, amine and alkyne (A^3-coupling) to synthesize propargylamines and for the Baeyer-Villiger oxidation of cyclic and aromatic ketones under mild reaction conditions.

3.2. Experimental

3.2.1. Preparation of Support

Montmorillonite K10 (10 g) was refluxed with 200 ml 2M HCl for 2 hour. After cooling, the supernatant liquid was discarded and the activated montmorillonite clay was repeatedly washed with deionised water until no Cl$^-$ ions could be detected by the AgNO$_3$ test. The activated clay was dried in air oven at 50°C over for 12 h. The solid product obtained was designated as modified montmorillonite. The surface characterizations of modified Montmorillonite clay were presented in Table 4.1.

3.2.2. Preparation of supported silver nanoparticles (Ag-NPs)

1 g of modified montmorillonite was impregnated with 20 mL (0.5 m mol) aqueous solution of AgNO$_3$ under vigorous stirring for 8 h. The mixture was then evaporated to dryness in a rotary evaporator. 0.4 g of the dry composite was dispersed in 20 mL of water and 151.4 mg of NaBH$_4$ (4 m mol) in 10 mL of distilled water were added slowly over 10 min under constant stirring conditions. The grey reaction product was recovered and washed with deionised water several times and then dried in a desiccator for 15 h. The composite was designated as Ag-NPs@mmt and stored in airtight bottle for further use.

3.2.3. General procedure for the one-pot synthesis of propargylamines

Aldehyde (1 m mol), amine (1 m mol), alkyne (1.2 m mol), 20 mg catalyst and 5 mL toluene were taken in a 25 mL round bottom flask and the reaction mixture was refluxed at 100 ^{o}C for stipulated time period (2h). The progress of the reactions was monitored by TLC. After completion of the reaction, the solid catalyst was separated from the mixture by filtration through a sintered funnel (G3) and the solvent was removed under low pressure in a rotary evaporator. The recovered catalyst was washed with acetone, dried in a desiccator and stored for another consecutive reaction run. The crude product obtained was then purified by silica gel column chromatography using ethyl acetate and hexane as eluents. The products were characterized by ^{1}H and ^{13}C NMR spectrometry.

3.2.4. General procedure for oxidation of ketone

Ketone (2 m mol), H_2O_2 (20 m mol) and 25 mg Ag-NPs@mmt were taken in 10 mL round bottom flask and the reaction mixture was stirred at room temperature for 4 h. After completion of the reaction, the solid catalyst was recovered by filtration. The byproduct water obtained in the reaction was removed by using anhydrous sodium sulphate. The conversion of the reaction was determined using gas chromatography (GC).

3.3. Results and discussion

3.3.1. Characterization of Support

The characterization of modified montmorillonite was thoroughly carried out with the help of different sophisticated analytical instruments like Powder-XRD, FTIR, N_2 adsorption-desorption, SEM-EDX and HRTEM analysis.

3.3.1.1. X-ray diffraction

The parent montmorillonite K10 showed an intense basal reflection at 7.10^o 2θ corresponding to a basal spacing of 12.7 Å (Fig. 3.1). During acid treatment, the reflection intensity decreased with time and no basal reflection was seen after 2h. The layered structure of the clay disrupted during acid treatment and only a low intense broad reflection was observed at $20\text{-}30^o$ 2θ confirmed the formation of amorphous silica [65].
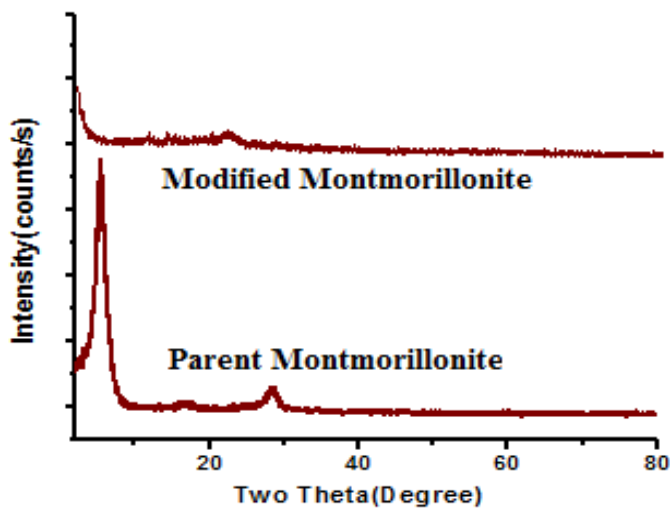
Fig. 3.1. Powder XRD pattern of different Montmorillonite clay.

3.3.1.2. Specific surface area and pore size distribution

The modified montmorillonite contained micro (< 2 nm) and mesopores (2-50 nm) with average pore diameters ~ 4.88 nm, a high specific surface area upto 416 m^2/g and a large specific pore volume of ~ 0.65 cm^3/g (Table 3.1.). This observation may be due to the formation of micro and mesopores during acid treatment which leached out Al^{3+} ion from the octahedral sites of the clay matrix and introduced permanent porosity on the clay surface. The adsorption-desorption study of modified montmorillonite indicated the formation of mesoporous solid. The isotherm obtained was of type-IV [Fig. 3.2] with a H3 hysteresis loop at P/P$_o$ ~ 0.4-0.9. The differential volumes versus pore diameter plot [Fig. 3.3] indicated relatively narrow pore size distributions and these nanorange pores can be advantageously utilized for the *in situ* synthesis of various metal nanoparticles.
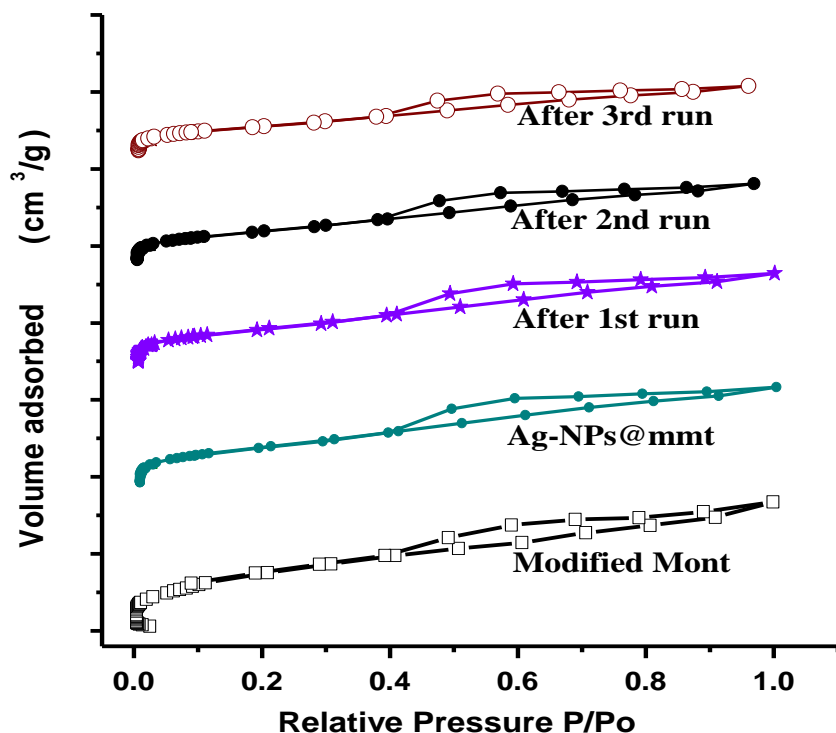
Fig. 3.2. N$_2$ adsorption / desorption isotherms of Modified Mont, Ag-NPs@mmt and recovered catalysts.
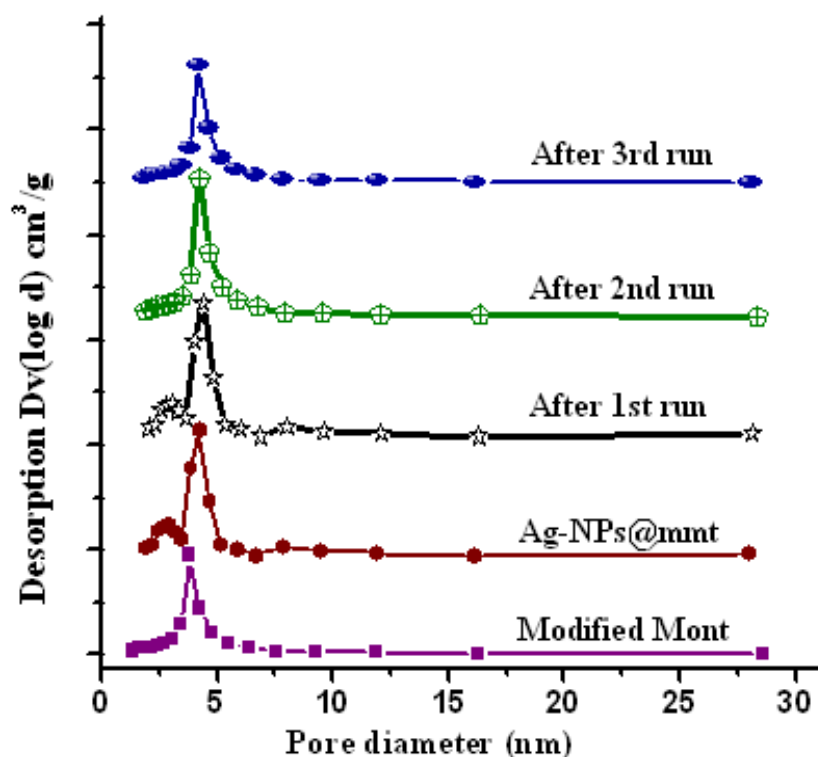
Fig. 3.3. BJH pore size distribution curves of Modified Mont., Ag-NPs@mmt and recovered catalysts.

3.3.1.3. FTIR spectra

The parent montmorillonite exhibited an intense absorption band at ~1051 cm^{-1} for Si-O stretching vibrations of tetrahedral sheet. The bands obtained at 525 and 462 cm^{-1} were due to Si-O-Al and Si-O-Si bending vibrations [Fig. 3.4]. During acid treatment, the band shifts from ~1051 cm^{-1} to ~1091 cm^{-1} indicating the change in bonding environment in tetrahedral layer and formation of amorphous silica phase. The increasing amount of free SiO_2 with acid treatment is reflected in the alteration of the band at 799 cm^{-1} which is attributed to the stretching vibration of amorphous SiO_2 [29 b]. Montmorillonite also showed absorption bands at 3628 cm^{-1} due to stretching vibrations of OH groups of Al-OH.
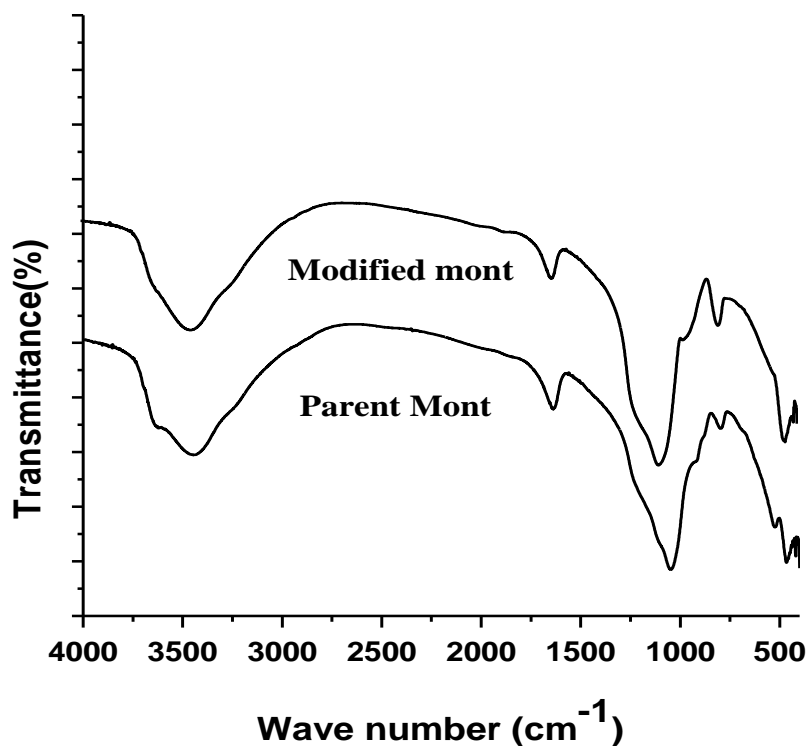
Fig. 3.4. FTIR spectra of different Montmorillonite clays.

3.3.1.4. SEM-EDX investigation

The typical SEM image of modified montmorillonite [Chapter 2; Fig. 2.5(c)] showed the formation of pores on the clay surface. The EDX analysis at the surface [Chapter 2; Fig. 2.5(d)] revealed that predominant amounts of Si compared to Al was present on the surface.

3.3.1.5. TEM investigation

The typical TEM image of modified montmorillonite is shown in Fig. 3.5 (a). During controlled acid treatment, most of the layered structure of clay minerals is disrupted and only a few are retained. In Fig. 3.5(b), both the layered and non-layered structures of clay mineral are seen along with silver nanoparticles.
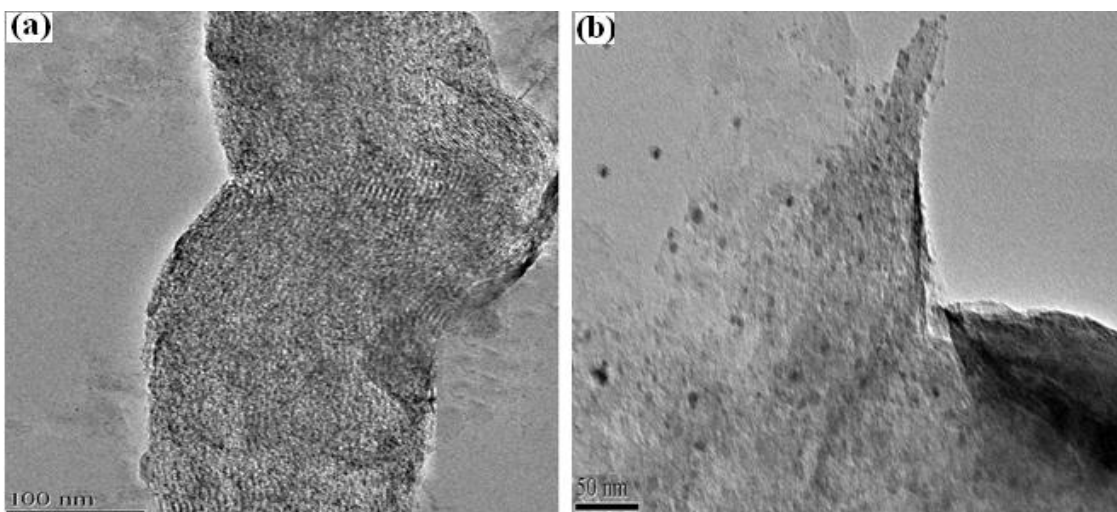
Fig. 3.5. Typical TEM images of (a) modified montmorillonite and (b) modified montmorillonite with silver nanoparticles.

3.3.2. Characterization of supported silver nanoparticles (Ag-NPs@mmt)

The preliminary investigation of the formation of the silver nanoparticles (Ag-NPs) was obtained from UV–Visible spectroscopy. The appearance of surface plasmon resonance band at around ~400 nm of Ag-NPs@mmt substantiated the formation of silver nanoparticles (Fig. 3.6).
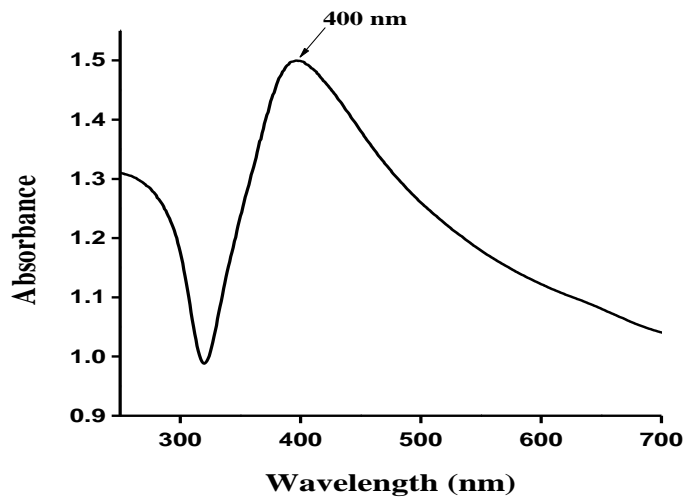
Fig. 3.6. UV-Visible spectrum of Ag-NPs@mmt.

The SEM-EDX analysis showed the presence of silver nanoparticles on the surface of modified montmorillonite (Fig. 3.7 a, b). The elemental dot mapping shows the distribution of silver throughout the surface of modified montmorillonite (Fig. 3.8).
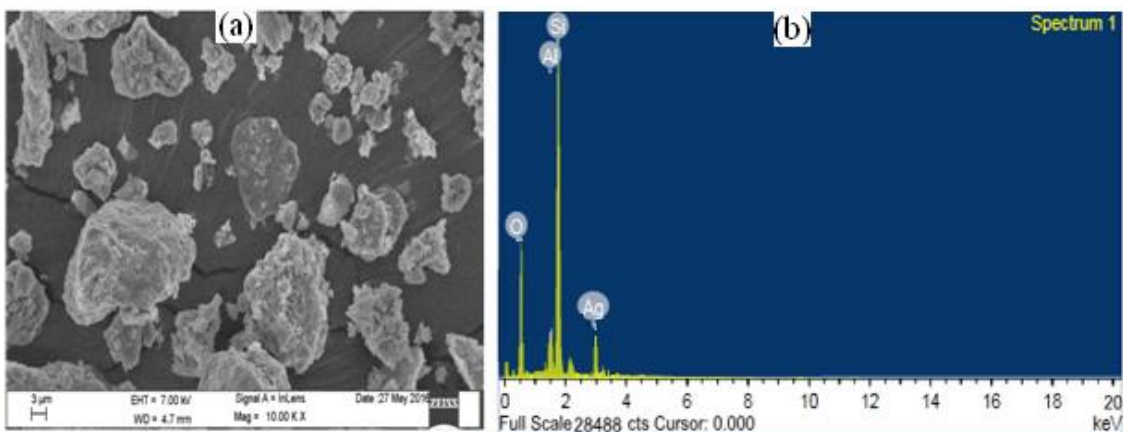
Fig. 3.7. (a) SEM image and **(b)** EDX pattern of Ag-NPs@mmt
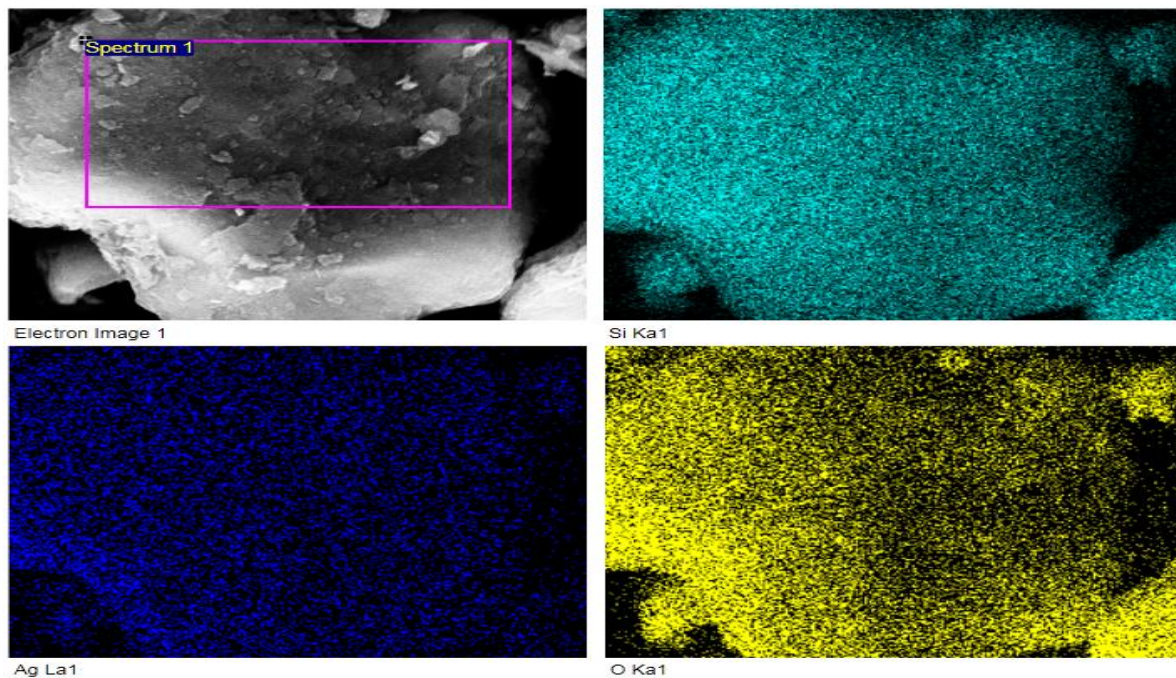
Fig. 3.8. Electron image and elemental dot mapping of Si, O and Ag on the surface of Ag-NPs@mmt.

TEM study [Fig.3.9. a, c, d] showed that the silver nanoparticles were uniformly dispersed throughout the surface of modified montmorillonite and the nanoparticles were spherical in shape with sizes of 1-10 nm. The HRTEM [Fig.3.9. b] and SAED (Selected Area Electron Diffraction) pattern [Fig.3.9. b (inset)] of Ag-NPs@mmt corresponds to crystalline nature of the silver nanoparticles.
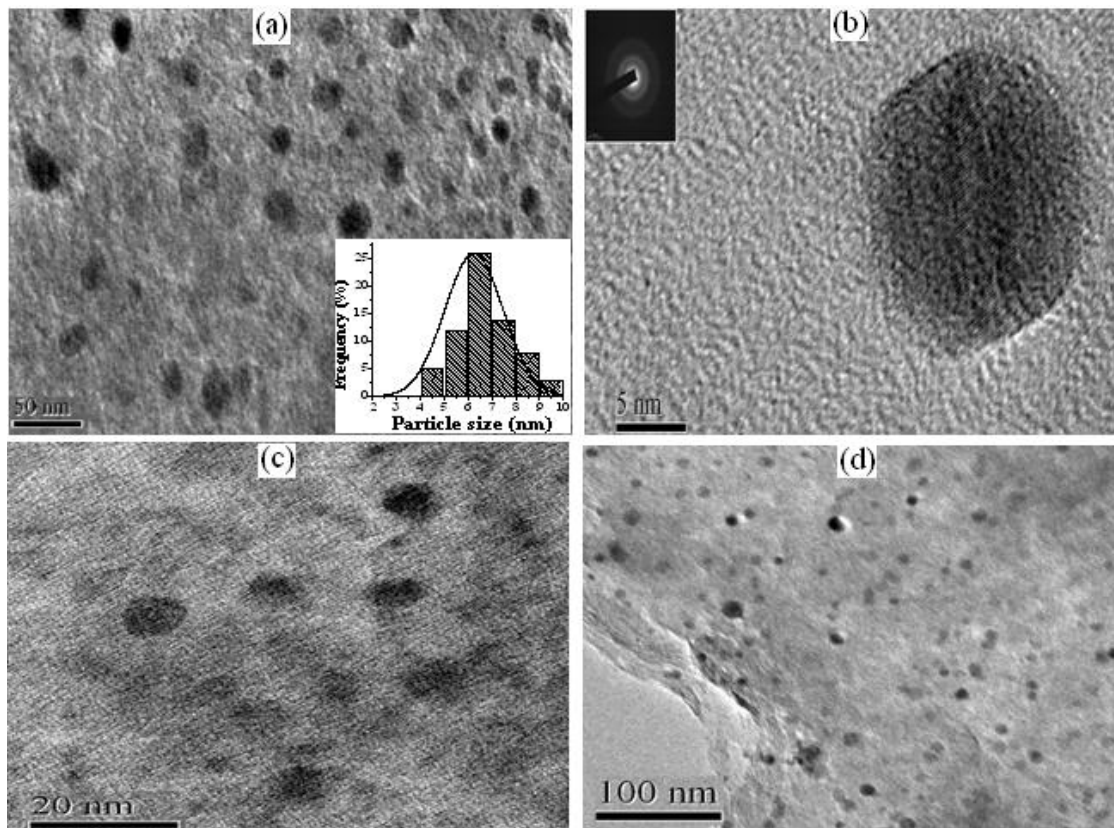
Fig. 3.9. TEM image (a), (c), (d) and Representative HRTEM image (b) and corresponding SAED pattern (inset) of Ag-NPs@mmt.

The powder XRD study also showed the crystalline nature of the silver nanoparticles (Fig. 3.10.). The four prominent peaks of 2θ values 38.24, 44.30, 64.54 and 77.62^0 were assigned to the (111), (200), (220) and (311) diffraction of a fcc lattice of silver.
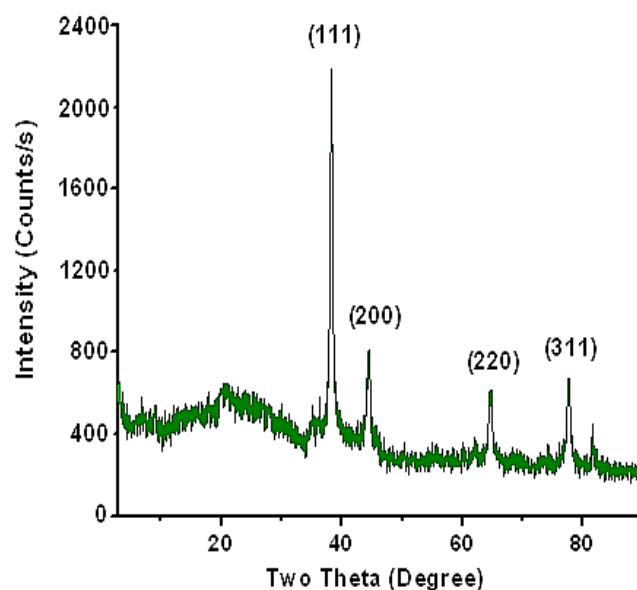
Fig. 3.10. Powder XRD for Ag-NPs@mmt

From N_2 adsorption-desorption study, it is observed that there is a change in the textural parameters such as specific surface area and pore volume of modified montmorillonite after supporting silver nanoparticles (Ag-NPs). The N_2 adsorption-desorption isotherms of the clay matrix obtained in this study [Fig. 3.2] before and after the formation of the silver nanoparticles (Ag-NPs), showed type IV isotherm with a H3 hysteresis loop at P/P_o ~0.4-0.9. These observations confirm that the highly ordered porous structure of clay is maintained even after supporting the Ag-NPs. But there is an appreciable decrease in the specific surface area and the specific pore volume after supporting Ag-NPs (Table 3.1). This might be due to clogging of some pores by silver nanoparticles. However, increase in pore diameter may be due to rupture of some smaller pores to generate bigger ones during the formation of Ag-NPs into the pores. The Ag contents in Ag-NPs@mmt as analyzed by ICP-AES, reveals the presence of 0.0082 m mol Ag in 20 mg Ag-NPs@mmt catalyst (0.410 m mol/g).

Table 3.1. Surface properties of Ag-NPs@mmt and modified montmorillonite.

	Samples	Surface properties of support/catalysts		
		Specific surface area (m^2/g)	Average pore diameter (nm)	Specific pore volume (cm^3/g)
Modified Mont		416	4.39	0.65
Ag-NPs@mmt	After run Fresh	324	6.34	0.54
	1	276	6.96	0.46
	2	238	7.72	0.39
	3	212	8.68	0.34

3.3.3. Catalytic activity

3.3.3.1. Synthesis of propargylamines using Ag-NPs@mmt as catalyst

The three component coupling reaction of aldehyde, amine and alkyne known as A^3-coupling is widely used reaction for the synthesis of different propargylamine derivatives via C-H alkyne activation. To investigate the utility of the modified montmorillonite clay stabilized silver nanoparticles (Ag-NPs@mmt), the synthesized Ag-NPs@mmt was tested as catalyst precursor for the well-known A^3-coupling reaction. By using benzaldehyde, piperidine and phenylacetylene as the model substrates, a series of three-component reactions were carried out to determine the best reaction condition (i.e. solvent, reaction time etc.). First, the reaction was carried out under solvent free condition, where about 45% of the propargylamine product was obtained in 5 h using synthesized Ag-NPs@mmt catalyst. After that different solvent such as water, dichloromethane, ethanol, acetonitrile and DMF for the model reaction were used, but no encouraging results were obtained (Table 3.2.). But when toluene was used as a solvent at 100^oC, surprisingly, the maximum yield (95%) of the product was obtained in 2 h for the model reaction. Therefore, toluene is used as the solvent for the synthesis of different propargylamine derivatives by considering its high yield and selectivity.

Table 3.2. Optimization of reaction conditions for the synthesis of propargylamines.

Sl no.	Solvent	Temperature (°C)	Time (h)	Isolated yield (%)
1	Solvent free	70	5	45
2	Water	90	5	28
3	Dichloromethane	40	5	62
4	Ethanol	78	5	42
5	Toluene	100	2	95
6	Acetonitrile	80	5	56
7	DMF	110	5	58

Reaction conditions: Aldehyde (1 mmol), Amine (1 mmol), Alkyne (1.2 mmol), Catalyst (20 mg, contain 0.0082 m mol of Ag).

The effect of various catalyst amounts were also studied in the Ag-NPs@mmt catalysed A^3-coupling reaction. The effect of catalyst amount was studied with 10, 15, 20 and 25 mg of the catalyst in the model reaction (Table 3.3.). With increase in amount of catalyst the yield increased, but almost same yields were observed for 20 and 25 mg catalyst. Thus, all the reactions were performed using 20 mg catalyst.

Table 3.3. Effect of catalyst amount in the propargylamine synthesis.

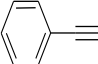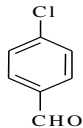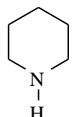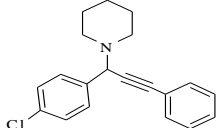| Entry	Catalyst	Temp (°C)	Catalyst amount (mg)	Yield(%)
1	Ag-NPs@mmt	100	10	68
2	Ag-NPs@mmt	100	15	76
3	Ag-NPs@mmt	100	20	95
4	Ag-NPs@mmt	100	25	96
5	Modified mont	100	20	8
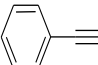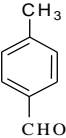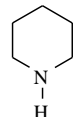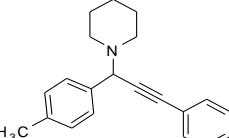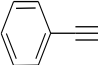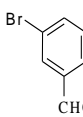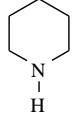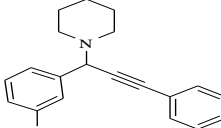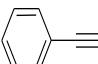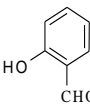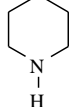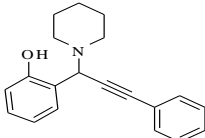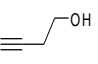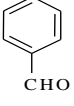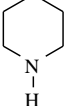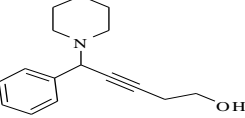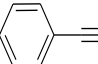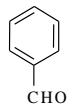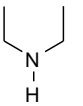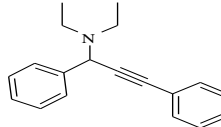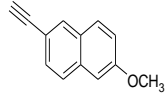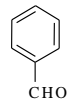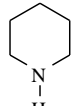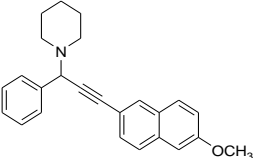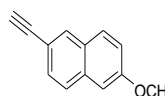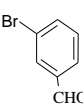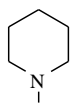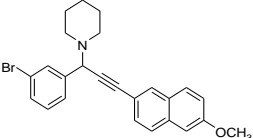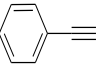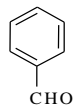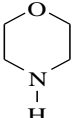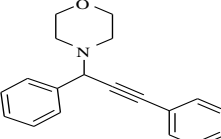
The various substrates and products are represented in Table 3.4. The mild reaction condition, high yield of the product (Maximum 95%) and less reaction time (2 hour) for the reaction indicates the efficacy of the Ag-NPs@mmt catalyst (Table 3.4.). To test the requirement of a catalyst, a control reaction was carried out using the model substrates in absence of the catalyst. No progress of the reaction was observed in this case. When the same reaction was carried out using only the modified clay as catalyst,

only 8% yield of the desired product was obtained. Since, the use of primary amines did not show any encouraging result in our preliminary investigation, only secondary amines were used in the present study. Here, we used different secondary amines, aldehydes and terminal alkynes and all the substrates give the expected propargylamines with excellent yields and selectivity. The model reaction where benzaldehyde, piperidine and phenylacetylene were used as substrates gave maximum (95%) isolated yield using our Ag-NPs@mmt catalyst (entry S1). There was no significant effect of electron donating or withdrawing nature of substituent on the aromatic aldehyde in the synthesis of propargylamines as all the aldehydes gave the product with excellent yield and selectivity. But aliphatic aldehyde gave a slightly lower yield than aromatic aldehyde (Table 3.4.) Again the use of cyclic amines, i.e., piperidine and morpholine (entry S1 and S11) showed higher conversion than of aliphatic amine, i.e., diethylamine (entry S8). In this work, all the reactions were carried out with 20 mg silver nanocatalyst which contains 0.0082 mmol Ag.

Table 3.4. Ag-NPs@mmt catalyzed A[3]-coupling of aldehyde, alkyne and amine.
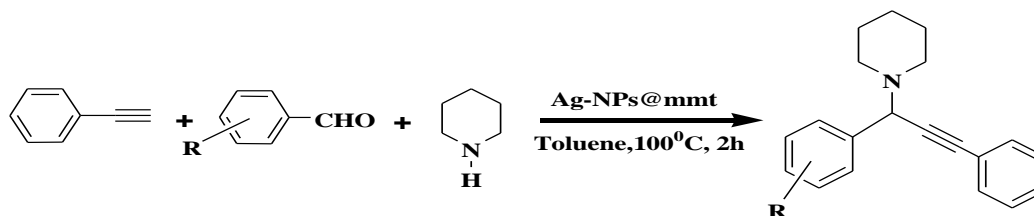
Entry	Alkyne	Aldehyde	Amine	Products	Yield[*] (%)	TON[a]
S1					95	115
					93(2nd run)	
					91(3rd run)	
					88(4th run)	
S2					92	112

57

	Alkyne	Aldehyde	Amine	Product	Yield	
S3	(phenylacetylene)	4-Cl-C6H4-CHO	piperidine (N-H)	(product structure)	94	114
					93(2nd run)	
					91(3rd run)	
					89(4th run)	
S4	(phenylacetylene)	4-CH3-C6H4-CHO	piperidine (N-H)	(product structure)	90	109
S5	(phenylacetylene)	3-Br-C6H4-CHO	piperidine (N-H)	(product structure)	93	113
S6	(phenylacetylene)	2-HO-C6H4-CHO	piperidine (N-H)	(product structure)	87	106
S7	(propargyl alcohol)	C6H5-CHO	piperidine (N-H)	(product structure)	87	106
S8	(phenylacetylene)	C6H5-CHO	diethylamine (N-H)	(product structure)	83	101
					82(2nd run)	
					80(3rd run)	
					78(4th run)	
S9	(6-ethynyl-2-methoxynaphthalene)	C6H5-CHO	piperidine (N-H)	(product structure)	88	107
S10	(6-ethynyl-2-methoxynaphthalene)	3-Br-C6H4-CHO	piperidine (N-H)	(product structure)	86	104
S11	(phenylacetylene)	C6H5-CHO	morpholine (O, N-H)	(product structure)	93	113

S12	(propargyl alcohol: ≡—OH)	(benzaldehyde CHO)	(morpholine, N-H)	(product structure with OH)	85	103
S13	(phenylacetylene)	(vanillin: OH, O-methoxy, CHO)	(morpholine, N-H)	(product structure, HO, O-methyl)	87	106
S14	(phenylacetylene)	(pentanal, O)	(piperidine, N-H)	(product structure)	85	103
S15	(phenylacetylene)	(benzaldehyde CHO)	(pyrrolidine, N-H)	(product structure)	90	109

*Yields are isolated products based on benzaldehyde after silica-gel column chromatography, **Reaction conditions: Aldehyde (1 mmol), Amine (1 mmol), Alkyne (1.2 mmol), Catalyst (20 mg), Solvent: toluene, Temperature: 100°C, Time: 2 h.
[a] Turn over number (TON) calculated as moles of product formed/moles of catalyst used.

3.3.3.1.1. Recyclability of the catalyst

For practical application, the recyclability of the catalyst is a very important factor in any catalytic study. Here, the recyclability of the catalyst was investigated with the substrates of entry S1, entry S3 and entry S8. The catalyst was recovered by filtration after each experiment. The recovered catalyst was then washed with acetone, dried and reused directly with fresh reaction mixture without further purification up to 4th run for the desired A[3]-coupling and showed only a slight decrease in its catalytic activity (Table 3.4.). The recovered catalyst was further investigated through N2 adsorption–desorption analysis. In comparison to the fresh catalyst of surface area 324 m^2g^{-1}, the specific surface areas of the recovered catalysts decreased (Table 3.1.), which may be due to blockage of the pores by the reactant molecules after each reaction.

3.3.3.1.2. Leaching investigation

To study the heterogeneous nature of the catalyst, a hot filtration test was carried out to investigate whether any leaching of silver occurs during the course of the reaction.

Here, the three component coupling reaction of benzaldehyde, piperidine and phenylacetylene was carried out in toluene for 1 h at 100°C using the Ag-NPs@mmt catalyst. After 1 h, the yield of the product was 65%. The Ag-NPs@mmt nanocatalyst was then filtered off in hot conditions and with the filtrate the reaction was run for another 1 h. But no further increase in the yield of the propargylamine product was observed in the second run. Before the catalytic reaction, the silver content in Ag-NPs@mmt was 0.410 m mol/g (0.0082 m mol Ag in 20 mg catalyst). After 3rd run, silver content in the Ag-NPs@mmt catalyst was found to be 0.405 mmol/g which was marginally decreased. Thus, the nanocatalyst maintains its heterogeneous nature and no leaching of silver occurs during the course of the reaction.

3.3.3.1.3. Proposed mechanism

A plausible reaction mechanism for the one-pot, three component synthesis of propargylamines catalyzed by Ag-NPs@mmt was proposed. It was pictorially illustrated in Scheme 3.1.
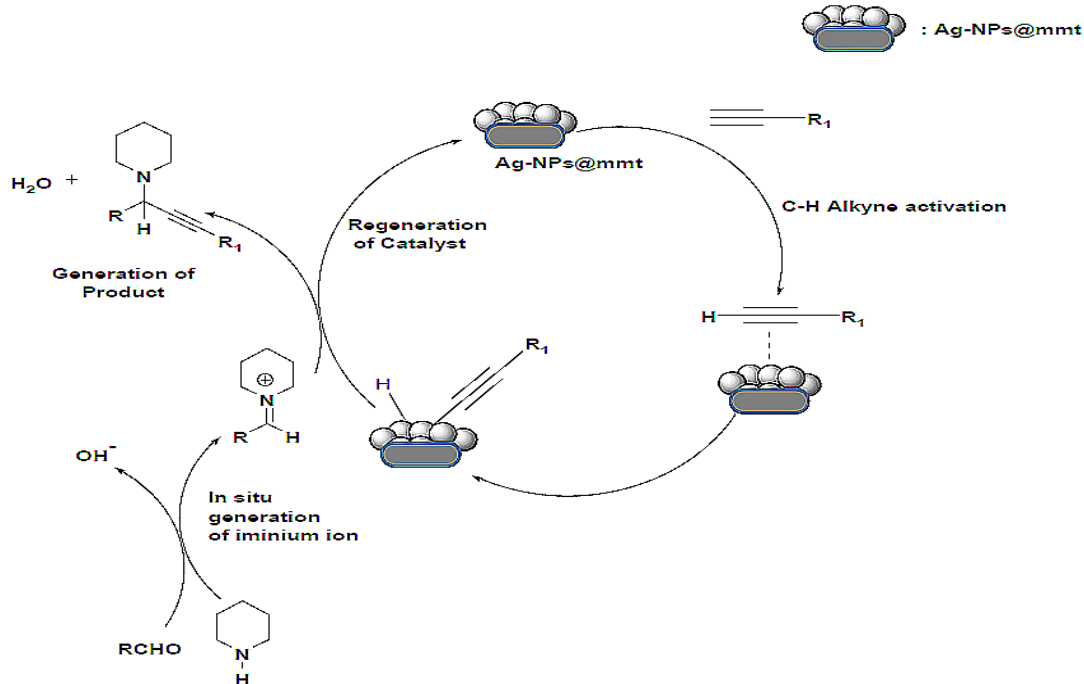
Scheme 3.1. Proposed mechanism for the A^3-coupling reaction.

In the first step, the silver nanoparticles activated the C–H bond of the terminal alkyne to generate a silver-alkylidine complex on the surface of the modified montmorillonite. The second step involved the reaction between the silver-alkylidine complex formed, and the iminium ion which was generated in situ from the reaction between aldehyde and amine, to give the desired product and the catalyst was regenerated. The theoretical by product obtained from the reaction is only water.

3.3.3.1.4. ^{1}H and ^{13}C NMR data of some of the synthesized products.

S1. 1-(1,3-diphenylprop-2-ynyl)piperidine
^{1}H NMR (300 MHz, CDCl$_3$, ppm): δ 1.37-1.65 (m, 6H), δ 2.53-2.57 (t, 4H), δ 4.79 (s, 1H), δ 7.24-7.35 (m, 6H), δ 7.50-7.53 (m, 2H), δ 7.61-7.68 (m, 2H); ^{13}C NMR (75 MHz, CDCl$_3$, ppm): δ 24.66, 26.21, 50.74, 62.43, 86.11, 87.94 , 123.38, 127.23, 128.13-128.34, 128.51-128.75, 131.87, 138.58.

S2. 1-(1-(4-Methoxyphenyl)-3-phenylprop-2-ynyl)-piperidine
^{1}H NMR   (300 MHz, CDCl$_3$, ppm): δ 1.42-1.67(m, 6H), δ 2.53-2.55 (t, 4H): δ 3.81 (s, 3H), δ 4.72 (s, 1H), δ 6.87-6.90 (m, 2H), δ 7.31-7.38 (m, 3H), δ 7.48-7.54 (m, 4H); ^{13}C NMR (75 MHz, CDCl$_3$, ppm): δ 24.54, 26.20, 50.64, 55.27, 61.83, 86.44, 87.75, 113.46-113.68, 123.43, 128.10, 128.34, 129.75,130.64,131.85, 159.06.

S3. 1-(1-(4-Chlorophenyl)-3-phenylprop-2-ynyl) piperidine
^{1}H NMR (300 MHz, CDCl$_3$, ppm): δ 1.32-1.51 (m, 6H), δ 2.51-2.54 (t, 4H), δ 4.76 (s, 1H), δ 7.31-7.34 (m, 6H), δ 7.49-7.58 (m, 4H). ^{13}C NMR (75 MHz, CDCl$_3$, ppm): δ 24.54, 26.27, 50.74, 61.79, 74.30, 81.79, 85.45, 123.20, 128.33-128.56, 129.47, 129.97, 131.94, 132.59, 134.81.

S4. 1-(3-phenyl-1-p-tolylprop-2-ynyl) piperidine

^{1}H NMR (300 MHz, CDCl$_3$, ppm): δ 1.35-1.60 (m, 6H), δ 2.34 (s, 3H), δ 2.41-2.61 (m, 4H), δ 4.75 (s, 1H), δ7.05-7.14 (1H,m), δ 7.30-7.49 (m, 4H), δ7.49-7.53 (m, 4H) . ^{13}C NMR (75 MHz, CDCl$_3$, ppm): δ 21.24, 24.61, 26.30, 50.77, 62.24, 81.75, 86.48, 121.89, 123.51, 128.14-129.93, 131.91, 132.60, 135.62, 137.18.

S7. 5-phenyl-5-(piperidin-1-yl) pent-3-yn-1-ol

^{1}H NMR (300 MHz, CDCl$_3$, ppm): δ 1.37-1.42 (m, 4H), δ 2.08-2.17 (m, 4H), δ2.45-2.61(m,5H), δ3.72-3.79(m,2H), δ 4.53 (s, 1H), δ7.26-7.61 (5H, m). ^{13}C NMR (75 MHz, CDCl$_3$, ppm): δ 23.31, 24.56, 25.85, 50.68, 60.63, 61.22, 62.08, 66.70, 74.72, 78.57, 84.36, 126.76, 127.62, 128.08-128.66, 137.90.

3.3.3.2. Baeyer-Villiger oxidation of different ketones catalysed by Ag-NPs@mmt

The synthesized Ag-NPs@mmt was utilized as catalyst precursor for the well-known Baeyer-Villiger oxidation of different cyclic and aromatic ketones under solvent free conditions using H$_2$O$_2$ as oxidant at room temperature (RT). To optimize the reaction conditions (i.e. catalyst amount, reaction time), a series of oxidation reactions were carried out using cyclohexanone as the model substrate. A control reaction was carried out to test the requirement of a catalyst by stirring the model substrate at RT in the absence of the catalyst. No conversion was observed in this case. The use of Ag-NPs@mmt as catalyst under solvent free condition gave a maximum conversion 99% in 4h in the model reaction. When the same reaction was carried out using only modified montmorillonite clay as catalyst, no conversion was observed. Thus the catalytic reaction takes place in presence of Ag-NPs. The effect of various catalyst amounts was also studied to optimize Ag content on the catalytic activity and we have found that 25 mg catalyst is sufficient for the catalytic Baeyer-Villiger oxidation (Table 3.5.).

Table 3.5. Effect of catalyst amount on Baeyer-Villiger oxidation

Entry	Catalyst	Time (h)	Catalyst amount (mg)	*Conversion (%)
1	Ag-NPs@mmt	4	10	72
2	Ag-NPs@mmt	4	15	79
3	Ag-NPs@mmt	4	20	88
4	Ag-NPs@mmt	4	25	99
5	Ag-NPs@mmt	4	30	99

* **Based on GC analysis.**

The high conversion of the product (Maximum 99%), excellent selectivity and less reaction time (4 hour) for the reaction indicate the efficacy of the catalyst at RT (Table 3.6). In this work, we used different cyclic and aromatic ketones and all the ketones yield the desired product with a very good conversion. The model reaction gives maximum 99% conversion with 100% selectivity when Ag-NPs@mmt is used as catalyst (entry S2 in Table 3.6.). In this study, it is observed that cyclic ketones showed a slightly higher conversion than aromatic ketones. This may be due to higher stability of aromatic ketones than cyclic ketones which decreases their reactivity. Again substituted ketones showed slightly lower conversion than unsubstituted one.

The recyclability of the catalyst for Baeyer-Villiger oxidation of ketones was investigated with the substrate of entry S2, entry S4 and entry S7 (Table 3.6.). The catalyst was recovered by simple filtration technique after each experiment. It was then washed with acetone, dried and reused directly for another run without further purification for the desired Baeyer-Villiger oxidation. The recovered catalyst was used up to the 4th run and showed only a slight decrease in activity (Table 3.6.). The recovered catalyst was further investigated through TEM analysis. In the TEM analysis of the recovered catalyst (after 4th run), it was found the sizes of Ag-NPs are still below 10 nm (Fig. 3.11).

Table 3.6. Ag-NPs@mmt catalysed Baeyer-Villiger oxidation of ketones.
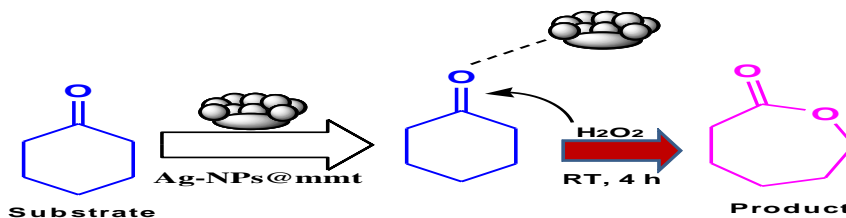
Entry	Substrate	Product	Conversion*(%)	Selectivity (%)
S1.			90	100
S2.			99 98 (2nd run) 96 (3rd run) 93 (4th run)	100
S3.			90	96
S4.			89 87 (2nd run) 85 (3rd run) 82 (4th run)	94
S5.			84	99
S6.			79	98
S7.			91 89 (2nd run) 87 (3rd run) 86 (4th run)	96
S8.			88	93
S9.			86	90

*From GC analysis; Reaction conditions:** Substrate (2mmol), H_2O_2 (20 mmol), Catalyst (25 mg), solvent free, room temperature, Time: 4 h.
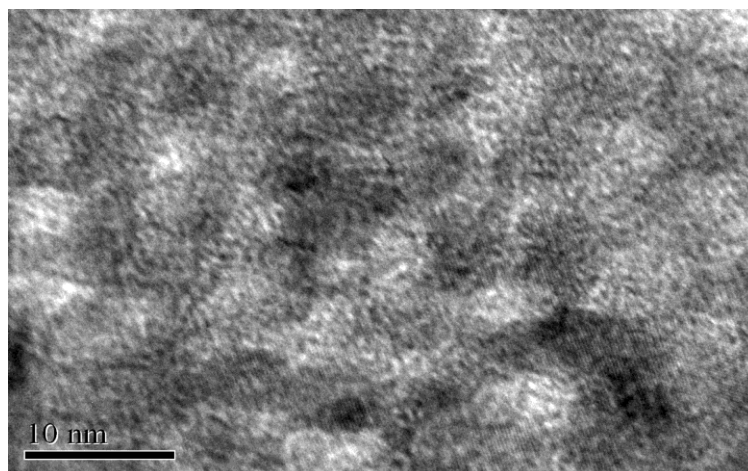
Fig. 3.11. TEM image of recovered Ag-NPs@mmt after 4th run.

A plausible mechanism for the Baeyer-Villiger oxidation with H_2O_2 as oxidant was proposed (Scheme 3.2.). Initially, the substrate is adsorbed on the catalyst surface and the carbonyl group gets activated. Hydrogen peroxide then attacks at the more electrophilic carbonyl carbon forming the Criegee intermediate. After rearrangement, a new product (cyclic ester) is obtained with a theoretical byproduct H_2O.
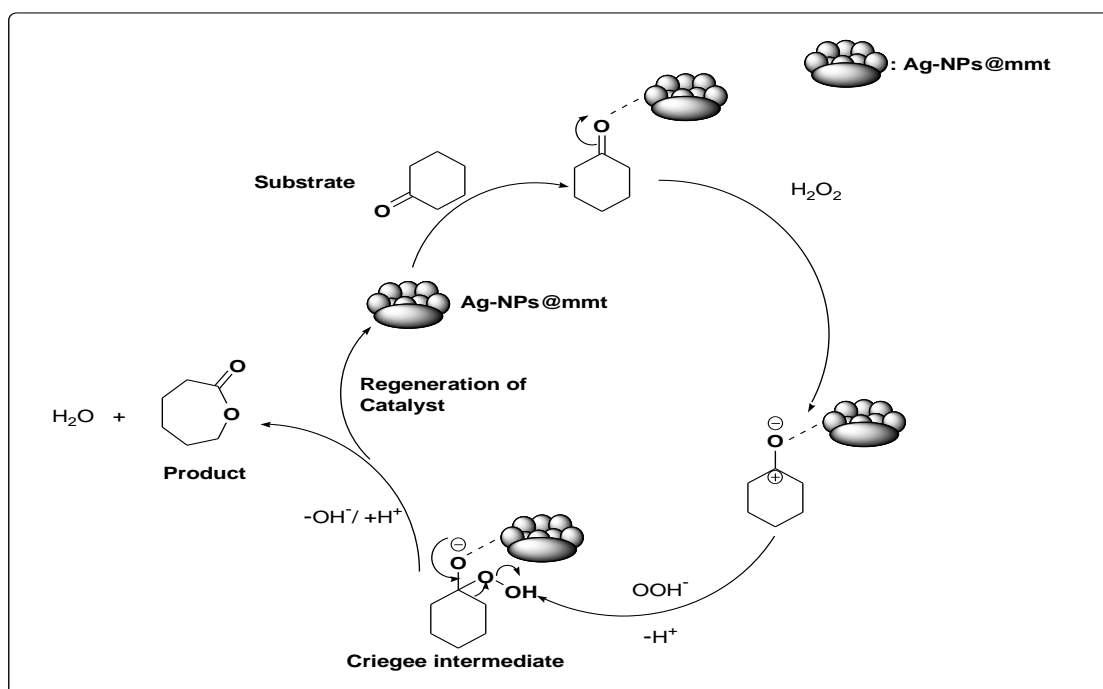
Scheme 3.2. Proposed mechanism for Baeyer-Villiger oxidation.

3.4. Conclusion

The modified Montmorillonite clay served as an excellent support for nanoparticles formation and limited the growth of the particles up to desired nanosize range. Electron microscopic and spectroscopic data confirmed the formation of Silver nanoparticles (Ag-NPs) into the micro and mesopores of modified montmorillonite. The Ag-NPs were spherical in shape and size below 10 nm. These nanoparticles demonstrated high catalytic activities in A^3-coupling reactions of aldehyde, amine and alkyne for synthesizing propargylamine derivatives with high yield under mild reaction conditions in a heterogeneous system. The silver nanocatalysts also showed excellent catalytic activity in the catalytic Baeyer-Villiger oxidation of cyclic and aromatic ketones using H_2O_2 as oxidant under solvent free conditions. Further, the nanocatalysts were reused for new batch of reactions without significant loss of their activity.

Chapter-4

Synthesis, characterization and applications of Fe_3O_4 nanoparticles stabilized on montmorillonite

4. Synthesis, characterization and applications of Fe_3O_4 nanoparticles stabilized on montmorillonite

4.1. Introduction

Metals and metal oxide nanoparticles exhibit a wide range of applications in recent time intrigued by distinguishable differences compared to their corresponding bulk metals [1, 7]. The potential exploitation of nanoparticles based materials in different fields such as catalysis, sensor, biosciences etc. is a challenge for the researchers [72, 91]. In the recent years, there has been increasing interest in 'iron' for use in catalysis and in the development of sensor as it is the cheapest, most abundant metal for use. Among the class of nanostructured materials, the works on magnetic nanoparticles is of current interest, due to their high importance in fundamental science and advanced technology [92]. But the magnetic nanoparticles of particle size below 10 nm have a great tendency to deform and aggregate during the course of any chemical applications which decreases the reactivity of the material [94-95]. The aggregation of nanoparticles also changes the thermal and chemical stability of the nanomaterials. Thus to prevent the agglomeration, the nanoparticles must be stabilized by using some suitable supports for better applications. Recently, the uses of micro and mesoporous materials as stabilizer have gained importance in their use in catalysis, sensors, adsorbents and electrochemical studies [96]. Montmorillointe clay is environmentally benign, cheap, easy to modify and is a very good stabilizer / support and catalyst [4, 26]. The acid modification of montmorillonite clay breaks the layered structure of the clay to give a high surface area and porous matrix having micro and mesopores with diameters in the range 0-10 nm [75, 97]. In the present work, we have reported synthesis of magnetic Fe_3O_4 nanoparticles using both modified and unmodified montmorillonite clay as stabilizer under mild condition. The magnetic nanopartilcles with modified clay has been utilized as magnetically recoverable heterogeneous catalyst precursor (MRC) for the synthesis of different dihydropyrimidinones via the Biginelli reaction under green condition. The magnetic nanoparticles with unmodified clay has been used in surface modification of Gold and Platinum working electrodes for the development of new electrochemical

sensor for selective determination of Dopamine and Ascorbic acid by square wave voltammetric technique. The montmorillonite K10 clay was modified by refluxing it with mineral acid (HCl) under controlled conditions to generate a matrix having high surface area and contain micro and mesopores. These micro and mesopores act as 'host' for the *in situ* generation of magnetic Fe_3O_4 nanoparticles and limits the growth of the nanoparticles upto desired range.

Dopamine (DA) is one of the most important catecholamine neurotransmitter which plays an important role in several important physiological functions, such as renal, hormonal, central nervous and cardiovascular functions [98-99]. The deficiency of dopamine leads to neurological diseases such as Parkinson's disease, Alzheimer's disease and Schizophrenia [100-101]. In addition to that dopamine also plays an important role in drug addiction and some manifestations of HIV [102-103]. Thus, the detection of concentration of dopamine in body fluids is of great significance in the field of clinical diagnostics. Ascorbic acid (AA), on the other hand, is one of the important vitamins which can prevent scurvy. Besides, ascorbic acid also takes part in a number of biological reactions. Ascorbic acid (vitamin c) is often added to various food products and pharmaceuticals due to its antioxidant and pH regulatory properties [104]. In recent years, the voltammetric studies on neurotransmitters in the extracellular fluid of the central nervous system have received significant interest for the development of new voltammetric sensors [104]. Both DA and AA are electrochemically active compounds and show similar electrochemical properties. As a result, they complicate their electrochemical identification when both DA and AA are present in the solution. The concentration of AA, in human bio-fluids, is generally reported to be 100 to 1000 times higher than that of DA [105]. When conventional electrodes are used, ascorbic acid oxidizes at a potential close to that of DA and exhibits an overlapping voltammetric response. Then it becomes difficult for the user to identify their respective electrochemical signal. To solve this problem, the working electrodes are modified chemically by using different electrode modifying agents. The advantage of using modified electrode is that the modified electrode can lower the oxidation potential of the target analyte and also increase the sensitivity, thus improving the selectivity [105].

Various sensing materials with high stability, catalytically active and excellent conductivity, such as metal and metal oxide nanocomposites, polymers, carbonaceous materials, have been used for the modification of bare electrode surfaces [98-100]. Some of the recent works on electrode modification for simultaneous detection of DA and AA are- bi-nuclear copper^{2+} complex as modified GC electrode [99], 2,4-dinitrophenylhydrazine@phosphatidylcholine modified GC electrode [101], composite polymer film modified electrode [106], GC electrode modified with dendrimers containing gold metal nanoparticles [107], carbon paste electrode modified with polypyrrole / ferrocyanide film [108], gold nanoparticles distributed poly(4-aminothiophenol) modified electrode [109], poly(acrylic acid) multi walled carbon nanotube (MWCNT) composite film modified GC electrode [110]. But improvement for the stability, sensitivity and selectivity of the modified electrode towards dopamine and ascorbic acid is still an important issue among researchers. In this work, we have reported synthesis of Fe_3O_4 nanoparticles using montmorillonite K-10 as support by an *in situ* approach. The synthesized nanocomposite was used to modify the surface of Gold and Platinum electrode. The modified gold and platinum electrodes were able to distinguish voltammetrically between DA and AA in presence of other biologically important compounds / ions.

Pyrimidinones or Dihydropyrimidinones (DHPMs) are well known for their wide range of pharmaceutical and therapeutic activities such as anticancer, anti-inflammatory, antibacterial, antifungal activities [20-21]. Some of the clinically important antiretroviral agents such as AZT, DDC and DDI possess the pyrimidine scaffold [111-113]. The marine natural alkaloid product Batzlladine B is found to be potent HIV gp-120-CD4 inhibitors and it contains the dihydropyrimidine-5-carboxylate as a sole unit [111-116]. The Biginelli reaction involves three component one-pot condensations of β-ketoester, aldehyde and urea to give dihydropyrimidinone derivative. But the main problem occurred in the reaction is the low to moderate yield of product is obtained when substituted aldehydes are used [115-116]. In recent years, different types of homogeneous and heterogeneous catalysts were used for the synthesis of different dihydropyrimidinone

derivatives [115-119]. Although both homogeneous and heterogeneous catalysts were used in this reaction, the uses of heterogeneous catalysts get the advantages over homogenous ones, because of easy separation and reusability of the catalyst and simple isolation of the desired product. Some of the recently used heterogeneous catalytic system for DHPMs synthesis are- Al-MCM-41, $FeCl_3$ embedded in Al-MCM-41, EPZ10, heteropolyacids such as $H_3PW_{12}O_{40}$ and $H_3PMo_{12}O_{40}$, Nanomagnetic-supported sulphonic acid, β-Cyclodextrin-propyl sulfonic acid and Lewis acid-surfactant-combined catalyst are used for the synthesis of dihydropyrimidinones [115-119]. But, due to stringent and growing environmental regulations, the researchers try to develop ecofriendly and sustainable synthetic methods which become one of the important requirements for any chemical industry [26]. The strategy of magnetic separation of the catalysts attracted much attention over any other technique as it prevents the loss of catalyst. Here, we have reported synthesis of magnetic Fe_3O_4 nanoparticles using modified montmorillonite clay as stabilizer by an *in situ* approach. The synthesized nanocomposite has been used as a magnetically recoverable heterogeneous catalyst (MRC) precursor for the synthesis of different dihydropyrimidinones derivatives under green reaction conditions. The magnetic nanocatalyst shows its catalytic activity for several runs without any significant loss in activity. The montmorillonite K10 clay is modified by treatment with mineral acid (HCl) under controlled conditions to generate a matrix having high surface area and contain micro and mesopores. The modified montmorillonite clay acts as a support for the *in situ* generation of magnetic Fe_3O_4 nanoparticles (Fe_3O_4@mmt) and controls the sizes of the nanoparticles with in 10 nm.

In this chapter, we report synthesis of Fe_3O_4 magnetic nanoparticles using both unmodified and modified montmorillonite clay as stabilizer and their utilization in the development of voltammetric sensor for dopamine and ascorbic acid and as magnetically recoverable heterogeneous catalyst for the one pot synthesis of dihydropyrimidinones.

4.2. Experimental

4.2.1. Preparation of Support

Montmorillonite K10 (10.0 g) was dispersed in 200 mL 2M HCl in a round bottom flask. The mixture was then refluxed for 2 hour. After cooling, the supernatant liquid was discarded and the activated montmorillonite clay was washed repeatedly by deionised water. The removal of chloride ions from the clay was confirmed by the AgNO$_3$ test. The activated clay was dried at 50°C in air oven for 12 h. The solid product obtained was named as modified montmorillonite.

4.2.2. Preparation of clay supported magnetic Fe$_3$O$_4$ nanoparticles

0.5 g of both unmodified and modified montmorillonite was dispersed in 50 mL double distilled water separately and 0.5 mmol of FeCl$_2$.4H$_2$O and 1 mmol FeCl$_3$ were added to both the solutions. The solution mixtures were stirred vigorously for 6 h and degassed with nitrogen. After that 10 mL of aqueous NH$_3$ solution was added drop wise to both the stirring solutions. The solutions turned black immediately and were stirred for another 1 h. The black reaction products were recovered and washed with deionised water several times and then dried in desiccator for 15 h. The composites were designated as Fe$_3$O$_4$@K10 and Fe$_3$O$_4$@mmt respectively.

4.2.3. Preparation of modified electrode

10 mg of Fe$_3$O$_4$@ K10 nanocomposite was dispersed in a solution of 0.5 mL of dichloromethane and 0.2 mL of styrene. 1.0 μL of the solution was placed on the tip of pre-cleaned platinum (Pt) and gold (Au) electrode surface with the help of a micropipette. The electrodes were allowed to dry. The modified platinum and gold electrodes were designated as Pt/ Fe$_3$O$_4$@K10 and Au/ Fe$_3$O$_4$@K10 respectively.

4.2.4. Typical procedure for the synthesis of Dihydropyrimidinones (DHPMs)

Aldehyde (1 mmol), β-ketoester (1 mmol), urea (1.5 mmol), 20 mg catalyst (Fe$_3$O$_4$@mmt) and 5 mL ethanol were stirred at 78 ^{o}C in a 25 mL round bottom flask for stipulated time period. The progress of the reaction was checked from time to time by thin layer chromatography (TLC). At the end of the reaction, the solid catalyst was

recovered magnetically with the help of a magnetic needle retriever. The solid product obtained was finally recrystallized to give the pure product. The isolated pure products were characterized by ^{1}H and ^{13}C NMR and CHNS elemental analysis.

4.3. Results and discussion

4.3.1. Characterization of Support

The parent montmorillonite K10 and modified montmorillonite were well characterized with the help of different sophisticated analytical instruments like Powder-XRD, N_2 adsorption-desorption, FTIR, SEM-EDX analysis.

4.3.1.1. X-ray diffraction

The parent montmorillonite K10 showed an intense basal reflection at 7.10^o 2θ corresponding to a basal spacing of 12.7 Å (Fig. 4.1). During acid treatment, the reflection intensity of the peak decreased with time and no peak was observed after 2h acid activation. Acid treatment disrupted the layered structure of the clay and appearance of a low intense reflection at 20-30° 2θ confirmed the formation of amorphorous silica [65].
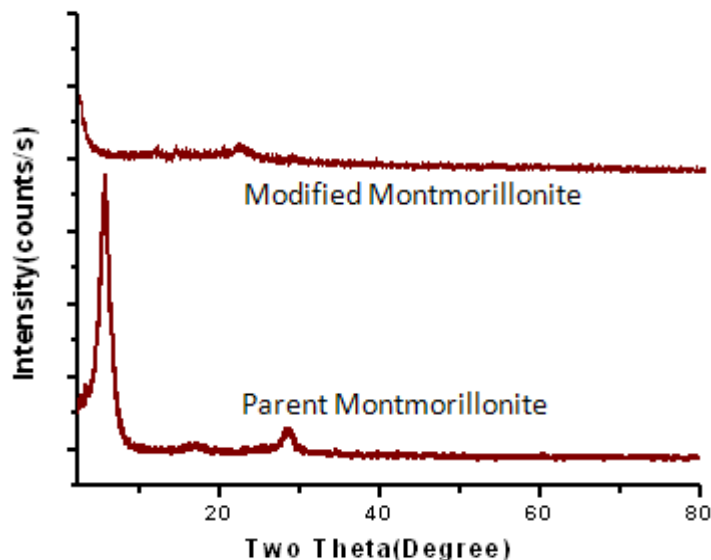

Fig. 4.1. Powder XRD pattern of parent and modified montmorillonite.

4.3.1.2. Specific surface area and pore size distribution

The modified montmorillonite contained micro (< 2 nm) and mesopores (2-50 nm) with average pore diameters ~ 4.88 nm, a high specific surface area upto 416 m^2/g and a large specific pore volume of ~ 0.65 cm^3/g (Table 4.1). This observation may be due to the leaching of Al from the octahedral sites of the clay matrix during acid treatment which generated micro and mesopores on the clay surface. The adsorption-desorption study showed type-IV isotherm [Fig. 4.2. (a)] with a H3 hysteresis loop at P/P$_o \sim 0.4$-0.9, indicating mesoporous solid. The differential volumes versus pore diameter plot [Fig. 4.2. (b)] showed relatively narrow pore size distributions. On the other hand, the unmodified clay showed a relatively low surface area of 192 m^2/g, average pore diameters ~ 3.82 nm and specific pore volume of ~ 0.30 cm^3/g.
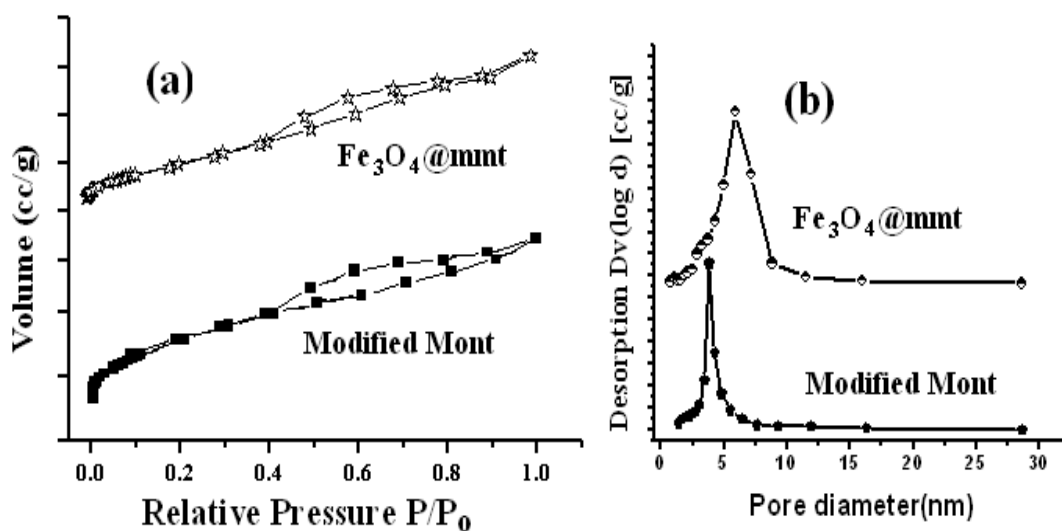

Fig. 4.2. (a) N$_2$ adsorption / desorption isotherms and (b) BJH pore size distribution curves of modified montmorillonite and Fe$_3$O$_4$@mmt.

4.3.1.3. FTIR spectroscopic study

The raw montmorillonite K10 showed an intense absorption band at ~ 1051 cm^{-1} for Si-O stretching vibrations of tetrahedral sheet [Fig. 4.3.]. After acid modification, the band shifts from ~ 1051 cm^{-1} to ~ 1091 cm^{-1} indicating the change in bonding environment

in the clay matrix. The formation of amorphous silica phase is also substantiated by the alteration of the band at 799 cm^{-1} which is attributed to the vibrations of amorphous SiO_2 [29 b].
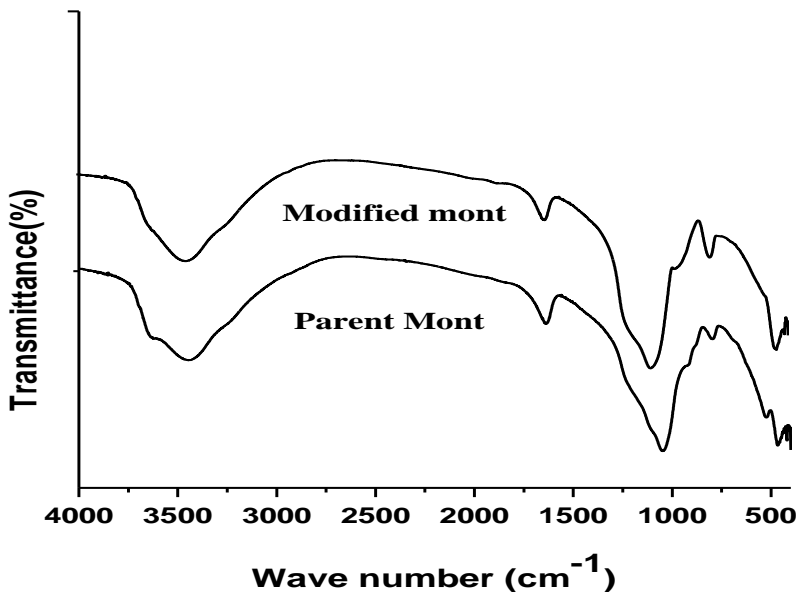

Fig. 4.3. FTIR spectrum of parent and modified clay.

4.3.1.4. SEM-EDX investigation

The SEM study of unmodified clay showed the uniform layered structure of the clay [Chapter 2; Fig. 2.5(a)]. EDX analysis of unmodified clay [Chapter 2; Fig. 2.5(b)] also showed the presence of predominant amounts of Si and Al on the clay surface. Acid treatment leached out most of Al from octahedral sites and developed pores on the clay matrix. The typical SEM image of modified montmorillonite [Chapter 2; Fig. 2.5(c)] showed the formation of pores on the clay surface. The EDX analysis at the surface [Chapter 2; Fig. 2.5(d)] revealed that predominant amounts of Si compared to Al was present on the surface.

4.3.2. Characterization of clay supported magnetic Fe_3O_4 nanoparticles

The powder XRD pattern suggested face centred cubic lattice (fcc) lattice type arrangement of Fe_3O_4-nanoparticles in both unmodified and modified clay [Fig. 4.4 (a) and (b)] [120].
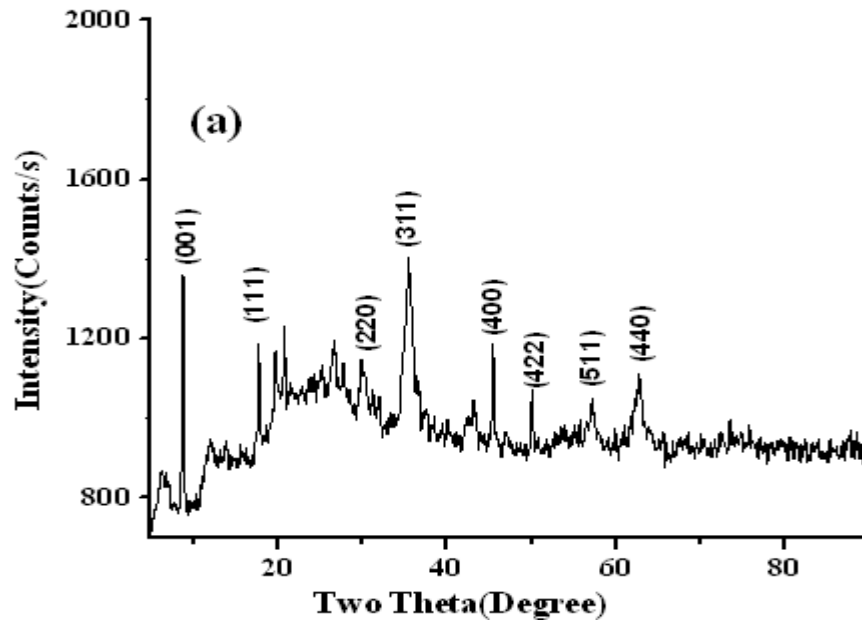

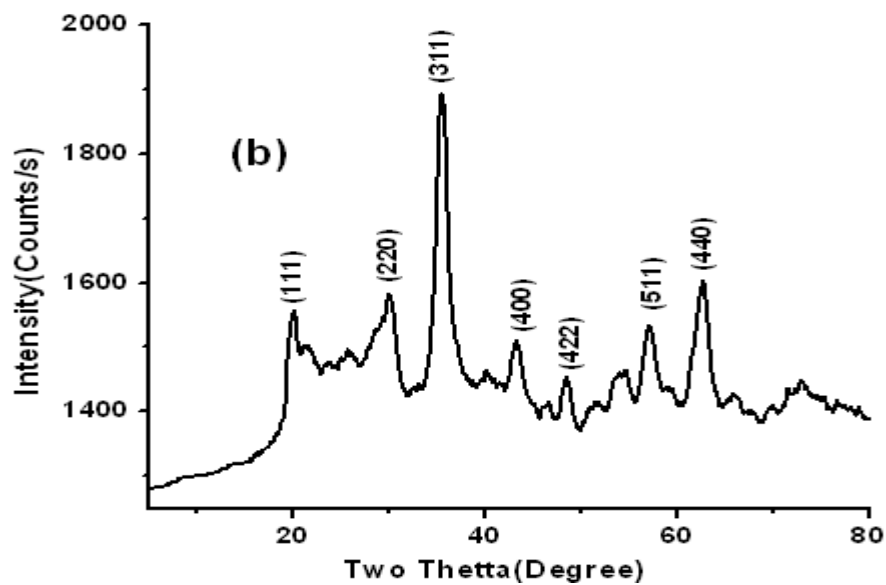**Fig. 4.4.** (a) Powder XRD pattern of Fe_3O_4@K10

Fig. 4.4. (b) Powder XRD pattern of Fe_3O_4@mmt.

The seven reflections were assigned to the (111), (220), (311), (400), (422), (511) and (440) diffraction of a cubic face-centered (fcc) lattice of magnetic Fe_3O_4 nanoparticles. The nanocomposite with unmodified clay showed an additional diffraction peak at $7.10^o 2\theta$ due to basal reflection (001) of montmorillonite clay.

TEM analysis showed well dispersed Fe_3O_4 nanoparticles on the surface of both K10 [Fig. 4.5. (a)] and modified montmorillonite [Fig. 4.5. (b)]. It was observed that the nanoparticles formed a magnetic nanocluster with particle size below 10 nm. The HRTEM [Fig. 4.5.(c)] and SAED (Selected Area Electron Diffraction) pattern [Fig. 4.5. c (inset)] of Fe_3O_4@mmt indicated the crystalline nature of the magnetic nanoparticles was maintained on the clay surface.
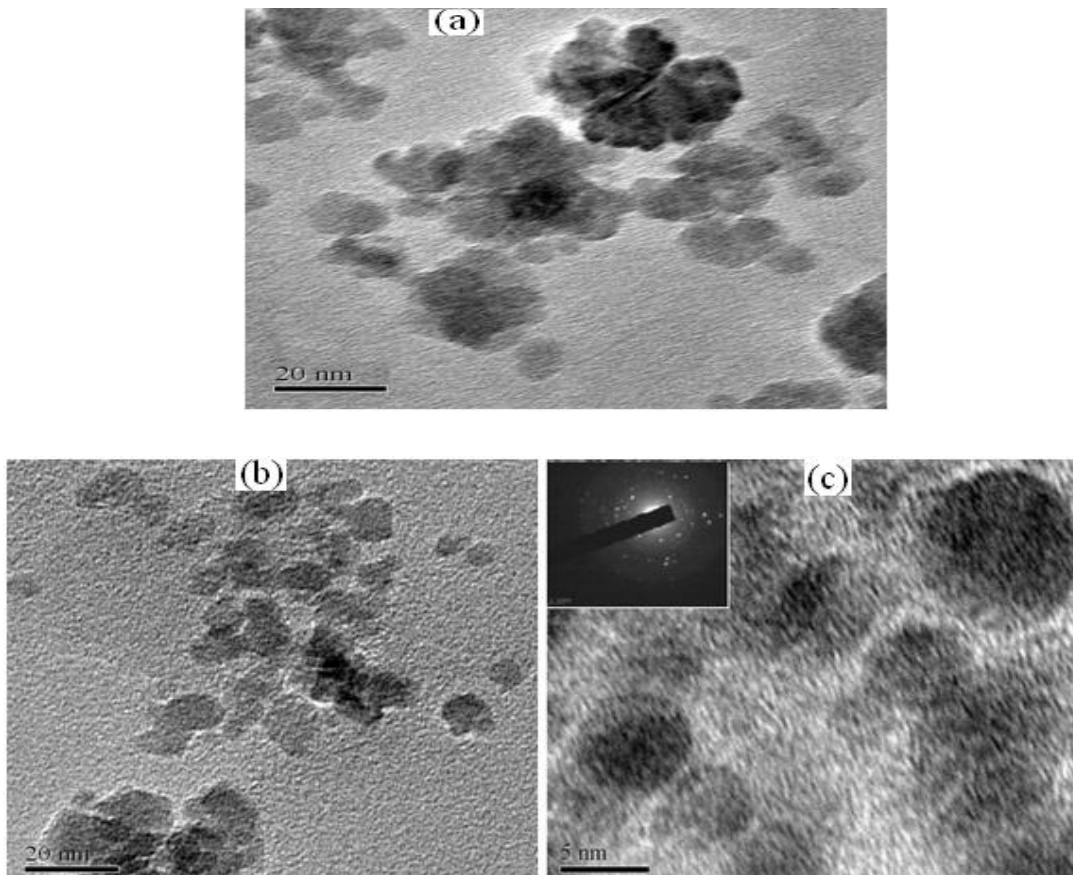

Fig. 4.5. **(a)** TEM image of Fe_3O_4@K10 (unmodified clay), (b) TEM image and (c) HRTEM and SAED pattern (inset) of Fe_3O_4@mmt.

To determine the electronic state of the elements and purity, XPS analysis was performed for Fe_3O_4 nanoparticles. XPS analysis gave a broad and narrow scan spectrum of Fe_3O_4 nanoparticles [Fig. 4.6.]. Fe_3O_4 nanoparticles stabilized on modified montmorillonite showed peaks at 710.8 eV for $Fe2p_{3/2}$ doublet and at 724.1 eV for $Fe2p_{1/2}$ doublet from iron oxide. The peak obtained at 529.4 eV was due to O_{1s} [Fig. 4.6. (inset)]. Further, no any other satellite peak at 719 eV was observed in the XPS spectrum and this confirmed the absence of Fe^{3+} in γ-Fe_2O_3 in the nanocomposite [121].
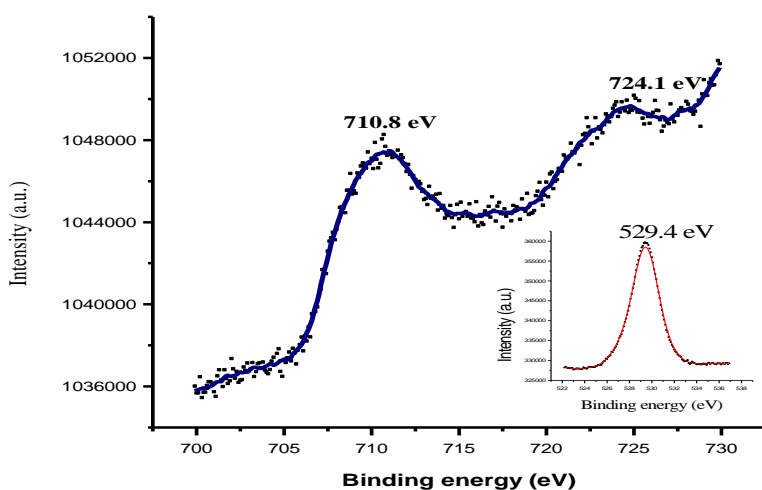

Fig. 4.6. XPS spectrum of Fe_3O_4@mmt.

From N_2 adsorption-desorption study, it is observed that there is an appreciable decrease of the specific surface area and the specific pore volume after supporting Fe_3O_4 nanoparticles (Table 4.1.) which might be due to clogging of some pores by Fe_3O_4 nanoparticles. Fe_3O_4 supported modified montmorillonite show type IV isotherm with a H3 hysteresis loop at P/P_o ~0.4-0.9 [Fig. 4.2.]. This confirms that the highly ordered porous structure of clay is maintained even after supporting the Fe_3O_4 nanoparticles. But, increase of pore diameter may be due to rupture of some smaller pores to generate bigger ones during the formation of magnetic Fe_3O_4 nanoparticles into the pores [4]. The Fe

contents in Fe_3O_4@mmt as analyzed by ICP-AES, reveals the presence of 0.295 mmol Fe in 100 mg Fe_3O_4@mmt nanocomposite (0.059 mmol Fe in 20 mg nanocomposite).

Table 4.1. Surface properties of Fe_3O_4@mmt and modified clay.

Samples	Surface properties of support/catalysts		
	Specific surface area (m^2/g)	Average pore diameter (nm)	Specific pore volume (cm^3/g)
Modified Mont	416	4.88	0.65
Fe_3O_4@mmt ⌐Catalysis⌐ After run Fresh →	308	6.46	0.51
1	265	7.10	0.42
2	225	8.02	0.36
3	204	9.14	0.32

4.3.3. Electrochemical applications of Fe_3O_4@K10 nanocomposite

Here, we have used the Fe_3O_4@K10 nanocomposite to modify surface of gold (Au) and platinum (Pt) working electrodes. The modified electrodes have been utilized as voltammetric sensors for selective determination of DA and AA.

4.3.3.1. Electrochemistry of Au/Fe_3O_4@K10 and Pt/Fe_3O_4@K10 modified electrode

Square wave voltammograms of Au/Fe_3O_4@K10 and Pt/Fe_3O_4@K10 electrode in phosphate buffer at pH 7.0 and at scan rate 0.1 Vs^{-1} were recorded using 0.1 M $NaNO_3$ as the supporting electrolyte (Fig. 4.7.). The modified Au and Pt electrode in phosphate buffer showed a peak with redox potential + 0.105 V and + 0.091V respectively. To study the effect of pH of the electrolytic medium on the electrochemistry of both the modified electrodes, the pH of the solution was adjusted from 5.0 to 8.5. But the change in pH did not show any affect to the peak position and redox potential.
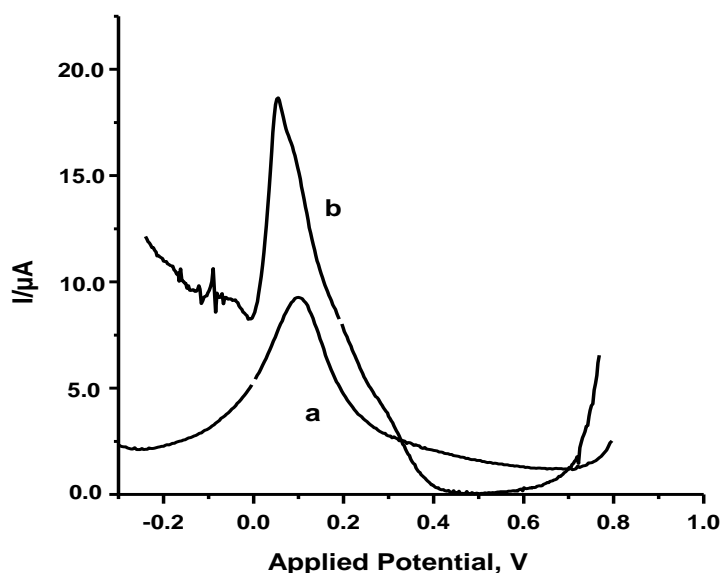
Fig. 4.7. Square wave voltammogram of (a) Au/Fe$_3$O$_4$@K10 and (b) Pt/Fe$_3$O$_4$@K10 modified electrode in phosphate buffer (Ag-AgCl is the reference electrode, scan rate: 0.1 V s^{-1})

4.3.3.2. Selective voltametric determination DA and AA by modified Au and Pt electrode

The bare gold (Au) and platinum (Pt) electrodes were first used to analyze the voltammetric responses in the mixture of DA and AA. The bare Au electrode showed a peak at redox potential − 0.102 V while the Pt electrode showed the same at redox potential + 0.108 V in the mixture of DA and AA having concentration 0.01mM and 0.1mM respectively [Fig. 4.8. (a)]. Thus, the bare Au and Pt electrodes are unable to detect DA and AA when both are present in the solution. On the other hand, the use of modified Au electrode in the mixture showed two peaks at   + 0.218V and + 0.672V respectively. The peak at + 0.218 V was due to DA and the peak at + 0.672 V was due to AA [Fig. 4.8. (b)]. The respective peak positions of DA and AA were confirmed by either increasing the concentration of DA keeping the concentration of AA fixed or vice versa. With increase in concentration of DA, the peak height i.e. peak current at + 0.218 V increased and it confirmed that the peak at + 0.218V was due to DA [Fig. 4.8. (c)]. Similarly, addition of AA to the mixture of DA and AA increased the peak

current at + 0.672 V and this substantiated the peak obtained at this potential was due to AA [Fig. 4.8. (d)].
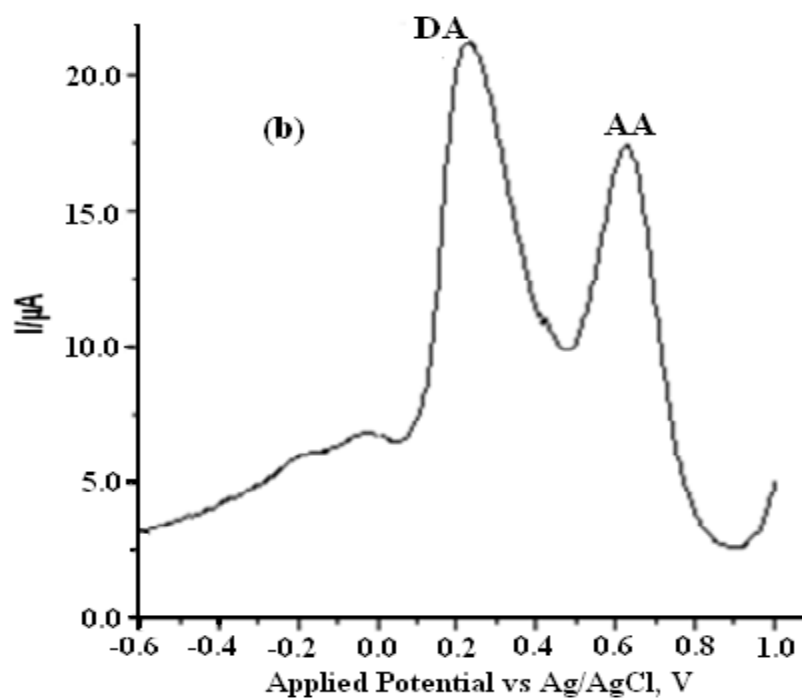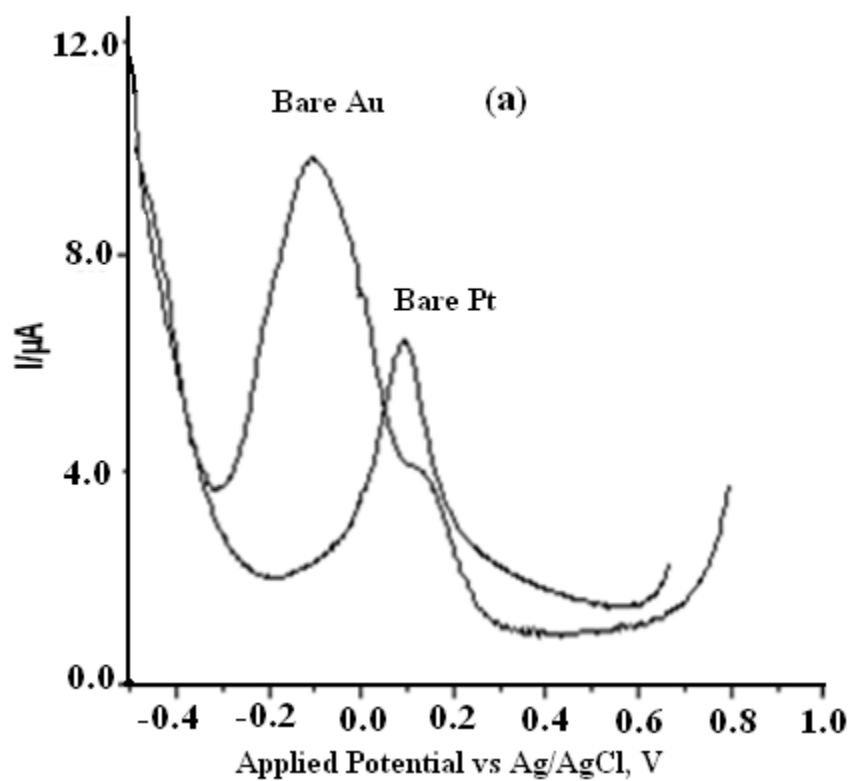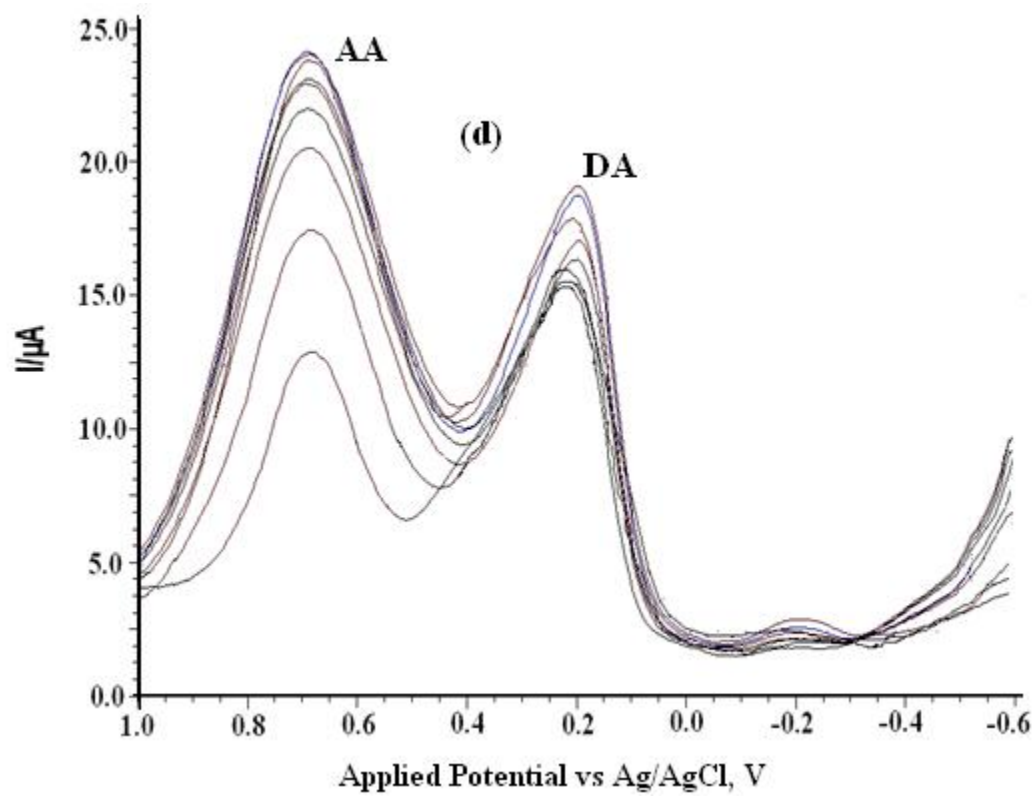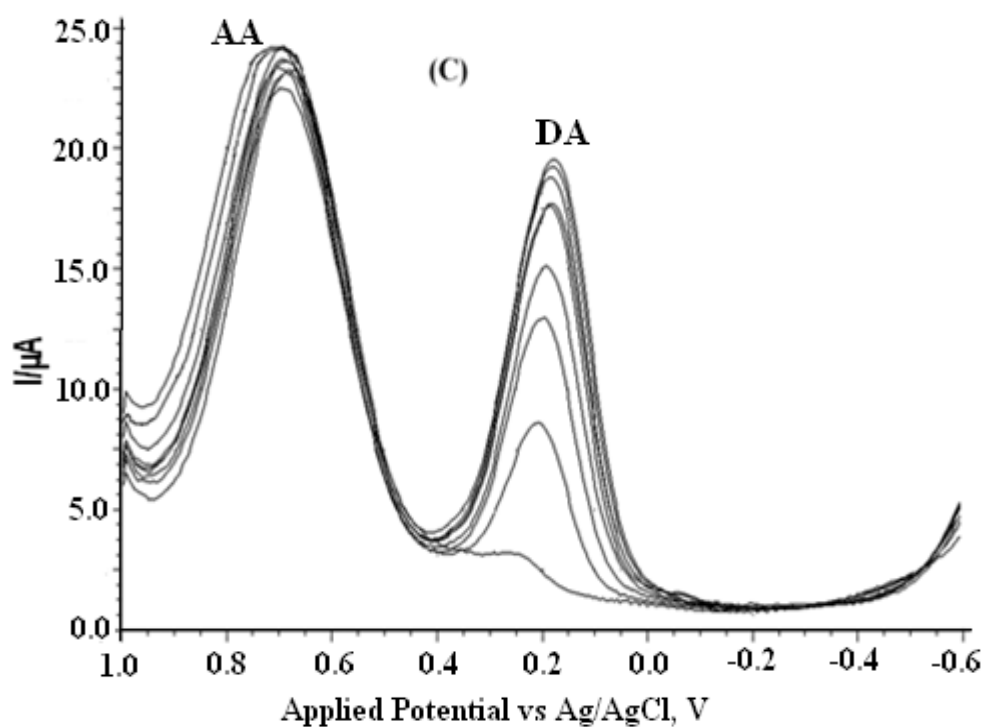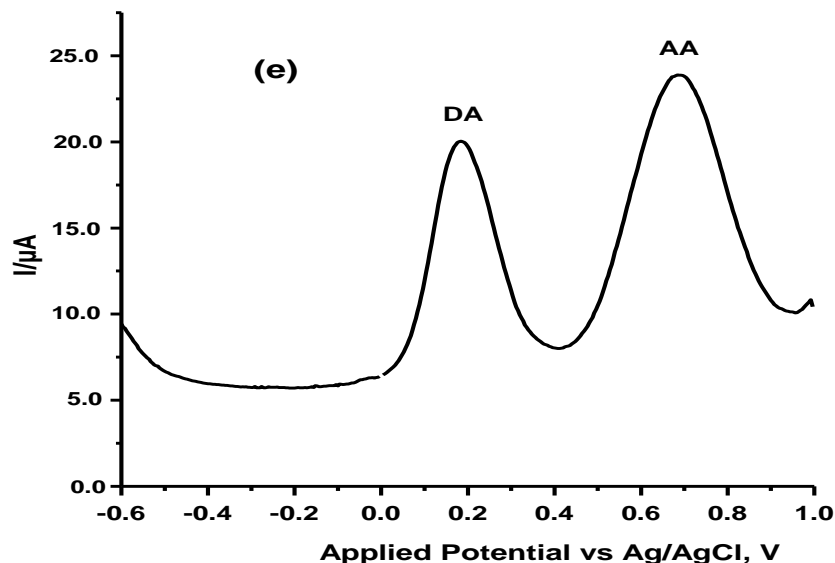
Fig. 4.8. The square wave voltammetric response of (a) the bare Au and Pt electrode in the mixture of DA and AA, (b) Modified Au electrode in the Mixture of DA and AA, (c) Modified Au electrode with increase concentration of DA, (d) Modified Au electrode with increase concentration of AA, and (e) Modified Pt electrode in the mixture of DA and AA.

The plots of current against concentrations of DA and AA were found to increase linearly with concentrations in the electrolytic medium (Fig. 4.9.). When the modified Pt electrode was used in the selective determination of DA and AA, two peaks were obtained, one due to DA at + 0.182V and the other due to AA at + 0.681V [Fig.4.8. (e)]. In this case, the respective positions of DA and AA were confirmed by same procedure as before.
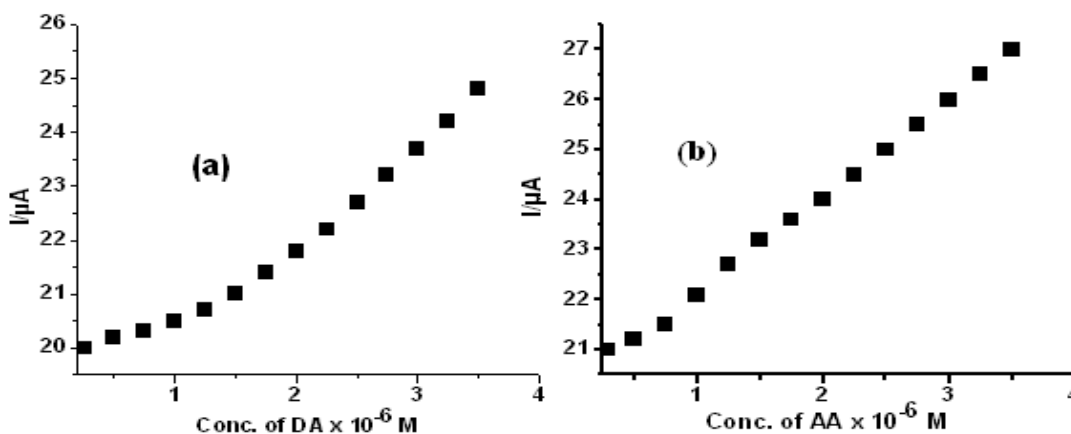
Fig. 4.9. Plot of SWV current versus concentration of DA (a) and AA (b).

83

4.3.3.3. Influence of other substances in the voltammetric detection of DA and AA

To study the influence of other substances in the voltammetric determination of DA and AA, the experiment was performed by using both the modified electrodes in presence of some biologically important ions / compounds such as Na^+, K^+, Mg^{2+}, Ca^{2+}, Zn^{2+}, Fe^{2+}, cholesterol and glucose. In the result, it was found that the presence of these biologically important ions / compounds did not show any interference in the electrochemistry of DA and AA (Fig. 4.10.).

Fig. 4.10. Square wave voltammogram of (a) modified Au and (b) modified Pt in mixture of DA and AA in presence of some biologically important ions/compounds.

4.3.4. Catalytic applications of Fe₃O₄@mmt magnetic nanocomposite

4.3.4. Catalytic applications of Fe$_3$O$_4$@mmt magnetic nanocomposite

4.3.4.1. Synthesis of dihydropyrimidinones (DHPMs) using Fe$_3$O$_4$@mmt as catalyst

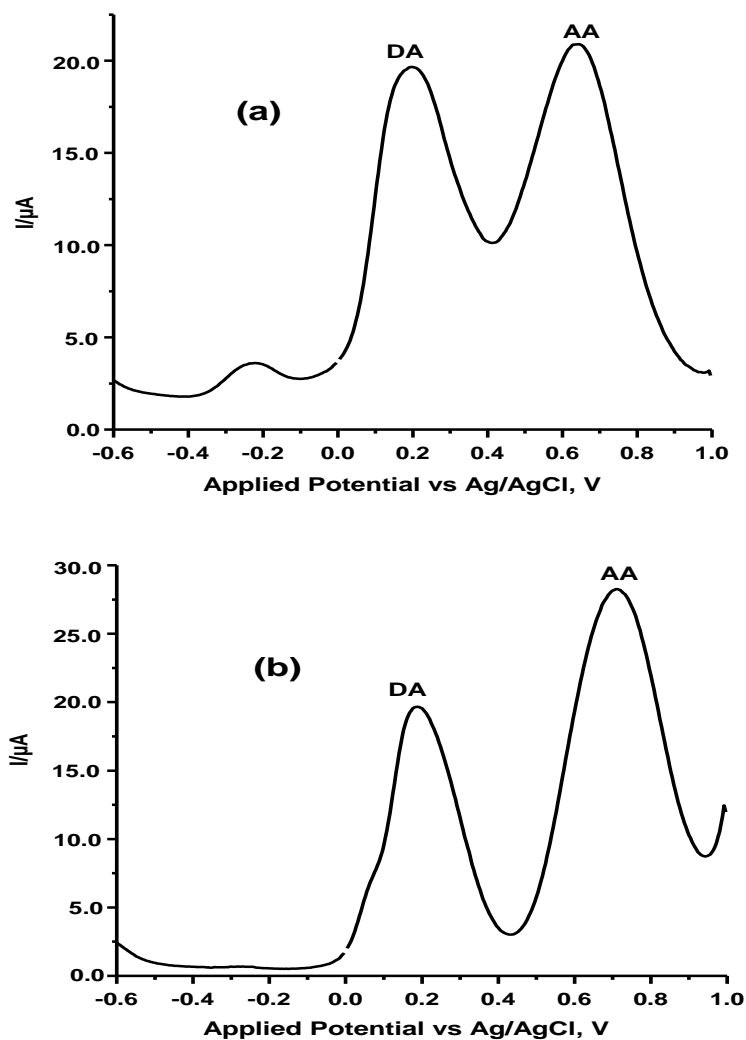The conditions for the synthesis of dihydropyrimidinones (DHPMs) via the Biginelli reaction were optimized by using the model substrates benzaldehyde, urea and ethylacetoacetate (β-ketoester). The effect of solvent was investigated first on the reaction. The reaction without solvent at 90^{0}C was the first choice where we obtained about 60% yield of the DHPMs product in 3 h. Then we used water as solvent at 90^{0}C which increased the yield to 68% in 3 h. But when we performed the reaction with ethanol as solvent 78°C, surprisingly, the yield of the product increased to 98% in 2 h. The use of other solvents such as methanol, acetonitrile and DMF were also tested (Table 4.2.) and finally ethanol was used as the solvent for the synthesis of different DHPMs derivatives by considering its high yield, selectivity and green solvent nature. To test the requirement of a catalyst, a control reaction was performed with the model substrates in the absence of the catalyst and we obtained only 6% yield of the product in 5 h. The use of modified montmorillonite as a catalyst gave only 55% yield in 5h. Thus the effective catalytic reaction takes place in presence of Fe$_3$O$_4$@mmt nanocomposite which gave 98% yield in 2 h in the model reaction. Here, all the reactions were performed using 20 mg Fe$_3$O$_4$@mmt catalyst (contains 0.059 mmol Fe).

The application of Fe$_3$O$_4$ nanoparticles on unmodified clay as catalyst precursor was also investigated in the model reaction but it gave only 75% yield of product which was comparatively low with respect to the reaction catalysed by the nanoparticles with modified clay (Fe$_3$O$_4$@mmt). This might be due to the higher surface area of the modified clay which increased the catalytic efficiency of the magnetic nanocomposite. In this work, we used different aldehydes, ethylacetoacetate and urea for synthesis of different DHPMs. The various substrates used and their corresponding products are represented in Table 4.3. The model reaction where the substrates were ethylacetoacetate, benzaldehyde and urea, gave maximum 98% isolated yield in presence of Fe$_3$O$_4$@mmt nanocatalyst (entry S1). It was observed that the presence of any substituent on the aromatic aldehyde had no significant effect on the yield of the DHPMs product (entry S1, S2 and S4) but the product synthesized by aliphatic aldehyde (entry S9, S10) gave

slightly lower yield than aromatic aldehyde (entry S1,S2). The use of substituted urea such as 1,3-dimethyl urea, thiourea and acetylacetone (β-diketone) instead of ethylacetoacetate as substrates were also investigated in this work (Table 4.3.). The use of thiourea as substrate gave slightly lower yield of product compared to the substrate urea and 1,3-dimethyl urea (entry S1, S14 and S15). Both ethylacetoacetate and acetylacetone completed the reaction smoothly without any difficulty. In this work, we obtained 85-98% yield of the synthesized products with 100% selectivity. After completion of the reaction, the nanocatalyst was separated from the mixture magnetically with the help of a magnetic needle retriever. The different products obtained were purified by recrystallization and characterized by ^{1}H and ^{13}C NMR and CHNS analysis. The recyclability of the Fe_3O_4@mmt nanocatalyst was investigated in the synthesis of DHPMs (Table 4.3.). After each experiment, the nanocatalyst was recovered by magnetic separation technique. It was then washed with acetone, dried and reused directly with for another run for the desired DHPMs synthesis and showed only a slight decrease in activity after 4th run.

Table 4.2. Optimization of reaction conditions for DHPMs synthesis.
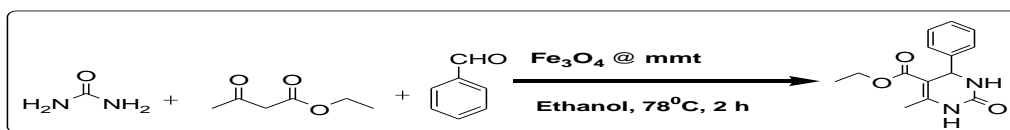
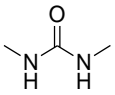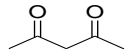| Entry	Solvent	Time (h)	Temperature (^{0}C)	*Yield (%)
1	Solvent free	3	90	60
2	Water	3	90	68
3	Methanol	3	65	66
4	Ethanol	2	78	98
5	DMF	3	110	28
6	Acetonitrile	3	80	35
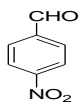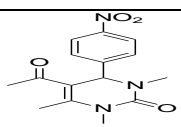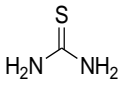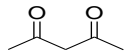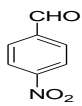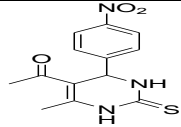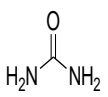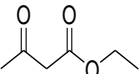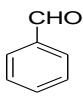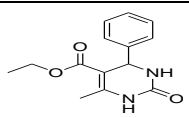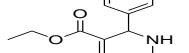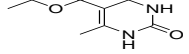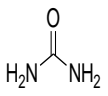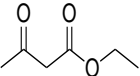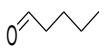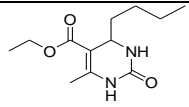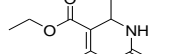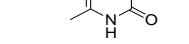
*__Yields__ are isolated products based on the aldehyde after recrystallization. **__Reaction conditions:__ Aldehyde (1 mmol), Ethylacetoacetate (1 mmol), Urea (1.5 mmol), Catalyst (20 mg, contains 0.059 mmol Fe) and Solvent (5 ml).

The recovered magnetic nanocatalyst was again investigated through N_2 adsorption-desorption, HRTEM analysis. Compared to the fresh Fe_3O_4@mmt nanocatalyst of surface area 308 m^2g^{-1}, the specific surface areas of the recovered catalysts decreased (Table 4.1.). The decreased in surface area after successive run may be due to blockage of the pores by the reactant molecules after each reaction.

Table 4.3. Three-component condensation reactions catalyzed by Fe_3O_4@mmt to synthesize DHPMs.

Entry	Urea	Ethylacetoacetate/ Acetylacetone	Aldehyde	Product	Yield[*](%)
S1					98
S2					97
S3					96
S4					98
S5					95
S6					96
S7					95

	Reactant 1	Reactant 2	Aldehyde	Product	Yield
S8					96
S9					89
S10					91
S11					92
S12					85
S13					88
S14					94
S15					96
S16					95
S17					93
S18					97
S19					93
S20					95
S21					95

					Yield (%)
S22	1,3-dimethylurea (structure)	acetylacetone (structure)	4-nitrobenzaldehyde (structure)	product (structure)	94
S23	thiourea (structure)	acetylacetone (structure)	4-nitrobenzaldehyde (structure)	product (structure)	93
S24	urea (structure)	ethyl acetoacetate (structure)	benzaldehyde (structure)	product (structure)	97 [2nd run] / 95 [3rd run] / 93 [4th run]
S25	urea (structure)	ethyl acetoacetate (structure)	pentanal (structure)	product (structure)	88 [2nd run] / 86 [3rd run] / 83 [4th run]

[*]**Yields** are isolated products based on the aldehyde after recrystallization.
[**]**Reaction conditions:** Aldehyde (1 mmol), Ethylacetoacetate (1 mmol), Urea (1.5 mmol), Catalyst (20 mg, contains 0.059 mmol Fe) and Ethanol (5 ml); Refluxing temp. $78^{o}C$, Time: 2 h.

The recovered nanocatalyst after 3rd run was further analyzed by HRTEM. HRTEM image of the catalyst showed that the sizes of Fe_3O_4 nanoparticles are still maintained below 10 nm after 3rd catalytic run (Fig. 4.11.).
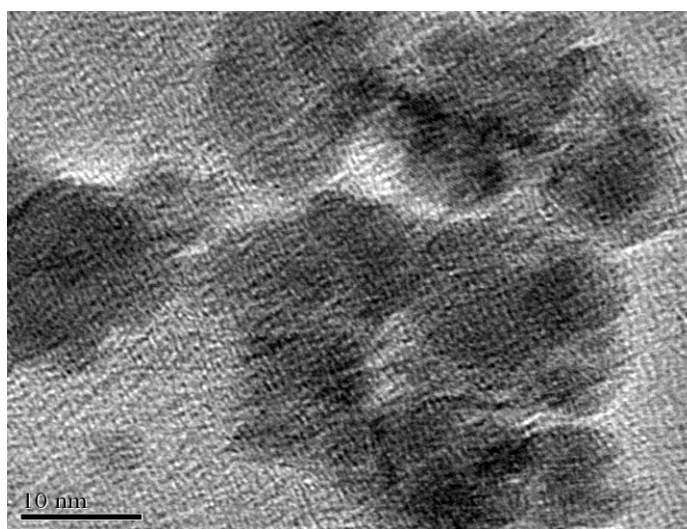
Fig. 4.11. HRTEM image of recovered Fe_3O_4@mmt nanocatalyst.

The possible reaction pathway for the Fe_3O_4@mmt catalysed reaction was given in Scheme 4.1. In the first step, the active methylene compound (ethylacetoacetate) coordinated with the Fe_3O_4@mmt catalyst. This coordination increased the electrophilicity of the carbonyl carbon atom of ethylacetoacetate. In the second step, aromatic aldehyde and ethyl acetoacetate combined to undergo aldol type condensation to give the corresponding aldol-type product. After that the urea molecule coordinated with the aldol type product through one of its N-atom to give 1,4-addition reaction of urea. The intermediate (A) obtained in this step generated ureides (B) which ultimately cyclize to give the desired DHPMs product and the catalyst was regenerated. The theoretical byproduct obtained from the reaction is water. The regenerated magnetic nanocatalyst continued the catalytic run till the completion of the process.
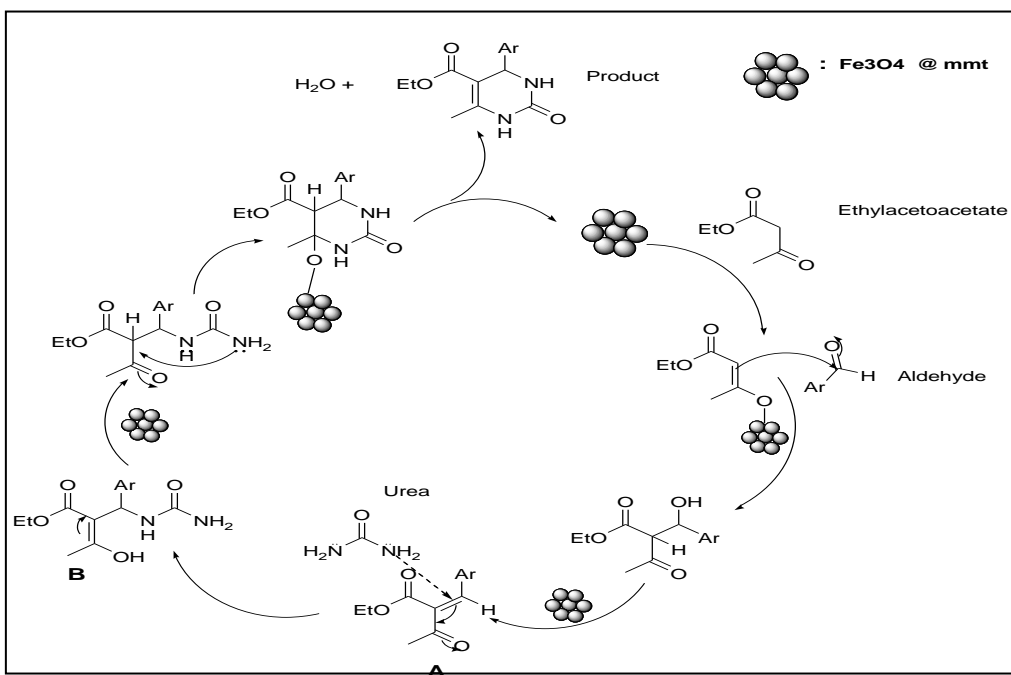
Scheme 4.1. Proposed mechanism for the synthesis of DHMPs.

4.3.4.3. Characterization of some of the synthesized products.

S1. Ethyl-1, 2, 3, 4-tetrahydro-6-methyl-2-oxo-4-phenylpyrimidine-5-carboxylate
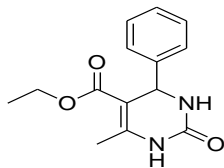
^{1}H NMR (300 MHz,DMSO-d6) : δ 1.09 (t, 3H), δ 2.25 (s, 3H), δ 3.94-4.02 (q, 2H), δ 5.15 (d, 1H), δ 7.22-7.35 (m, 5H), δ 7.74 (s, 1H), δ 9.2 (s,1H); ^{13}C NMR (75 MHz, DMSO-d6): δ 14.53, 18.24, 54.41, 59.66, 99.71, 126.70, 127.73, 128.86, 145.31, 148.82, 152.50, 165.80; C: 64.60%, H: 6.18%, N: 10.76%.

S2. Ethyl-1, 2, 3, 4-tetrahydro-6-methyl-4-(4-nitrophenyl)-2-oxopyrimidine-5-carboxylate
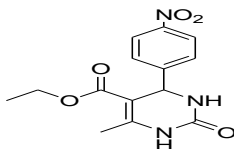
^{1}H NMR (300 MHz,DMSO-d6) : δ 1.09 (t, 3H), δ 2.50 (s, 3H), δ 3.95-4.04 (q, 2H), δ 5.26 (d, 1H), δ 7.49-7.52 (m, 1H), δ 7.90 (s, 1H), δ 8.15-8.44 (m,3H), δ 9.37 (s, 1H) ; ^{13}C NMR (75 MHz, DMSO-d6) : δ 14.50, 18.33, 54.12, 98.62, 124.75, 128.12, 131.11, 147.16, 149.86, 152.45, 165.51,192.83; C: 55.10%, H: 4.95%, N: 13.75%.

S3. Ethyl-1, 2, 3, 4-tetrahydro-4-(4-methoxyphenyl)-6-methyl-2-oxopyrimidine-5-carboxylate
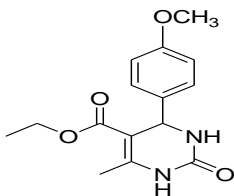
^{1}H NMR (300 MHz,DMSO-d6) : δ 1.12 (t, 3H), δ 2.23 (s, 3H), δ 3.71 (s, 3H) ,δ 3.94-4.01 (q, 2H), δ 5.09 (d, 1H), δ 6.86-6.89 (m, 2H), δ 7.12-7.15 (m, 2H), δ 7.68 (s,1H), δ 9.16 (s, 1H) ; ^{13}C NMR (75 MHz, DMSO-d6) : δ 14.55, 18.21, 53.78, 55.49, 59.62, 100.02, 114.14, 127.86, 137.49, 148.47, 152.64,158.89, 165.83; C: 62.06%, H: 6.23%, N: 9.63%.

S4. Ethyl-1, 2, 3, 4-tetrahydro-6-methyl-2-oxo-4-p-tolylpyrimidine-5-carboxylate
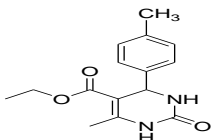
^{1}H NMR (300 MHz,DMSO-d6) : δ 1.11 (t, 3H), δ 2.25 (s, 3H), δ 2.50 (s, 3H) ,δ 3.93-4.0 (q, 2H), δ 5.10 (s, 1H), δ 6.86-6.89 (m, 2H), δ 7.11 (m, 4H), δ 7.69 (s,1H), δ 9.16 (s, 1H) ; ^{13}C NMR (75 MHz, DMSO-d6) : δ 14.50, 18.18, 21.05, 54.07, 59.71, 99.96, 126.60, 129.36, 136.93, 142.29, 148.56,152.74, 165.87; C: 65.70%, H: 6.61%, N: 10.19%.

S5. Ethyl-1, 2, 3, 4-tetrahydro-4-(2-hydroxyphenyl)-6-methyl-2-oxopyrimidine-5-carboxylate
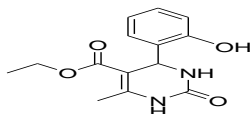
^{1}H NMR (400 MHz,DMSO-d6) : δ 1.19 (t, 3H), δ 1.69 (s, 3H), δ 4.15 (q, 2H), δ 4.43 (s, 1H), δ 5.38 (s, 1H), δ 6.72-7.12 (m, 4H), δ 7.14 (s, 1H), δ 7.57 (s,1H); ^{13}C NMR (100 MHz, DMSO-d6) : δ 14.54, 24.48, 44.1, 48.1, 61.03, 83.61, 117.06, 121.0, 125.92, 129.13, 129.83, 151.15, 155.07, 168.92; C: 60.86%, H: 5.82%, N: 10.12%.

4.4. Conclusion

Both the unmodified and modified montmorillonite clay was used as supports for the synthesis of magnetic Fe_3O_4 nanoparticles. The Fe_3O_4 nanoparticles with unmodified clay (Fe_3O_4@K10) were used to develop voltammetric sensors with gold and platinum working electrodes for selective determination of dopamine and ascorbic acid by square wave voltametry technique. The presence of other biologically important substances did not show any interference in the electrochemistry of dopamine and ascorbic acid. The magnetic nanoparticles with modified clay (Fe_3O_4@mmt) were used as magnetically recoverable heterogeneous catalysts for the synthesis various dihydropyrimidinones derivatives under green reaction conditions. The recovered magnetic nanocatalysts continued the reaction for several runs without any significant loss in activity.

Chapter-5

Synthesis, characterization and applications of Cu^0- nanoparticles stabilized on montmorillonite

5. Synthesis, characterization and applications of Cu^0-nanoparticles stabilized on montmorillonite

5.1. Introduction

The synthesis of metal nanoparticles by environmentally benign, efficient and greener procedure has become more important to address industrial and environmental concerns [122]. Due to the unique size dependent properties and higher surface reactivity, the applications of metal nanoparticles in different fields have attracted great attention in recent time [1, 123]. Various metal nanoparticles have been successfully utilized in different applications such as electronics, opto-electronics, antibacterial activities, sensor, biosciences, medicine and catalysis [124]. The advantage of using metal nanocomposites over bulk metal in catalysis is the reduction in catalyst loading and reaction time, and it also minimizes the chance of formation of undesired products [56, 125]. The nature of the supporting / stabilizing material also plays a vital role on the shape, size and reactivities of the metal nanoparticles. In this connection, different supports / stabilizers like organic ligands, polymers, dendrimers, micro and mesoporous materials, activated carbons, metal oxides etc. are used in the synthesis of metal nanoparticles [125-127]. Among the different supports, the uses of micro and mesoporous supports for stabilizing metal nanoparticles have attracted great attention in recent years due to their high surface area and narrow pore size distribution which helps to control the sizes of the nanoparticles within limited range. Nanoparticles stabilized on mesoporous support are advantageously used in catalysis, development of sensors, adsorbents and electrochemical studies [96, 128].

For practical applications, the development of eco-friendly and sustainable synthetic methods received the importance in recent years due to the growing environmental regulations. Thus, in the synthesis of metal nanoparticles by chemical reduction, the three main areas which determine the environmental acceptability of the process are: choice of solvent, reducing agent and nature of support material [129]. In this chapter, we report a procedure for the synthesis of size selective Cu^0-nanoparticles using

both unmodified and modified montmorillonite clay as support material. Montmorillonite K10 is environmentally benign and cheap, which is modified by refluxing with mineral acid (HCl) under controlled conditions to give a porous matrix with high surface area having micro and mesopores. The Cu^0-nanoparticles stabilized on unmodified clay (Cu^0@K10) has been utilized as voltammetric sensor for dopamine (DA) and ascorbic acid (AA) using gold and platinum working electrodes. The Cu^0-nanoparticles stabilized on modified clay (Cu^0-NPs@mmt) are applied as efficient heterogeneous catalysts for the synthesis of different dihydropyrimidinones derivatives under green reaction conditions.

DA belongs to a group of neurotransmitters called catecholamine which plays an important role in different physiological functions like renal, hormonal, central nervous and cardiovascular functions [98-99]. Its deficiency causes many neurological diseases such as Alzheimer's disease, Schizophrenia and Parkinson's disease [100-101]. DA affects the brain processes that control movement, emotional response, and ability to experience pleasure and pain. Thus, regulation of DA plays a crucial role in our mental and physical health. AA is one of the important vitamins which take part in a number of biological reactions. Deficiency of AA in the body can cause scurvy. It is a good antioxidant and maintains the pH regulatory properties [104]. So, the detection of both DA and ascorbic acid in body fluids is of great significance in the field of clinical diagnostics. The development of voltammetric sensors for different biologically active compounds has received significant interest in recent years [104]. Electrochemically, both dopamine (DA) and ascorbic acid (AA) are active compounds but they show similar electrochemical responses which complicate their electrochemical identification in presence of one another. When normal electrodes are used, both dopamine and ascorbic acid oxidizes at a potential very close to one another thereby giving a complicated voltammetric response. Then it becomes impossible to determine the electrochemical responses for DA and AA. Thus, various electrode modifying agents are used to develop better working electrode, which can voltammetrically distinguish between dopamine and ascorbic acid [100-104]. Different types of materials with sensing ability, high stability, catalytically active and with excellent conductivity, such as metal nanocomposites,

polymers, organic ligands, metal complexes, have been used for the modification of conventional working electrodes [99-101]. Some of the recently used electrode modifying agents for the determination of DA and AA are: bi-nuclear copper^{2+} complex, 2, 4-dinitrophenylhydrazine@phosphatidylcholine, dendrimers containing gold metal nanoparticles, composite polymer film, poly (acrylic acid) multi walled carbon nanotube (MWCNT), poly (4-aminothiophenol) with gold nanoparticles etc [106-110].

Pyrimidinones or Dihydropyrimidinones (DHPMs) are comprised of a pyrimidine scaffold having similar structural features to the nucleic acid bases present in DNA and RNA. They show different types of pharmaceutical and therapeutic activities such as antifungal, anti-inflammatory, antibacterial and anticancer activities [112-116]. One of the important DHPMs derivatives that show anticancer property is monastrol; it is an inhibitor of human kinesin Eg5 and considered one of the promising compounds in cancer chemotherapy [130-132]. Considerable work has also been performed to obtain the structure-activity relationship in the monastrol derivative series [133-134]. The synthesis of monastrol involves the three component condensation reaction of ethylacetoacetate, 3-hydroxybenzaldehyde and thiourea via the Biginelli reaction. But the main problem occurred in the reaction is the low yield of the product is obtained with the traditional ethanol/HCl catalysed reaction. Various homogeneous and heterogeneous catalysts were developed in recent years for the synthesis of different dihydropyrimidinone derivatives [117-119]. But the uses of heterogeneous catalysts have the advantages over homogenous ones, because of easy separation catalysts for reusability and simple isolation of the synthesized product.

In this chapter, the synthesized nanocomposite material (Cu^0@K10) has been used to modify the Platinum and Gold electrode surfaces. The modified electrodes served as efficient voltammetric sensors for DA and AA in presence of other biologically important species. Further, synthesis of racemic monastrol and its related derivatives catalysed by Cu^0-nanoparticles stabilized on modified montmorillonite (Cu^0-NPs@mmt) under green reaction conditions have also been reported. The clay modification was done by refluxing the montmorillonite K10 with HCl under controlled condition to give a

porous matrix with high surface area. This modified porous matrix acts as a support for the *in situ* synthesis of Cu^0-nanopartilces and controls particles size below 10 nm. Further, reusability of the Cu^0-NPs@mmt catalyst was investigated in this study and showed only a slight decrease in activity after 3rd catalytic run.

5.2. Experimental

5.2.1. Preparation of Support

About 10 g of montmorillonite K10 was dispersed in 200 mL 2M HCl in a round bottom flask. The mixture was then refluxed for 2 hour under vigorous stirring. After that the mixture was cooled and the supernatant liquid was discarded. The activated montmorillonite clay obtained was washed repeatedly by deionised water till the removal of Cl^- ions from the clay as confirmed by the $AgNO_3$ test. The modified clay was dried at 50^oC in air oven for 12 h and the solid mass obtained was named as modified montmorillonite.

5.2.2. Preparation of supported Cu^0-nanoparticles

0.8 g of both unmodified and modified clay was impregnated with 20 mL (1 m mol) aqueous solution of $CuCl_2$ under vigorous stirring conditions for 8 h. The solid composites were then obtained by evaporation to dryness in a rotary evaporator. 0.4 g of the dry composites of both were dispersed in 30 mL of ethylene glycol separately and 189.2 mg of $NaBH_4$ (5 m mol) in 10 mL of distilled water were added to both the solutions slowly over 10 min in nitrogen environment under constant stirring conditions. The black reaction products so obtained were recovered and washed with deionised water several times and then dried in a desiccator for 15 h. The nanocomposites were named as Cu^0@K10 and Cu^0-NPs@mmt respectively.

5.2.3. Procedure for modification of working electrode

10 mg of Cu^0@K10 nanocomposite was dispersed with 0.2 mL of styrene and 0.5 mL of dichloromethane in a 5 mL beaker. 1.0 μL of the solution was placed on the tip of a pre-cleaned platinum (Pt) and gold (Au) electrode surface with the help of a micropipette. This developed a film of the nanocomposite on the electrodes surface. The

electrodes were allowed to dry. The modified platinum and gold electrodes obtained were named as Pt/Cu^0@K10 and Au/Cu^0@K10 respectively.

5.2.4. General procedure for the synthesis of thiourea based dihydropyrimidinones (DHPMs)

Aldehyde (1 m mol), β-ketoester (1 m mol), thiourea (1.5 m mol), 25 mg catalyst (Cu^0-NPs@mmt) and 10 mL ethanol were stirred at room temperature in a round bottom flask for stipulated time period. The progress of the reaction was checked by TLC. At the end of the reaction, the solid catalyst was separated from the mixture simply by filtration and the solvent was removed using rotary evaporator. The crude product obtained was finally recrystallized to give the pure product. The isolated pure products were characterized by ^{1}H and ^{13}C NMR and CHNS analysis.

5.3. Results and discussion

5.3.1. Characterization of Support

The characterization of both parent montmorillonite K10 and modified montmorillonite were carried out with the help of different sophisticated analytical techniques like Powder-XRD, N$_2$ adsorption-desorption and SEM-EDX analysis.

5.3.1.1. X-ray diffraction

The parent montmorillonite K10 showed an intense basal reflection at 7.10^o 2θ due to a basal spacing of 12.7 Å (Fig. 5.1). Acid treatment of montmorillonite disrupted the layered structure of the clay and this is substantiated by the decreased in the basal reflection intensity with time and no peak was observed after 2 h acid activation.
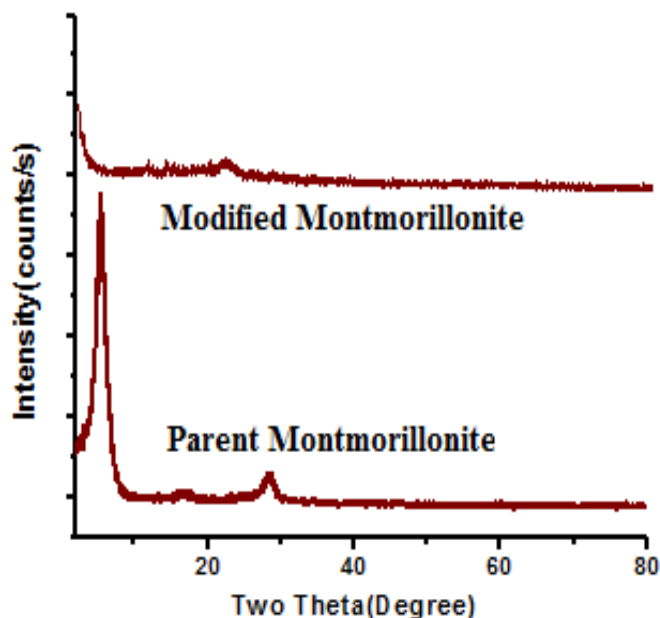
Fig. 5.1. PXRD pattern of parent and modified montmorillonite.

5.3.1.2. Specific surface area and pore size distribution

Specific surface area and pore size distribution analysis showed that the modified montmorillonite contained micro and mesopores with average pore diameters ~ 4.88 nm, a high specific surface area of 416 m^2/g and a large specific pore volume of ~ 0.65 cm^3/g (Table 5.1). The increase in surface area and pore volume may be due to the leaching of Al^{3+} from the octahedral sites of the clay matrix which generated micro and mesopores on the clay surface. The adsorption-desorption isotherm obtained was of type-IV [Fig. 5.2.] with a H3 hysteresis loop at P/P$_o$ ~ 0.4-0.9, indicating mesoporous solid. The plot of differential volumes against pore diameter [Fig. 5.3] showed narrow pore size distributions. Compared to modified montmorillonite, the unmodified clay showed a relatively low surface area of 192 m^2/g, average pore diameters ~ 3.82 nm and specific pore volume of ~0.30 cm^3/g.
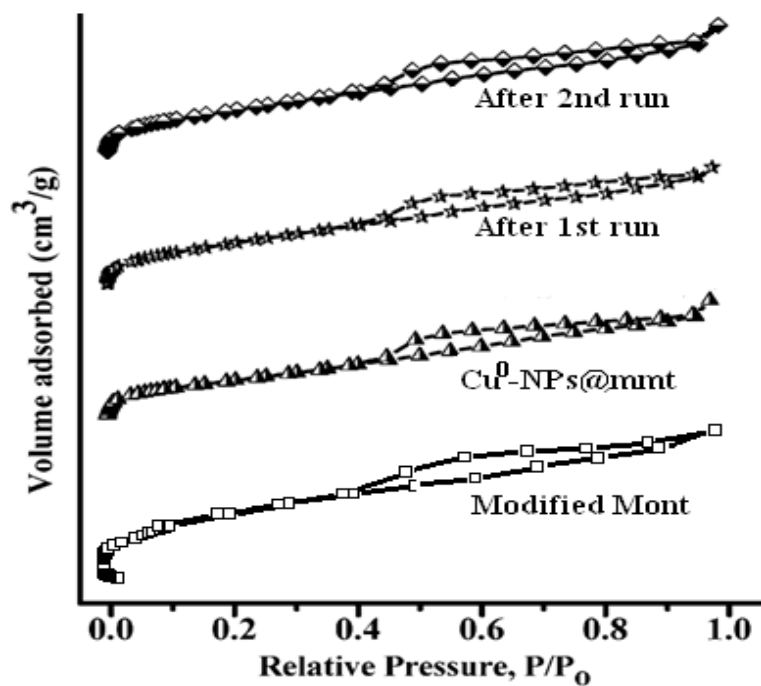
Fig. 5.2. N_2 adsorption / desorption isotherms of Modified Mont, Cu^0-NPs@mmt and recovered catalysts.
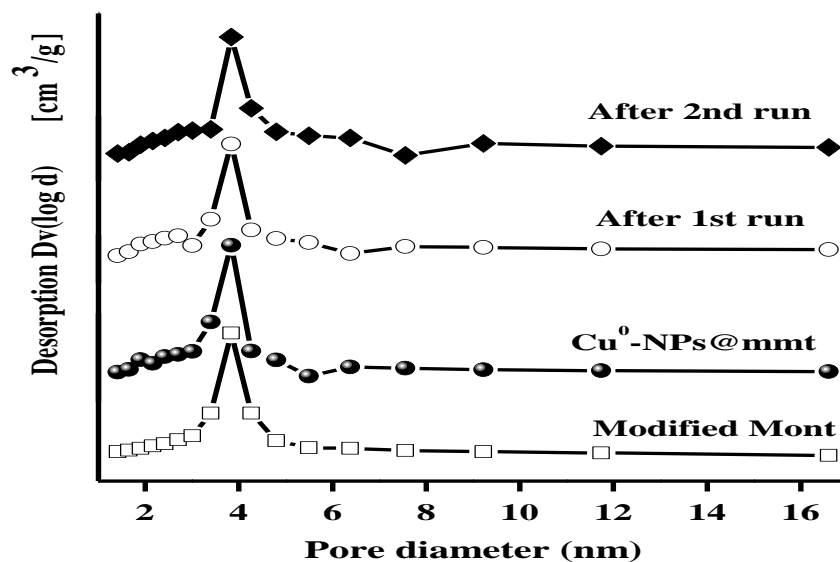
Fig. 5.3. BJH pore size distribution curves of Modified Mont, Cu^0-NPs@mmt and recovered catalysts.

5.3.1.3. SEM-EDX analysis

The SEM-EDX analysis of unmodified clay showed the layered structure of the clay [Chapter 2; Fig. 2.5(a)] and the presence of predominant amounts of Si and Al on the clay surface [Chapter 2; Fig. 2.5(b)]. Acid treatment leached out most of Al^{3+} from octahedral sites and developed micro and mesopores on the clay matrix. The typical SEM image of modified montmorillonite [Chapter 2; Fig. 2.5(c)] showed the formation of pores on the clay surface and the corresponding EDX analysis at the surface [Chapter 2; Fig. 2.5(d)] revealed that predominant amounts of Si compared to Al was present on the surface.

5.3.2. Characterization of clay supported Cu^0-nanoparticles

The evidence for the formation of Cu^0-nanoparticles was substantiated by powder XRD analysis. The powder XRD pattern suggested face centred cubic lattice (fcc) lattice type arrangement of Cu^0-nanoparticles in both unmodified and modified clay. The three broad peaks of 2θ values 43.4, 50.2 and 74.1^0 which were assigned to the (111), (200) and (220) indices of fcc lattice of metallic Cu [Fig. 5.4 (a) and (b)]. The nanocomposite with unmodified montmorillonite showed an additional diffraction peak at 7.10^o 2θ due to basal reflection (001) of montmorillonite clay.
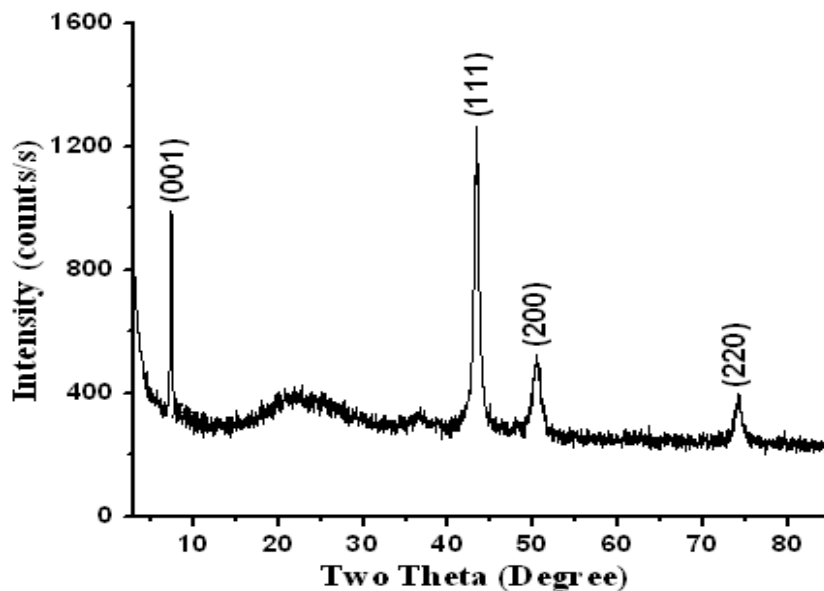
Fig. 5.4. (a) Powder XRD pattern of Cu^0@K10

101
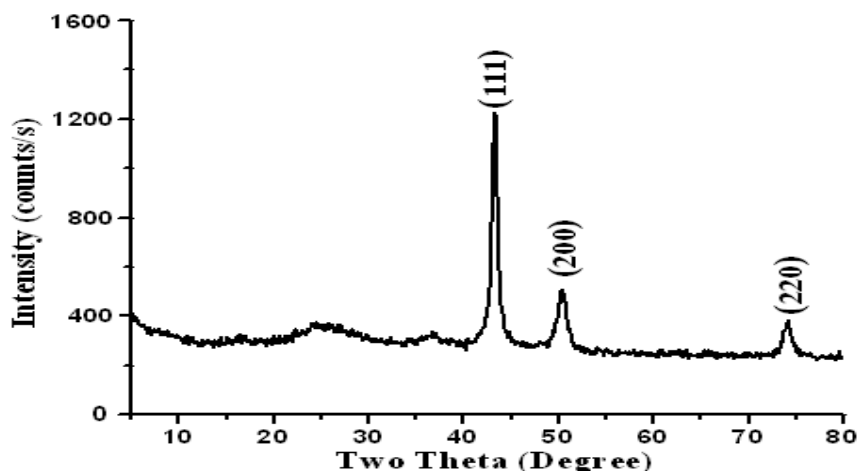
Fig. 5.4. (b) Powder XRD pattern of Cu^0-NPs@mmt

TEM study showed the Cu^0-nanoparticles were well dispersed on the surface of K10 [Fig. 5.5. (a)] and modified montmorillonite [Fig. 5.5. (b)]. The nanopartilcles were spherical in shape with sizes of 1-10 nm. The HRTEM [Fig.5.5. (c)] and SAED (Selected Area Electron Diffraction) pattern [Fig.5.5. (d)] of Cu^0-NPs@mmt corresponds to crystalline nature of the nanoparticles.

Specific surface area and pore size distribution analysis showed that there was an appreciable decrease of the specific surface area and the specific pore volume after supporting Cu^0-nanoparticles (Table 5.1.). The decrease in surface area and pore volume might be due to clogging of some pores of the clay matrix by Cu^0-nanoparticles. The Cu^0-NPs@mmt nanocomposite showed type IV isotherm with a H3 hysteresis loop at P/P_o ~0.4-0.9 [Fig. 5.2.] which confirmed that porous structure of clay was maintained even after formation Cu^0-nanoparticles. But, increased of pore diameter might be due to rupture of some smaller pores to generate bigger pores during the formation of Cu^0-nanoparticles into the pores. The Cu contents in Cu^0-NPs@mmt as analyzed by ICP-AES, reveals the presence 0.03 mmol Cu in 25 mg Cu^0-NPs@mmt.
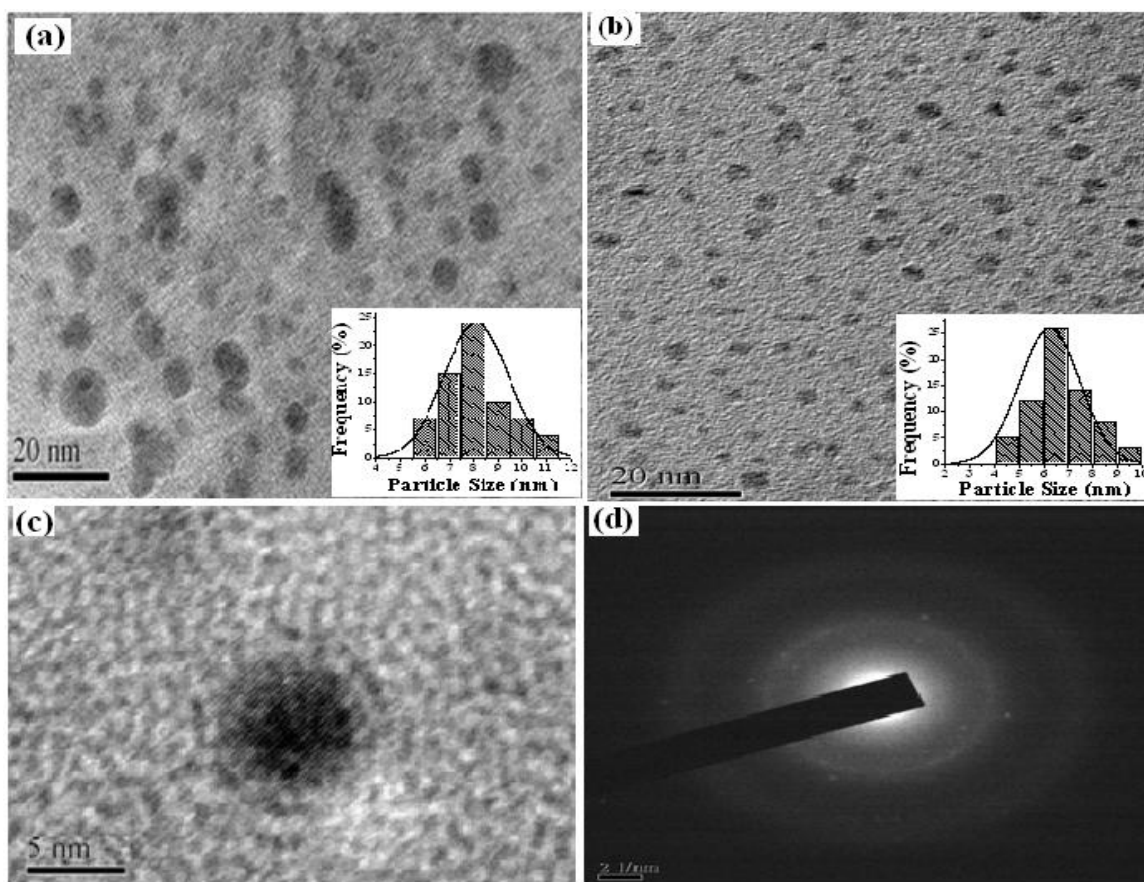
Fig. 5.5. **(a)** TEM image of Cu^0@K10 (unmodified clay), **(b)** TEM image of Cu^0-NPs@mmt and **(c)** HRTEM and **(d)** SAED pattern Cu^0-NPs@mmt.

Table 5.1. Surface properties of Cu^0-NPs@mmt and modified montmorillonite.

Samples		Surface properties of support/catalysts		
		Specific surface area (m^2/g)	Average pore diameter (nm)	Specific pore volume (cm^3/g)
Modified Mont		416	4.88	0.65
Cu^0-NPs@mmt	After run Fresh	336	6.20	0.56
	1	295	6.85	0.48
	2	258	7.68	0.41

5.3.3. Electroanalytical applications of Cu^0@K10 nanocomposite

In this study, we have used the Cu^0@K10 nanocomposite to modify surface of platinum and gold working electrodes. The modified electrodes act as voltammetric sensors for selective determination of dopamine and ascorbic acid by square wave voltammetric technique.

5.3.3.1. Electrochemistry of Pt/Cu^0@K10 and Au/ Cu^0@K10 modified electrode

Square wave voltammograms of Pt/Cu^0@K10 and Au/ Cu^0@K10 modified electrode in phosphate buffer at pH 7.0 and at scan rate 0.1 Vs^{-1} were recorded using 0.1M $NaNO_3$ as the supporting electrolyte (Fig. 5.6.). The Pt/Cu^0@K10 electrode in phosphate buffer showed a peak with redox potential + 0.193 V while the Au/ Cu^0@K10 electrode showed the peak at + 0.212 V. The effect of pH of the electrolytic medium on the electrochemistry of both the modified electrodes was investigated. The electrochemical response of the modified electrodes was observed in the pH range 5.0 to 8.5, but the changed in pH did not show any characteristic change the peak position and redox potential.
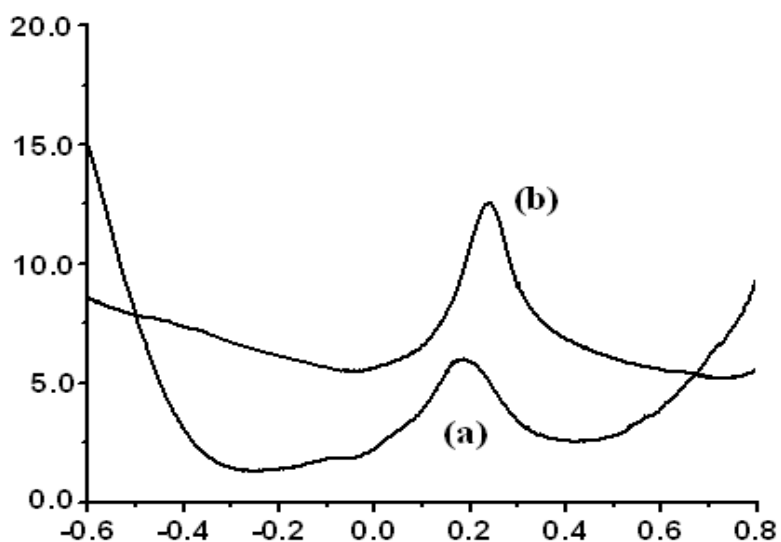
Fig. 5.6. Square wave voltammogram of (a) Pt/Cu^0@K10 and (b) Au/ Cu^0@K10 modified electrode in phosphate buffer (Ag-AgCl is the reference electrode, Scan Rate: 0.1V s^{-1}).

5.3.3.2. Selective voltametric detection of DA and AA by modified Pt and Au electrode

The unmodified Pt and Au electrodes were first used to analyze the voltammetric responses of DA and AA when both were simultaneously present in the solution. The unmodified Pt electrode showed a peak at redox potential + 0.108 V while the unmodified Au electrode showed the same at redox potential − 0.102 V in the mixture of DA and AA having concentration 0.01 mM and 0.1 mM respectively [Fig. 5.7. (a)]. Thus, the bare Pt and Au electrodes are unable to detect DA and AA both in presence of one another. The use of modified Pt/Cu^0@K10 electrode in the mixture showed two peaks at + 0.286V due to DA and + 0.745V due to AA respectively [Fig. 5.7. (b)]. To confirm the respective peak positions of DA and AA, the concentration of DA in the mixture was increased and it was found that the peak height i.e. peak current at + 0.286 V increased which substantiated the peak obtained at this potential was due to DA [Fig. 5.7. (c)]. Similarly, increased of concentration of AA increased the peak current at + 0.745 V and this confirmed the corresponding peak was due to AA. On the other hand, the modified Au/Cu^0@K10 electrode showed two redox peaks in the mixture of DA and AA [Fig. 5.7. (d)]. The redox peak obtained at + 0.291 V was due to DA and the redox peak obtained at + 0.738 V was due to AA. In this case, the respective electrochemical responses of DA and AA were confirmed by same procedure as before.
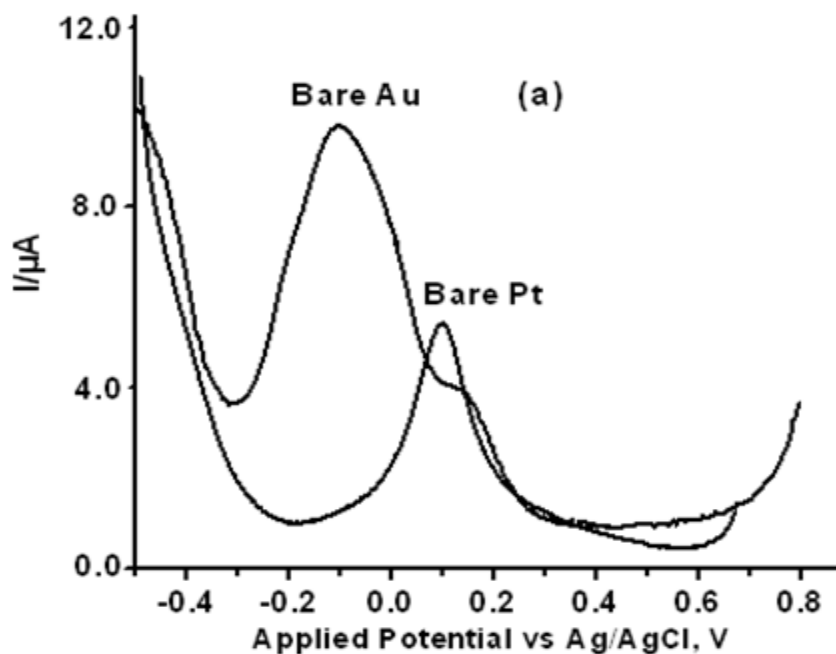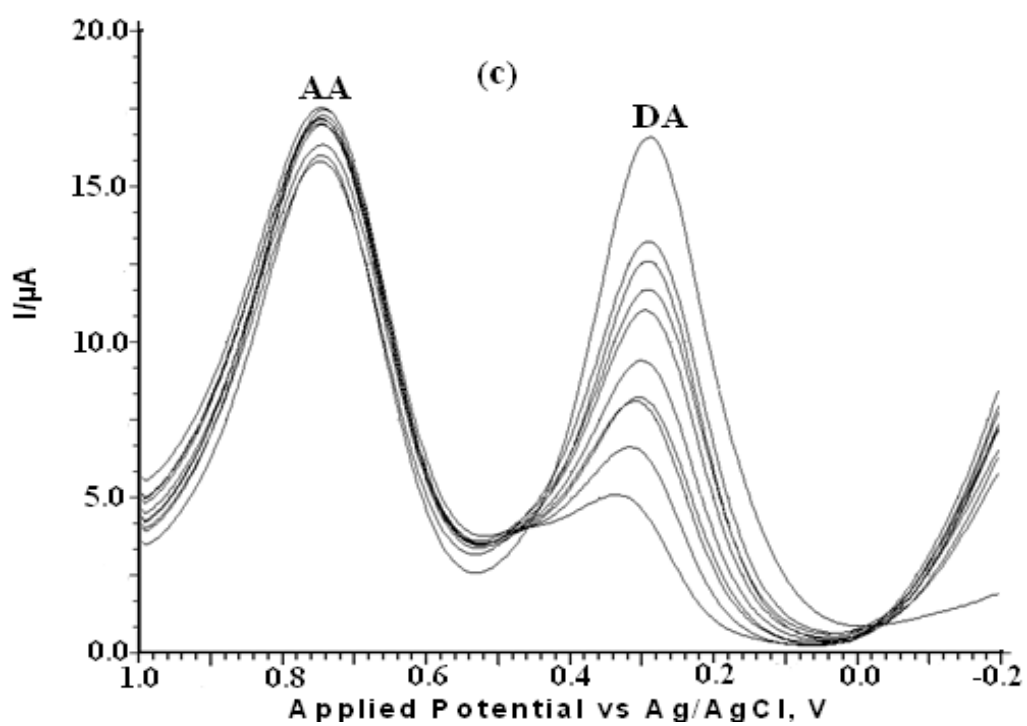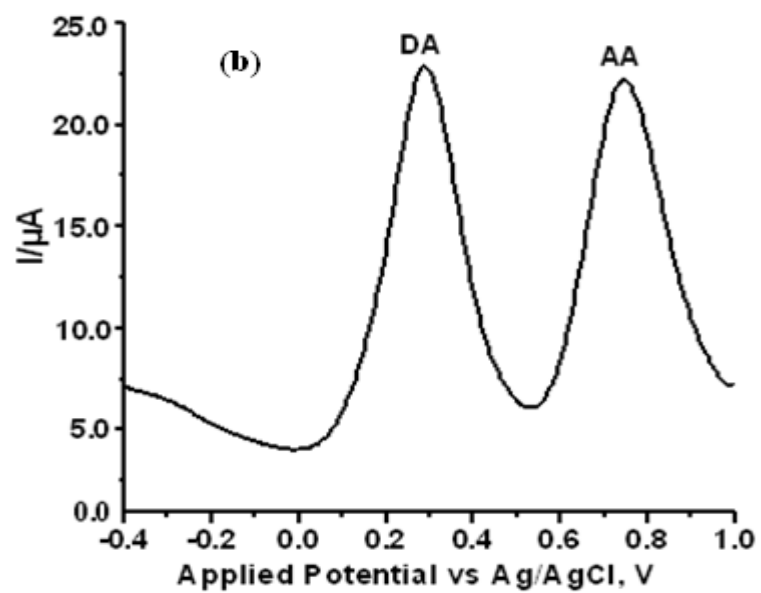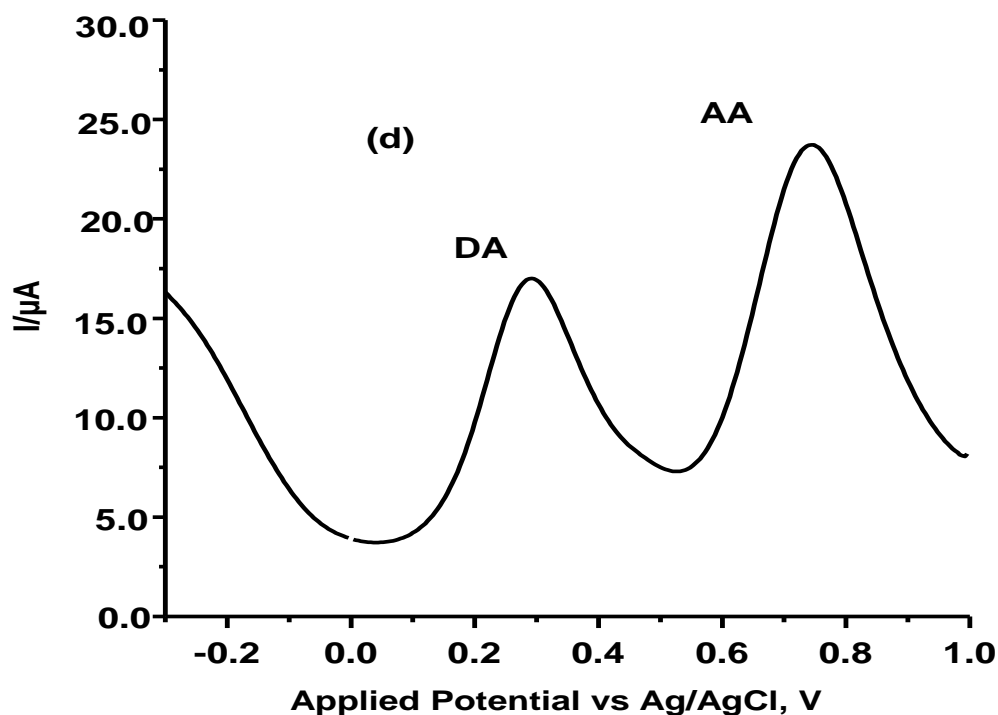
Fig. 5.7. The square wave voltammogram of (a) the bare Pt and Au electrode in the mixture of DA and AA, (b) Modified Pt electrode in the Mixture of DA and AA, (c) Modified Pt electrode with increasing concentration of DA, and (d) Modified Au electrode in the mixture of DA and AA.

The influence of a number of biologically important species such as Na^+, K^+, Mg^{2+}, Ca^{2+}, Zn^{2+}, Fe^{2+}, cholesterol and glucose was also investigated by both the modified electrodes on the selective voltammetric detection of DA and AA. But no significant interference was observed in the selective determination of DA and AA. Thus, the Cu^0-nanoparticles coated modified electrodes showed excellent electrochemical sensing of DA and AA in presence of other biologically important substances.

5.3.4. Catalytic applications of Cu^0-NPs@mmt nanocomposite

5.3.4.1. Synthesis of thiourea based dihydropyrimidinones (DHPMs) using Cu^0-NPs@mmt as catalyst
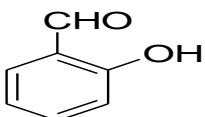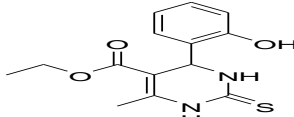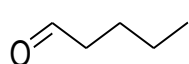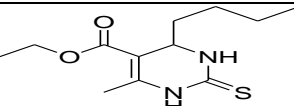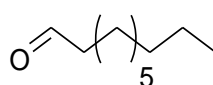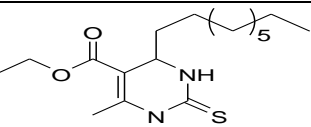
The conditions for the synthesis of thiourea based dihydropyrimidinones (DHPMs) were optimized by using the model substrates benzaldehyde, thiourea and ethylacetoacetate (β-ketoester). After screening a wide range of reactions, we have found that our catalytic system (Cu^0-NPs@mmt) is most efficient for the three-component condensation reaction in ethanol as a solvent at room temperature. The model reaction gave maximum 95% yield in 4 h in presence of Cu^0-NPs@mmt catalyst using ethanol as solvent. To test the requirement of a catalyst, the model reaction was performed without catalyst; but no progress in the reaction was observed. The use of modified montmorillonite as a catalyst gave only 42% yield in 4h. Thus the effective catalytic reaction takes place in presence of Cu^0-NPs@mmt catalyst. In this work, all the reactions were carried out with 25 mg Cu^0-NPs@mmt catalyst (contains 0.03 mmol Cu). Here, we used different aldehydes, ethylacetoacetate and thiourea for synthesis of different DHPMs derivatives. The various substrates and products were represented in Table 5.2. The highest yield obtained in this study was 95% where the substrates are benzaldehyde, ethylacetoacetate and thiourea (entry S1). It was observed that the presence of any electron withdrawing or donating substituent on the aromatic aldehyde had no significant effect on the yield of the DHPMs product (entry S1, S2 and S3) but the substrate 3-hydroxybenzaldehyde used in the synthesis of monastrol gave relatively low yield compared to the other aromatic aldehydes (entry S5). Again, the use of aliphatic aldehyde as substrate gave slightly lower yield of product than aromatic aldehyde (Table 5.2.). In this work, we obtained 79-95% yield of the desired products with 100% selectivity for the Cu^0-NPs@mmt catalysed reaction. After completion of the reaction, the Cu^0-NPs@mmt was separated from the mixture simply by filtration. The different products obtained were purified by recrystallization. The isolated pure products were characterized by ^{1}H and ^{13}C NMR and CHNS analysis.

The recyclability of the Cu^0-NPs@mmt catalyst was investigated in the synthesis of DHPMs (Table 5.2.). After each experiment, the nanocatalyst was recovered by filtration. It was then washed with acetone, dried and reused directly for another catalytic run. The recovered nanocatalyst was successfully reused up to 3rd catalytic run without any significant loss in activity. The recovered nanocatalyst was further investigated through N_2 adsorption-desorption analysis. The surface area of the recovered Cu^0-NPs@mmt catalyst decreased with respect to the fresh catalyst of surface area 336 m^2g^{-1} (Table 5.1.). The observations might be due to blockage of the pores by the reactant molecules after each catalytic run.

Table 5.2. Cu^0-NPs@mmt catalysed thiourea based dihydropyrimidinones (DHPMs).
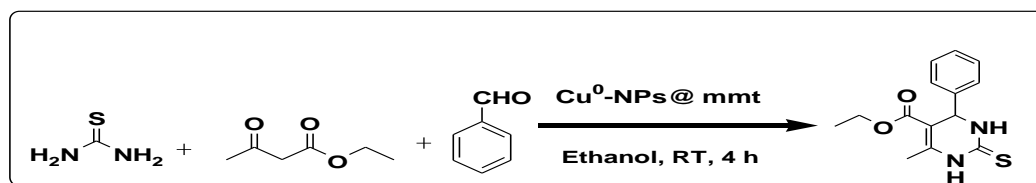
Entry	Aldehyde	Product	*Yield(%)
S1.			95^a 93^b 91^c
S2.			93
S3.			91
S4.			92
S5.			81

S6.	CHO ... OH	(structure)	88
S7.	(structure)	(structure)	79
S8.	(structure)	(structure)	83[a] 81[b] 78[c]

*Yields are isolated products based on the aldehyde after recrystallization.

Reaction conditions: Aldehyde (1 mmol), Ethylacetoacetate (1 mmol), Thiourea (1.5 mmol), Catalyst (25 mg, contains 0.03 mmol Cu) and Ethanol (5 ml); RT, Time 4 h.
[a]1st run, [b]2nd run, [c]3rd run.

A plausible reaction mechanism for the one-pot synthesis of DHPMs catalyzed by Cu^0-NPs@mmt was proposed (Scheme 5.1.).
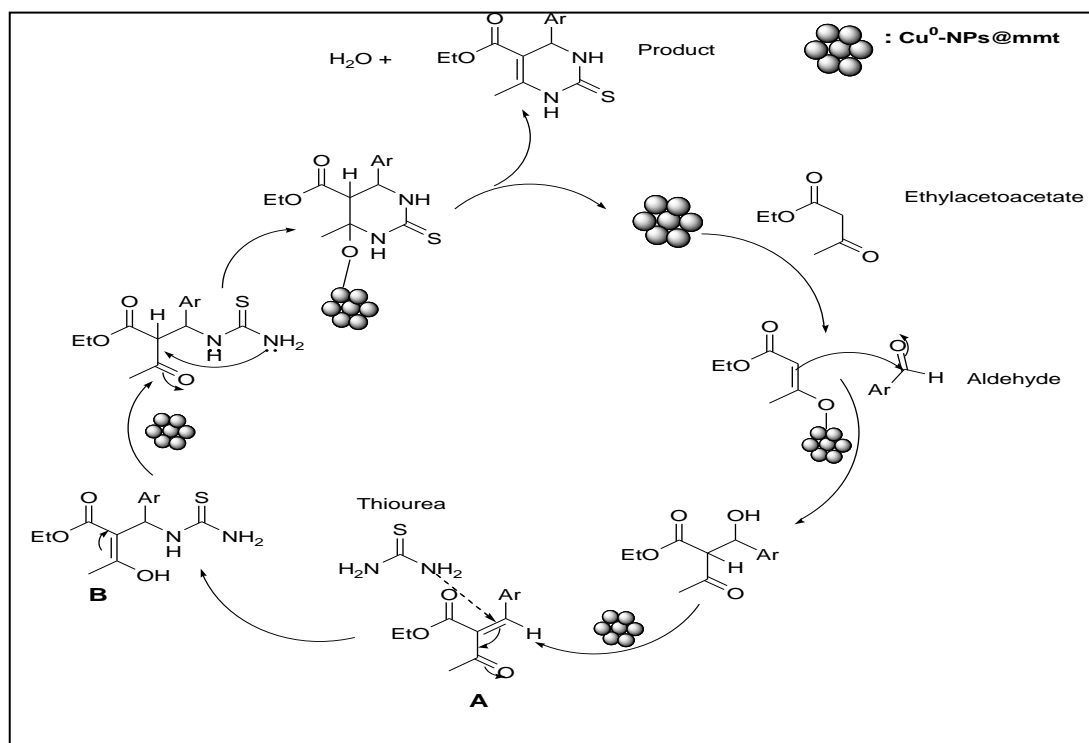
Scheme 5.1. Proposed mechanism for the synthesis of thiourea based DHMPs.

110

First, ethylacetoacetate coordinated with the Cu[0]-NPs@mmt catalyst and increased the electrophilicity of the carbonyl carbon atom of ethylacetoacetate. Then aromatic aldehyde and ethyl acetoacetate combined to undergo aldol type condensation to give the corresponding aldol-type product. The thiourea molecule then coordinated with the aldol type product through one of its N-atoms to give the intermediate (A) which generated ureides (B). The ureides (B) ultimately cyclize to give the desired DHPMs product and the catalyst was regenerated. The theoretical byproduct obtained from the reaction is only water. The regenerated Cu[0]-NPs@mmt catalyst continued the catalytic run till the completion of the process.

5.3.4.2. Characterization of some of the DHPMs products

S1. Ethyl-1, 2, 3, 4-tetrahydro-6-methyl-4-phenyl-2-thioxopyrimidine-5-carboxylate
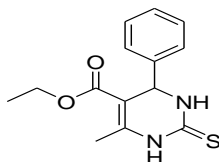
^{1}H NMR (400 MHz, DMSO-d[6]) : δ 1.06 (t, 3H), δ 2.03 (s, 3H), δ 3.93-3.98 (q, 2H), 5.12 (d, 1H) ,δ 7.16-7.29 (m, 5H), δ 9.61 (s, 1H), δ 10.29 (s, 1H); ^{13}C NMR (100 MHz, DMSO-d[6]) : δ 14.53, 17.68, 30.5, 54.53, 60.12, 101.20, 126.90, 129.09, 144.0, 145.57, 165.64, 174.72, 207.07; C: 60.80%, H: 5.79%, N: 10.07%, S: 11.52%.

S2. Ethyl- 1, 2, 3, 4-tetrahydro-6-methyl-4-(4-nitrophenyl)-2-thioxopyrimidine-5-carb-oxylate
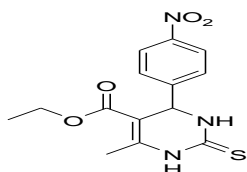
^{1}H NMR (400 MHz,DMSO-d[6]) : δ 1.16 (s, 3H), 2.44 (s, 3H), δ 5.1 (t, 2H), δ 5.5 (s, 1H), δ 7.55 (d, 2H),δ 8.09 (d, 2H), 8.27 (s, 1H) ,δ 10.08 (s, 1H); ^{13}C NMR (100 MHz, DMSO-d[6]): δ 15.18,16.20, 55.3, 61.56, 100.20, 123.62, 128.15, 146.76, 147.76,150.95, 184.25, 192.35; C: 52.28%, H: 4.65%, N: 12.96%, S: 9.91%.

S3. Ethyl-1, 2, 3, 4-tetrahydro-4-(4-methoxyphenyl)-6-methyl-2-thioxopyrimidine-5-carboxylate
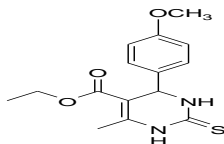
^{1}H NMR (400 MHz,DMSO-d^6) : δ 1.05 (t, 3H), δ 2.23 (s, 3H), δ 3.67 (s, 3H),δ 3.94-3.96 (q, 2H), 5.06 (d, 1H) ,δ 6.84-7.09 (m, 4H), δ 9.56 (s, 1H), δ 10.25 (s, 1H); ^{13}C NMR (100 MHz, DMSO-d6) : δ 14.33, 17.65, 53.95, 55.60, 60.07, 101.44, 114.38, 128.13, 136.21, 145.27, 159.24, 165.68, 174.50, 184.32; C: 58.67%, H: 5.85%, N: 9.09%, S: 10.42%.

S5. Ethyl-1, 2, 3, 4-tetrahydro-4-(3-hydroxyphenyl)-6-methyl-2-thioxopyrimidine-5-carboxylate
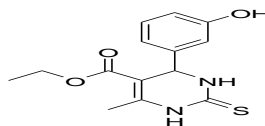
^{1}H NMR (400 MHz,DMSO-d6) : δ 1.14 (t, 3H), 2.45 (s, 3H), δ 4.19 (q, 2H), δ 5.04 (d, 1H), δ 7.19-7.36 (m, 4H), 9.42 (s, 1H), 9.86 (s, 1H) ,δ 10.26 (s, 1H); ^{13}C NMR (100 MHz, DMSO-d6): δ 14.24, 17.67, 54.43, 60.13, 61.66, 101.25, 113.73, 115.13, 121.64, 130.85, 138.14, 145.35, 157.95, 165.70, 174.64, 184.28; C: 57.41%, H: 5.45%, N: 12.96%, S: 9.46%, 10.87.

5.4. Conclusion

Both montmorillonite K10 and modified montmorillonite clay were used as supports for the synthesis of Cu^0-nanoparticles. The Cu^0-nanoparticles supported on montmorillonite K10 (Cu^0@K10) were used as electrode modifying agent for selective voltammetric detection of DA and AA by Pt and Au working electrodes. The presence of other biologically important substances did not show any characteristic interference in the electrochemical responses of DA and AA. The Cu^0-nanoparticles with modified clay (Cu^0-NPs@mmt) were used as efficient heterogeneous catalysts for the synthesis of various thiourea based dihydropyrimidinones under mild conditions. Further, the recovered nanocatalysts were reused upto 3rd catalytic run without any significant loss in activity.

Summary, Conclusions and Future scope

6. Summary, Conclusions and Future Scope

6.1. Summary

This thesis describes modification of montmorillonite K10 by treatment with mineral acid (HCl) to generate a high surface area and porous matrix. Nanoparticles of metals (Cu and Ag) and metal oxide (Fe_3O_4) have been generated on the porous surface of the clay matrix of modified and unmodified clay. The synthesized nanocomposites are characterized by powder XRD, SEM-EDX, HRTEM, XPS and N_2-adsorption analysis etc. The metal and metal oxide nanoparticles supported on modified clay were evaluated as heterogeneous catalysts for various organic transformations like A^3-coupling, Baeyer-Villiger oxidation, synthesis of dihydropyrimidinones and benzimidazoles. The metal and metal oxide nanoparticles with unmodified clay were utilized as electrode modifying agents to develop voltammetric sensor for dopamine and ascorbic acid. A brief summary and general conclusion of the research work are presented below.

Chapter 1: This chapter is an introductory chapter which describes the basic concept, history, importance of nanoscience and nanotechnology along with the different properties, types, synthetic routes and applications of metal nanoparticles. The role of supports used for the stabilization of metal nanoparticles is also described. This chapter deals with the review of literature for supported metal and metal oxide nanoparticles of Ag, Cu and Fe and their applications in catalysis and electrochemical studies. In addition to that, this chapter describes the different experimental procedure such as purification and modification of montmorillonite clay. The different instrumental techniques used to characterize different materials / products and their principles have also been described in this chapter.

Chapter 2: This chapter describes acid modification of montmorillonite K10 to generate a high surface area and porous matrix and its characterization by different sophisticated analytical instrument like FTIR, N_2-adsorption-desorption, powder XRD and SEM-EDX analysis. The application of modified clay as catalyst for the synthesis of benzimidazole

by the reaction between aromatic aldehyde and o-phenylenediamine has also been described.

Chapter 3: This chapter discusses the synthesis of silver nanoparticles (Ag-NPs) supported modified montmorillonite clay and their characterization by different analytical techniques such as UV-Visible spectroscopy, powder XRD, N_2-adsorption-desorption, SEM-EDX and HRTEM analysis. The applications silver nanoparticles as efficient catalysts for the three component coupling reaction of aldehyde, amine and alkyne to synthesize propargylamine and for the Baeyer-Villiger oxidation of cyclic ketones have been demonstrated. The recyclability of the catalysts for several runs is also described.

Chapter 4: In this chapter, synthesis of Fe_3O_4 nanoparticles using both modified and unmodified montmorillonite clay as support and their characterizations various analytical techniques like powder XRD, HRTEM, N_2-adsorption-desorption and XPS analysis are described. The application of Fe_3O_4 nanoparticles supported on unmodified clay in the development of voltammetric sensor for dopamine and ascorbic acid is discussed. It also describes the application of modified clay supported Fe_3O_4 nanoparticles as active catalyst for the synthesis of different dihydropyrimidinones via the Biginelli reaction under mild condition.

Chapter 5: This chapter discusses the synthesis, characterizations and applications of Cu^0-nanoparticles supported on both modified and unmodified montmorillonite. The Cu^0-nanoparticles are characterized by powder XRD, N_2 adsorption-desorption and TEM analysis. The unmodified clay supported Cu^0-nanoparticles as electrode modifying agents for the voltammetric determination of dopamine and ascorbic acid are described. The application of Cu^0-nanoparticles with modified clay as efficient catalyst for the synthesis different thiourea based dihydropyrimidinones has also been described.

6.2. Conclusions

(1) Montmorillonite K10 was modified by treatment with mineral acid (HCl) under controlled condition to achieve a high surface area and porous matrix and this modified clay was used as a support material for the synthesis of metal and metal oxide nanoparticles. The modified clay also shows catalytic activity towards the synthesis of benzimidazole by the reaction between aromatic aldehyde and o-phenylenediamine.

(2) Silver nanoparticles (Ag-NPs) of size below 10 nm were synthesized by impregnating $AgNO_3$ solution with modified montmorillonite clay followed by reduction with $NaBH_4$. UV-visible spectroscopy as well as other analytical techniques confirms the formation of silver nanoparticles. The silver nanoparticles are spherical in shape and are crystallized in fcc crystal lattice form.

(3) The synthesized modified clay supported silver nanoparticles were found as excellent heterogeneous catalyst for the one-pot three components coupling of aldehyde, amine and alkyne to synthesize propargylamine with high yield and selectivity. The silver nanoparticles also showed efficient catalytic activity towards the Baeyer-Villiger oxidation cyclic and aromatic ketones under mild reaction conditions. The catalysts were reused several times without any significant loss in catalytic activity.

(4) Fe_3O_4 nanoparticles of size below 10 nm were synthesized using both modified and unmodified montmorillonite as support material and were characterized by different analytical techniques like powder XRD, N_2 adsorption-desorption, TEM and XPS analysis etc.

(5) The Fe_3O_4 nanoparticles supported on unmodified montmorillonite was used to develop voltammetric sensor for dopamine and ascorbic acid by square wave voltammetry technique. The modified clay supported Fe_3O_4 nanoparticles was utilized as heterogeneous magnetically recoverable catalyst for the synthesis of different dihydropyrimidinones with high yield and selectivity. The nanocatalyst retained its

magnetic property and catalytic activity for several catalytic runs and served as efficient heterogeneous catalyst.

(**6**) Cu^0-nanopaticles were synthesized by impregnating $CuCl_2$ solution with both modified and unmodified montmorillonite followed by reduction with NaBH4 under nitrogen environment. TEM study reveals the nanoparticles are spherical in shape with particles size below 10 nm. The unmodified clay supported Cu^0-nanopaticles was applied as an electrode modifying agent for voltammetric determination of dopamine and ascorbic acid. The Cu^0-nanopaticles supported on modified montmorillonite showed catalytic activity for the synthesis of different thiourea based dihydropyrimidinones under mild reaction conditions.

6.3. Future scope

There are high scopes for scientific research towards the synthesis of various metal nanoparticles and their utilization in different fields. Some of the future scopes of the research work are listed below.

(**1**) The modified montmorillonite clay served as efficient, environmentally benign and excellent support material for Ag, Cu and Fe_3O_4 nanoparticles. The modified clay also showed catalytic activity for the synthesis of benzimidazoles. Thus, the modified clay can be advantageously used as support for other metal nanoparticles synthesis and can be used directly as catalyst for various organic transformations.

(**2**) The silver nanoparticles stabilized on modified montmorillonite are stable and showed efficient catalytic activity towards A^3-coupling reaction and Baeyer-Villiger oxidation. This silver nanocatalyst may be used as alternative catalyst in place of homogeneous metal catalyst in different other reactions such as C-H activation, oxidation reaction, C-C coupling reaction etc.

(**3**) The Fe_3O_4 nanoparticles stabilized on montmorillonite find applications in the development of voltammetric sensor for dopamine and ascorbic acid and showed efficient catalytic activity for the synthesis of different dihydropyrimidinones derivatives.

The simple synthetic procedure and robustness of Fe_3O_4 nanoparticles provides further useful applications in iron promoted transformation in the future.

(4) The Cu^0-nanoparticles stabilized on montmorillonite may be used as catalyst precursor for large scale synthesis of biologically active dihydropyrimidinones and other important organic reactions catalysed by copper. The Cu^0-nanoparticles may also be used for other electrochemical applications in the future.

References

7. References

[1] (a) K. J. Klabunde, S. Winecki, *Nanoscale Materials in Chemistry*, Wiley, New York (2001); (b) C. N. R. Rao, et al., *Chem. Soc. Rev.* **29**, 27 (2000); (c) C. P. Poole Jr., F. J. Owens, *Introduction to Nanotechnology*, Willy-Interscience (2003).

[2] (a) B. Zhou, S. Hermans, G. A. Somorjai, *Nanostructure science and technology*, Springer (**2004**); (b) J. M. Campelo, et al., *ChemSusChem* **2**, 18-45 (2009).

[3] (a) A. C. Templeton, W. P. Wuelfing, R. W. Murray, *Acc. Chem. Res*. **33**, 27 (2000); (b) H. Brune, et al., *Nanotechnology assessment and perspectives*, Springer (2006).

[4] (a) Y. Na, et al., *J. Am. Chem. Soc.* **126**, 250-258 (2004); (b) P. P. Sarmah, D. K. Dutta, *Green Chem.* **14**, 1086-1093 (2012).

[5] (a) F. Schröder, et al., *J. Am. Chem. Soc.* **130**, 6119-6130 (2008); (b) T. Tsukatani, H. Fujihara, *Langmuir* **21**, 12093-12095 (2005).

[6] (a) J. Virkutyte, R. S. Varma, *Chem. Sci.* **2**, 837 (2011); (b) H. Goesmann, C. Feldmann, *Angew. Chem. Int. Ed*. **49**, 1362-1395 (2010).

[7] (a) D. L. Feldheim, C. A. Foss, *Metal Nanoparticles: Synthesis, Characterization and Application*, CRC Press, New York (2002); (b) A. Fukuoka, P. L. Dhepe, *Chem. Record.* **9**, 224 (2009).

[8] (a) J. Turkevich, *Gold Bull*. **18**, 86 (1985); (b) H. Zhao, Y. Ning, *Gold Bull*. **33**, 103 (2000); (c) M. Faraday, *Phil. Trans.* **147**, 145-181 (1857).

[9] (a) G. A. Ozin, A. C. Arsenault, *Nanochemistry: A Chemical Approach to Nanomaterials*, RSC Publishing (2005); (b) M. Haruta, *Chem. Record.* **3**, 75 (2003).

[10] (a) A. Corma, H. Garcia, *Chem. Soc. Rev*. **37**, 2096 (2008); (b) M. Hu, et al., *Chem. Soc. Rev*. **35**, 1084 (2006).

[11] W. J. Parak, et al., *Quantum dots in nanoparticles*, Wiley-VCH (2004).

[12] (a) A. K. Geim, K. S. Novoselov, *Nat. Mater.* **6**, 183-191 (2007); (b) K. S. Novoselov, et al., *Science* **306**, 666-669 (2004).

[13] J. A. Dahl, B. L. S. Maddux, J. E. Hutchinson, *Chem. Rev*. **107**, 2228-2269 (2007).

[14] (a) G. M. Whitesides, J. P. Mathias, C. T. Sato, *Science* **254**, 1312-1319 (1991); (b) D. M. Dubbs, I. A. Aksay, *Ann. Rev. Phys. Chem.* **51**, 601-622 (2000).

[15] (a) B. Wiley, et al, *Chem. Eur. J.* **11**, 454-463 (2005); (b) J. M. Campelo, et al., *Chem. Eur. J.* **14** , 5988-5995 (2008); (c) O. S. Ahmed, D. K. Dutta, *Langmuir* **19**, 5540 (2003).

[16] (a) A. Barau, et al., *Catal. Lett.* **124**, 204-214 (2008); (b) H. Liu, et al., *Chem. Commun.* 2677-2679 (2008).

[17] M. Haruta, et al. **144**, 175-192 (1993).

[18] (a) B. L. Cushing, V. L. Kolesnichenko, C. J. O'Connor, *Chem. Rev*. **104**, 3893 - 3946 (2004); (b) A. Martinez, G. Prieto, *Catal. Commun*. **8** , 1479-1486 (2007).

[19] (a) J. Park, et al., *Angew. Chem. Int. Ed.* **46**, 4630-4660 (2007); (b) D. Wostek-Wojciechowska, et al., *J. Colloid Interface Sci.* **287**, 107-113 (2005).

[20] (a) R. Tatumi, T. Akita, H. Fujihara, *Chem. Commun*. 3349-3351 (2006); (b) M. Aslam, et al., *J. Mater. Chem.* **14**, 1795-1797 (2004).

[21] (a) Y. Chen, K. Yong, J. Li, *Mater. Lett.* **62**, 1018-102 (2007); (b) C. H. Walker, J. V. St. John, P. Wision-Neilson, *J. Am. Chem. Soc*. **123**, 3846 (2001); (c) F. Quignard, A. Choplin, A. Domard, *Langmuir* **16**, 9106-9108 (2000).

[22] (a) D. Astruc, F. Lu, J. R. Aranzaes, *Angew.Chem. Int. Ed.* **44** , 7852-7872 (2005); (b) N. Perkas, et al., *Catal. Lett.* **120**, 19-24 (2008).

[23] (a) J. P. M. Niederer, et al., *Top. Catal.* **18**, 265-269 (2002); (b) V. Budarin, et al., *Angew. Chem. Int. Ed.* **45**, 3782-3786 (2006).

[24] (a) A. Siani, et al., *J. Catal.* **266**, 331-342 (2009); (b) A. Sandoval, et al., *J. Mol. Catal. A : Chem.* **278**, 200-208 (2007); (c) A. Gniewek, et al., *J. Catal.* **254**, 121-130 (2008).

[25] (a) K. Layek, et al., *Green Chem.* **13**, 2878 (2011); (b) L. M. Rossi, et al., *Green Chem*. **9**, 379-385 (2007).

[26] (a) S. J. Borah, D. K. Das, *Catal. Lett.* **146**, 657 (2016); (b) X. Zhou, et al., *RSC Adv*. **3**,1732 (2013).

[27] (a) P. Laszlo, *Science* **235**, 1473-1477 (1987); (b) T. J. Pinnavaia, et al., *J. Chem. Soc. Faraday Disc.* **87**, 227-237 (1989); (c) R. S. Varma, *Tetrahedron* **58**, 1235-1255 (2002).

[28] (a) D. Manikandan, et al., *Appl. Clay Sci.* **37**, 193-200 (2007); (b) J. E. Gillot, *Clay in engineering geology*, Chapter 11, Elsevier (1968).

[29] (a) S. K. Bhorodwaj, D. K. Dutta, *Appl. Catal. A: Gen.* **378**, 221 (2010); (b) P. J. Wallis, et al., *Green Chem.* **9**, 980-986 (2007).

[30] (a) J. Safaei Ghomi, M. Ghasemzadeh, *J. Chem. Sci.* **125**, 1003 (2013); (b) Y. Saito, et al., *Langmuir* 182959 (2002).

[31] (a) H. Cong, et al., *J. Am. Chem. Soc.* **132**, 7514 (2010); (b) D. B. Kushal, et al., *Catal. Commun.* **11**, 1233, 2010.

[32] (a) S. Haq, A. Carew, R. Raval, *J. Catal.* **221**, 204 (2004); (b) F. Alonso, et al., *Eur. J. Org. Chem.* 1875 (2010).

[33] M. Kantam, et al, *Tetrahedron Lett.* **49**, 3083 (2008).

[34] D. Bhuyan, M. Saikia, L. Saikia, Catal. Commun. **58**, 158 (2015).

[35] (a) H. Firouzabadi, et al., *Adv. Synth. Catal.* **353**, 125-132 (2011); (b) X.J. Wu, et al., *Adv. Synth. Catal.* **351**, 3150-3156 (2009).

[36] (a) X. Luo, et al., Electroanalysis **18(4)**, 319 (2006); (b) V. Mani, et al., *Electrochim. Acta* **176**, 804 (2015); (c) Q. Chen, L. Zhang, G. Chen, *Anal. Chem.* **84(1)**, 171-178 (2012).

[37] (a) Y. He, et al., *Electroanalysis* **29(4)**, 965 (2017); (b) G. Zohreh, et al., *J. Nanostruct. Chem.* **5**, 237 (2015); (c) S. Zheng, et al., *Int. J. Electrochem. Sci.* **8**, 12296 (2013).

[38] (a) S. Erogul, et al., *Electrochim. Acta* **186**, 302 (2015); (b) G. S. Cao, et al., *Micro & Nano Lett.* **9(1)**, 16-18 (2014); (c) S. Sang, et al., *Int. J. Electrochem. Sci.* **12**, 1306-1317 (2017); (d) L. D. Tran, et al., *Mat. Sci & Eng. C.* **31**, 477 (2011).

[39] (a) H. Cui, et al., *Anal. Methods* **4**, 4176-4181 (2012); (b) M. Tayyebeh, et al., *Ionics* **23(4)**, 1005-1015 (2017).

[40] J. E. Gilliot, *Clay in Engineering Geology*, 1st Edition, Chapter 5, Elsevier (1968).

[41] O. S. Ahmed, D. K. Dutta, *J. Mol. Catal. A: Chem.* **202**, 279 (2003).

[42] C. R. Theocharis, K. J. Jacob, A. C. Gray, *J. Chem. Soc. Faraday Trans.* **84**, 1509-1515 (1988).

[43] J. Osteryoung, J.J. O'Dea, Electroanal. Chem. **14** (1980).

[44] (a) D. L. Andrews, Lasers in Chemistry, 2nd Edition, Springer-Verlag, Berlin, 69-70 (1990); (b) A. J. Bard, L. R. Faulkner, *Electrochemical Methods: Fundamentals and Applications*, John Wiley and Sons, Inc. 833 (2001); (c) D. R. James, A. Siemiarczuk, W. R. Ware, Review of Scientific Instrument **63**, 1710 (1992).

[45] B. J. Borah. D. Dutta, D. K. Dutta, *Appl. Clay Sci.* **49**, 320 (2010).

[46] (a) W. W. Chen, R. V. Nguyen, C. J. Li, *Tetrahedron Lett.* **50**, 2895 (2009); (b) R. Stern, M. J. Jedrzejas, *Chem. Rev.* **108**, 5061 (2008).

[47] (a) G. Nagendrappaa*, Resonance*. 64 (2002); (b) N. Kaur, D. Kishore, *J. Chem. Pharm. Res.* **4(2)**, 991 (2012).

[48] (a) L. Rout, S. Jammi, T. Punniyamurthy, *Org. Lett*. **9**, 3397 (2007); (b) R. Saladino, C. Crestini, et al., *ChemBioChem* **5**, 1558 (2004).

[49]. (a) G. Nagendrappaa, *Appl. Clay Sci.* **53**, 106 (2011); (b) R. J. M. J. Vogels, J. T. Kloprogge, J. W. Geus, *J. Catal.* **231**, 443 (**2005)**.

[50] (a) L. Fowden, R. M. Barrer, R. B. Tinker, *(Eds.), Clay Minerals: Their Structure, Behaviour and Use.* Philosophical Transactions of the Royal Society of London, Series A, Mathematical and Physical Sciences, **311**, 219 (1984).

[51] M. I. Carretero, *Appl. Clay Sci.* **21**, 155 (2002).

[52] (a) M. Lachar, N. Lahav, S. Yariv, *J. Therm. Anal.* **40**, 41 (1993); (b) M. Fusi, et al., *Soil Biochem.* **21**, 911 (1989).

[53] (a) R. A. Schoonheydt, et al., *Clays and Clay Minerals*, **27**, 269 (1979); (b) A. Moronta, et al., *Appl. Catal. A: Gen.* **334**, 173-178 (2008).

[54] (a) C. Waterlot, D. Couturier, B. Rigo, *Tetrahedron Lett.* **41**, 317 (2000); (b) D. M. Troast, J. Yuan, J. A. Jr. Porco, *Adv. Synth. Catal.* **350**, 1701 (2008).

[55] (a) J. T. Li, C. Y. Xing, T. S. Li, *J. Chem. Tech. Biotech.* **79**, 1275 (2004); (b) B. Thomas, S. Prathapan, S. Sugunan, *J. Chem. Res.* **79**, 21 (2005); (d) M. R. Dintzner, et al., *Tetrahedron Lett.* **45**, 79 (2004).

[56] D. Dutta, et al., *Appl. Clay Sci*. **53**, 650 (2011).

[57] (a) D. A. Horton, G. T. Bourne, M. L. Smythe, *Chem. Rev.* **103**, 893, (2003); (b) C. Zhang, L. Zhanga, N. Jiao, *Green Chem.* **14**, 3273 (2012).

[58] (a) J. E. Payne, et al., *J. Med. Chem.* **53**, 7739 (2010); (b) M. J. Tebbe, et al., *J. Med. Chem.* **40**, 3937 (1997).

[59] (a) A. M. Palmer, et al., *J. Med. Chem.* **53**, 3645 (2010); (b) C. Mukhopadhyay, et al., *RSC Adv.* **1**, 1033 (2011).

[60] (a) W. J. Ebenezer, et al., *Tetrahedron Lett.* **48**, 1641 (2007); (b) K. F. Ansari, C. Lal, *Eur. J. Med. Chem.* **44**, 4028 (2009).

[61] (a) J. Peng, et al., *J. Org. Chem.* **76**, 716 (2011); (b) S. Gupta, P. K. Agarwal, B. Kundu, Tetrahedron Lett., **51**, 1887 (2010)

[62] (a) M. Shen, T. G. Driver, *Org. Lett.* **10**, 3367 (2008); (d) M. M. Heravi, et al., *Catal. Commun.* **9**, 504 (2007); (b) G. M. Raghavendra, et al., *Tetrahedron Lett.* **52**, 5571 (2011).

[63] (a) L. M. Dudd, et al., *Green Chem.* **5**, 187 (2003); (b) M. C. Willis, *Chem. Rev.* **110**, 725 (2010).

[64] (a) C. L. Allen, J. M. J. Williams, *Chem. Soc. Rev.* **40**, 3405 (2011); (b) J. Ruan, J. Xiao, *Acc. Chem. Res.* **44**, 614 (2011); (c) A. T. Biju, N. Kuhl, F. Glorius, *Acc. Chem. Res.*, **44**, 1182 (2011).

[65] L. Wang, et al., *J. Colloid and Interface Sci.* **295**, 436 (2006).

[66] G. Schmid, B. Corain, *Eur. J. Inorg. Chem.* 3081 (2003).

[67] (a) M. Haruta, et al., *Chem. Lett.* 405 (1987); (b) R. W. Sun, et al., *Chem. Commun.* 5059 (2005).

[68] D. Lee, R. E. Cohen, M. F. Rubner, *Langmuir.* **21**, 9651 (2005).

[69] M. A. M. Khan, et al., *Nanoscale Res. Lett.* **6**, 434 (2011).

[70] (a) H. Miyamura, et al., *Angew. Chem. Int. Ed.* **46**, 4151 (2007); (b) J. D. Aiken III, R. G. Finke, *J. Am. Chem. Soc.* **121**, 8803 (1999).

[71] X. Sun, S. Dong, E. Wang, *Langmuir* **21**, 4710 (2005).

[72] (a) L. D. Rogatis, et al., *ChemSusChem* **3**, 24 (2010); (b) J. Michalik, et al., *J. Phys. Chem.* **100**, 4213 (1996).

[73] (a) H. A. Patel, H. C. Bajaj, R. V. Jasra, *J. Nanoparticles Res.* **10**, 625 (2008); (b) H. A. Patel, H. C. Bajaj, R. V. Jasra, *J. Nanosci. Nanotech.* **9**, 5946 (2009); (c) S. M. Peak, et al., *J. Phys. Chem. Solids* **67**, 1020 (2006).

[74] (a) S. Ayyappan, et al., *Solid State Ionics* **1996**, *84*, 271; (b) Z. Kiraly, et al., *J. Catal.* **1996**, *16*, 401; (c) H. Tsunoyama, et al., *Langmuir* **2004**, *20*, 11293.

[75] F. Bergaya, B. K. G. Theng, G. Lagaly, (Eds), *Handbook of Clay Science, Developments in Clay Science*, Vol. 1, Elsevier, Amsterdam, 2006, Chapter 7.1.

[76] M. A. Huffman, et al., *J. Org. Chem.* **60**, 1590 (1995).

[77] M. Konishi, et al., *J. Am. Chem. Soc.* **112**, 3715 (1990).

[78] G. Dyker, *Angew Chem. Int. Ed.* **38**, 1698 (1999).

[79] (a) V. A. Peshkov, O. P. Pereshivko, E. V. Van der Eycken, *Chem. Soc. Rev.* **41**, 3790 (**2012**); (b) W. J. Yoo, L. Zhao, C. J. Li, *Aldrichimica Acta* **44**, 43 (2011).

[80] (a) C. Binda, et al., *J. Med. Chem.* **47**, 1767 (2004); (b) C. W. Olanow, *Neurology* **66**, S69–S79 (2006).

[81] D. A. Gallagher, A. Schrag, *CNS Drugs* **22**, 563 (2008).

[82] (a) C. Wei, C. J. Li, *J. Am. Chem. Soc.* **125**, 9584 (2003); (b) B. J. Borah, et al., *Catal. Sci. Technol.* **4**, 1047 (2014).

[83] (a) B. Sreedhar, et al., *Tetrahedron Lett.* **46**, 7019 (2005); (b) S. B. Park, H. Alper, *Chem Commun.* 1315 (2005).

[84] (a) M. J. Albaladejo, et al., *Eur. J. Org. Chem.* 3093 (2012); (b) X. Zhang, A. Corma, *Angew Chem. Int. Ed.* **47**, 4358 (2008).

[85] M. Paul, et al., *Chem. Eng. Sci.* **71**, 564 (2012).

[86] R. Otomo, et al., *Catal. Sci. Technol.* **6**, 2787 (2016).

[87] G.J. ten Brink, I. W. C. E. Arends, R. A. Sheldon, *Chem. Rev.* **104**, 4105 (2004).

[88] (a) A. Chrobok, et al., *Appl. Catal. A: Gen.* **366**, 22 (2009); (b) C. G. Piscopo, et al., *Adv. Synth. Catal.* **352**, 1625 (2010).

[89] (a) A. Corma, et al., *Nature* **412**, 423 (2001); (b) A. Corma, M. T. Navarro, M. Renz, *J. Catal.* 219, 242 (2003).

[90] (a) T. Hara, et al., *Green Chem.* 14, 771 (2012); (b) P. Saikia, et al., *Green Chem.* **18**, 2843 (2016); (c) U.R. Pillai, E.S. Demessie, *J. Mol. Catal. A: Chem.* **191**, 93 (2003).

[91] (a) K. Kaneda, et al., *Molecules* 15, 8988 (2010); (b) J. Lu, et al., *Nanotechnology* 17, 5812 (2006).

[92] (a) J. Gao, et al., *J. Am. Chem. Soc.* **130**, 3710 (2008); (b) B. Sreedhar, A. S. Kumar, P. S. Reddy, *Tetrahedron Lett.* **51**, 1891 (2010).

[94] J. Mondal, T. Sen, A. Bhaumik, *Dalton Trans.* **41**, 6173-6181 (2012).

[95] (a) A. H. Latham, M. E. Williams, *Acc. Chem. Res.* **41**, 411-420 (2008);   (b) M. Arruebo, et al., *Nano Today* **2**, 22-32 (2007).

[96] (a) W. G. Borghard, et al., *Langmuir* **25**, 12661 (2009), (b) K. Sarkar, K. Dhara, M. Nandi, P. Roy, A. Bhaumik, P. Banerjee, *Adv. Funct. Mater.* **19**, 223 (2009).

[97] (a) C. N. Rhodes, D. R. Brown, *J. Chem. Soc. Faraday Trans.* **89(9)**, 1387 (1993); (b) N. Kaur, D. Kishore, *J. Chem. Phar. Res.* **4(2)**, 991 (2012).

[98] S. R. Ali., et al., *Analytical Chemistry* **79**, 2583-2587 (2007).

[99] D.K. Das, B. Sarma, S. Haloi, *Chemical Papers* **68(2)**, 153-163 (2014).

[100] (a) C. Martin, *Chem. Br.* **34**, 40 (1998); (b) A. Heinz, et al., *Nervenarzt.* **66**, 662 (1995).

[101] P. Goswami, D.K. Das, *J. Surface Sci. Technol.* **28**, 25 (2012).

[102] (a) I. Franken, J. Booij, W. Brink, *Eur. J. Pharmacol.* **526**, 199 (2005); (b) M. Heien, et al., *Proc. Natl. Acad. Sci.* **102**, 10023 (2005).

[103] (a) O. Rohr, B. et al., *Nucleic Acids Res.* **27**, 3291 (1999); (b) C. Scheller, et al., *J. Neural Transm.***107**, 1483 (2000).

[104] (a) J. B. Raoof, A. Kiani, *J. Electroanal. Chem.* **515**, 45 (2001); (b) M. E. Rice, et al., *Brain Res.* **340**, 151 (1985); (c) C. L. Suna, et al., *Biosens. Bioelectronics.* **26**, 3450 (2011).

[105] (a) M. A. Dayton, A. G. Ewing, R. M. Wightman, *Anal. Chem.* **52**, 2392 (1980); (b) R. N. Goyal, et al., *Electroanalysis.* **20**, 757-764 (2008).

[106] E. B. Bustos, et al., *Talanta.* **2007**, *72*, 1586;

[107] J. B. Raoof, R. Ojani, S. Rashid-Nadimi, *Electrochim. Acta.* **50**, 4694 (2005).

[108] A. I. Gopalan, et al., *Talanta*, **71**, 1774 (2007).

[109] A. Liu, I. Honma, H. Zhou, *Biosens. Bioelectron.* **23**, 74 (2007).

[110] A. Suzuki, et al., *Anal. Chem.* **79**, 8608 (2007).

[111] R. A. Janis, P. J. Silver, D. J. Triggle, *Adv. Drug Res.* **16**, 309 (1987).

[112] (a) C. O. Kappe, *J. Org. Chem.* **62**, 3109 (1997); (b) F. Bossert, W. Vater, *Med. Res. Rev.* **9**, 291 (1989).

[113] (a) K. I. Sakata, et al., *Cancer Sci.* **102**, 1712 (2011); (b) I. T. Phucho, et al., *Rasayan J. Chem.* **23**, 662 (2009).

[114] (a) A. D. Patil, et al., *J. Org. Chem.* **60**, 1182 (1995).

[115] (a) G. K. S. Prakash, et al., *Catal. Lett.* **144**, 2012 (2014).

[116] (a) B. Ramesh, C. M. Bhalgat, *Eur. J. Med. Chem.* **46**, 1882-1891 (2011); (b) G. B. D. Rao, B. Anjaneyulu, M. P. Kaushik, *Tetrahedron Lett.* **55**, 19 (2014).

[117] V. R. Choudhary, et al., *Catal. Commun.* **4**, 449 (2003).

[118] (a) S. E. Hankari, et al., *Chem. Commun.* **47**, 6704 (2011); (b) K. Y. Lee, K. Y. Ko, *Bull. Korean Chem. Soc.* **25**, 1929 (2004).

[119] (a) Y. Qiua, et al., *J. Mol. Cat. A: Chem.* **392**, 76 (2014); (b) E. Kolvari, N. Koukabi, O. Armandpour, *Tetrahedron* **70**, 1383 (2014).

[120] Y. Deng, et al., *J. Am. Chem. Soc.* **130**, 28-29 (2008).

[121] (a) X. Teng, et al., *Nano Lett.* **3**, 261 (2003); (b) S.Y. Lian, et al., *Solid State Commun.*, **127**, 605 (2003).

[122] (a) R. Narayanan, *Green Chem. Lett. Rev.* **5**, 707 (2012); (b) T. Zeng, et al., *Green Chem.* **12**, 570 (2010).

[123] (a) J. M. Campelo, et al., *ChemSusChem* **2**, 18 (2009); (b) A. C. Templeton, W. P. Wuelfing, R. W. Murray, *Acc. Chem. Res.* **33**, 27 (2000).

[124] (a) D. K. Dutta, et al., *Catal Sci. Technol.* **4**, 4001 (2014); (b) S. Pande, et al., *Organic Lett.* **10**, 5179 (2008).

[125] (a) V. K. Sharma, R. A. Yngard, Y. Lin, *Adv. Coll. Inter. Sci.* **145**, 83 (2009); (b) Y. Zhang, et al., *J. Am. Chem. Soc.* **130**, 5868 (2008); (c) P. Goswami, N. Borah, *J. Chem. Pharm. Res.* **6**, 697 (2014).

[126] W. Huang, et al., *Nano Lett*. **8**, 2027 (2008).

[127] (a) D. Manikandan, et al., *Appl. Clay Sci.* **37**, 193 (2007); (b) M. Chetia, et al., *NJC* **39**, 5902 (2015).

[128] S. S. Park, et al., *J. Mater. Chem.* **2010**, *20*, 7854.

[129] (a) M. N. Nadagouda, V. Polshettiwar, R. S. Varma, *J. Mater. Chem*., **19**, 2026 (2009); (b) V. Polshettiwar, R. S. Varma, *Green Chem*. **12**, 743 (2010).

[130] S. DeBonis, et al., *J. Med. Chem.* **51**, 1115-1125 (2008).

[131] K. Matsuno, et al., *Bioorg. Med. Chem. Lett.* **19**, 1058 (2009).

[132] U. Soumyanarayanan, et al., *Org. Med. Chem. Lett.* **2**, 23 (2012).

[133] E. Klein, et al., *Bioorg. Med. Chem.* **15**, 6474 (2007).

[134] D. Horton, G. T. Bourne, M. L. Smythe, *Chem. Rev.* **103**, 893-930 (2003).